

UC Riverside

UC Riverside Electronic Theses and Dissertations

Title

Hybrid Porous Materials for Controlled Release and Catalysis

Permalink

<https://escholarship.org/uc/item/3tw595d5>

Author

Liu, Rui

Publication Date

2010

Peer reviewed|Thesis/dissertation

UNIVERSITY OF CALIFORNIA
RIVERSIDE

Hybrid Porous Materials for Controlled Release and Catalysis

A Dissertation submitted in partial satisfaction
of the requirements for the degree of

Doctor of Philosophy

in

Chemistry

by

Rui Liu

December 2010

Dissertation Committee:

Dr. Pingyun Feng, Chairperson

Dr. Christopher A. Reed

Dr. Guy Bertrand

Copyright by
Rui Liu
2010

This Dissertation of Rui Liu is approved:

Committee Chairperson

University of California Riverside

Acknowledgements

Here I would like to take this opportunity to express my sincere gratitude to my advisor, Prof. Pingyun Feng, for her guidance and enthusiasm. She has provided me with valuable ideas, support and encouragement. She also gave me great freedom in research and provided a lot of opportunities to collaborate with other research groups. This dissertation would not have been possible without her guidance and help.

I also thank our excellent collaborators, Prof. Richard J Hooley in Chemistry Department at UCR and his postdoc Dr. Puhong Liao. Prof. Hooley and Dr. Liao provided deep insight in supramolecular chemistry. They also kindly provided cavitation to help me construct the novel materials. It is a great pleasure and experience to collaborate with them.

I greatly appreciate Prof. Xianhui Bu at CSULB for helpful discussion and kindly allowing me to use the equipments in his lab. I also would like to thank Prof. Len Mueller and his student Arun Agarwal in Chemistry Department at UCR for solid NMR measurement, Dr. Yi Meng and Dr. Dan Borchardt for NMR and Raman measurement, Dr. Richard Kondrat for GC-MS.

I am also very grateful to the rest of my dissertation committee, Prof. Christopher A. Reed and Prof. Guy Bertrand, for their valuable comments on my dissertation.

I thank all the past and present members of the Feng's group for providing a rich working experience, intellectual stimulation and support: Dr. Xiqing Wang, Dr.

Qichun Zhang, Dr. Lei Han, Dr. Zhenyu Zhang, Dr. Zhien Lin, Dr. Yang Liu, Dr. Ying Zhang, Dr. Guiyuan Jiang, Dr. Qipu Lin, Tao Wu, Xiang Zhao, Fan Zuo, Le Wang, Jikai Liu, Fei Bu.

Finally, I would like to thank to my parents. Without their love, encouragement and support, I couldn't finish my Ph. D. study smoothly.

Dedication

To my parents

ABSTRACT OF THE DISSERTATION

Hybrid Porous Materials for Controlled Release and Catalysis

by

Rui Liu

Doctor of Philosophy, Graduate Program in Chemistry
University of California, Riverside, December 2010
Dr. Pingyun Feng, Chairperson

First reported in 1992, ordered mesoporous materials exhibit unique features, such as regular pore geometry, high surface area, and large pore volume, and have shown great potential in various applications. This dissertation combines the knowledge from the field of ordered mesoporous materials and several other research areas to design advanced hybrid porous materials for controlled release and catalysis applications.

The demand for better treatment of illness has led to ever-increasing efforts in the development of efficient drug delivery system that can transport drug molecules to the targeted site and release the loading in a controlled manner. The emerging ordered mesostructured materials exhibit great potential in controlled release because of their stable structures, large surface areas, tunable pore sizes and pore volumes, well-defined surface properties, and biocompatibility. The great diversity in surface functionalization offers mesoporous silica a unique advantage in site-specific delivery and stimuli-responsive release. My research is focused on developing novel controlled

release systems using physiologically compatible chemical or physical stimuli by integrating organic materials with inorganic nanostructured porous materials. The release system uses mesoporous materials as reservoir and functional organic or nanomaterials as valves to perform the controlled responsive functionalities. With this strategy, a series of stimuli responsive and physiologically compatible release systems have been developed, which provide a promising new direction in the bio-applications of nanostructured materials.

Poly(4-vinyl pyridine) is coated on mesoporous silica through facile “grafting to” method. The grafted polymer nanoshell works as pH-sensitive barrier to control the release of trapped molecules from mesoporous silica. We also use nanoparticle as capping agent to block the silica mesopore by pH-responsive acetal linker to obtain acid-sensitive delivery system. By designing a polymeric network (capable of being cross-linked and de-cross-linked) as a “gatekeeper” at the pore opening of mesoporous silica-based materials, a series of hybrid porous materials for controlled release have been developed. For example, the pore of silica materials loaded with guest molecules are blocked by the addition of cystamine, a disulfide-based bifunctional primary amine, which allows polymer chains around the silica surface to be cross-linked. The polymeric network thus formed around the pore opening can be reopened by cleaving the disulfide bond of cystamine in the presence of disulfide reducing agents such as dithiothreitol (DTT), leading to the redox-controlled release. The further introduction of cyclodextrin introduced into the polymer network

expands the responsive diversity by supramolecular host-guest interaction, which is sensitive to photoirradiation, redox signal, or competitive binding.. In addition, cavitands are introduced into the hybrid system and work as supramolecular releasing trigger.

Sulfonated ordered mesoporous carbons have been synthesized by covalent attachment of sulfonic acid containing aryl radicals on the surface of mesoporous carbons. The hybrid materials work as novel solid acid catalysts, which show stable and highly efficient catalytic performance in biodiesel production.

Table of Contents

| | |
|---|----------|
| Acknowledgements | iv |
| Abstract | vii |
| Table of Contents | x |
| List of Figures | xiii |
| List of Tables | xvii |
| List of Schemes | xviii |
| | |
| Chapter One An Overview of Ordered Mesoporous Materials | 1 |
| 1.1 Introduction | 1 |
| 1.2 Synthesis of ordered mesoporous materials | 2 |
| 1.3 Control of structure and surface property | 4 |
| 1.3.1 Pore geometry | 4 |
| 1.3.2 Morphology | 6 |
| 1.3.3 Pore size | 7 |
| 1.3.4 Surface functionalization | 8 |
| 1.4 Ordered mesoporous silica in drug delivery and controlled release | 10 |
| 1.4.1 Sustained release system | 11 |
| 1.4.2 Stimuli-responsive release system | 15 |
| 1.4.2.1 Nanoparticles as gatekeepers | 15 |
| 1.4.2.2 Organic molecule and biomolecule as gatekeepers | 18 |

| | | | |
|----------------------|---------|---|----|
| | 1.4.2.3 | Supramolecular assemblies as gatekeepers | 23 |
| | 1.4.2.4 | Polymer and dendrimer as gatekeepers | 29 |
| | 1.5 | Ordered mesoporous materials in catalysis | 34 |
| | 1.6 | Summary and Outlook | 36 |
| | 1.7 | References | 37 |
| Chapter Two | | Responsive Polymer Coated Mesoporous Silica as pH-sensitive Nanocarrier for Controlled Release | 43 |
| | 2.1 | Introduction | 43 |
| | 2.2 | Experimental Section | 46 |
| | 2.3 | Results and Discussion | 47 |
| | 2.4 | Conclusion | 51 |
| | 2.5 | References | 52 |
| Chapter Three | | pH-Responsive Nanogated Ensemble Based on Gold-Capped Mesoporous Silica through an Acid-Labile Acetal Linker | 54 |
| | 3.1 | Introduction | 54 |
| | 3.2 | Experimental Section | 56 |
| | 3.3 | Results and Discussion | 60 |
| | 3.4 | Conclusion | 64 |
| | 3.5 | References | 65 |
| Chapter Four | | Tunable Redox-responsive Hybrid Nanogated Ensembles | 67 |
| | 4.1 | Introduction | 67 |
| | 4.2 | Experimental Section | 69 |

| | | |
|----------------------|---|-----|
| 4.3 | Results and Discussion | 72 |
| 4.4 | Conclusion | 79 |
| 4.5 | References | 79 |
| Chapter Five | Multiresponsive Supramolecular Nanogated Ensembles | 81 |
| 5.1 | Introduction | 81 |
| 5.2 | Experimental Section | 84 |
| 5.3 | Results and Discussion | 87 |
| 5.4 | Conclusion | 92 |
| 5.5 | References | 93 |
| Chapter Six | A Water-Soluble Deep Cavitand Acts as a Release Trigger for a Supramolecular Nanocap | 95 |
| 6.1 | Introduction | 95 |
| 6.2 | Experimental Section | 98 |
| 6.3 | Results and Discussion | 99 |
| 6.4 | Conclusion | 105 |
| 6.5 | References | 105 |
| Chapter Seven | Sulfonated Ordered Mesoporous Carbon for Catalytic Preparation of Biodiesel | 108 |
| 7.1 | Introduction | 108 |
| 7.2 | Experimental Section | 110 |
| 7.3 | Results and Discussion | 113 |
| 7.4 | Conclusion | 121 |
| 7.5 | References | 121 |

List of Figures

- Figure 1.1** Schematic representation of the synthesis of ordered mesoporous silica
- Figure 1.2** Schematic representation of preparation of ordered mesoporous carbon using ordered mesoporous silica (e.g., SBA-15) as the template
- Figure 1.3** Typical mesophases and corresponding mesoporous materials
- Figure 1.4** Functionalization of ordered mesoporous silicas by (A) post-synthesis grafting and (B) co-condensation methods, and (C) the formation of periodic mesoporous organosilicas (PMOs).
- Figure 1.5** Alendronate adsorption on hexagonally ordered mesoporous silica functionalized with propylamine groups
- Figure 1.6** Schematic representation of the CdS nanoparticle-capped mesoporous silica based drug/neurotransmitter delivery system.
- Figure 1.7** Schematic representation of gold nanoparticle-capped mesoporous silica through photocleavable linker
- Figure 1.8** Schematic representation of pH and laser light triggered release system
- Figure 1.9** Photo-responsive delivery system based on coumarin modified mesoporous silica.
- Figure 1.10** Schematic representation of dual responsive system based on CD-covered mesoporous silica through enzyme- and photo-cleavable linker..
- Figure 1.11** pH- and anion-controlled gate-like system by attaching oligoamine onto the surface of mesoporous silica
- Figure 1.12** Antigen-responsive gate-like system by attaching antibody onto the surface of mesoporous silica
- Figure 1.13** Schematic representation of the glucose-responsive mesoporous silica based delivery system for controlled release of bioactive G-Ins and cAMP

- Figure 1.14** Schematic representation of redox-responsive supramolecular nanovalve.
- Figure 1.15** Schematic representation of reversible supramolecular nanovalve
- Figure 1.16** Schematic representation of pH-Responsive mesoporous silica with dibenzo[24]crown-8
- Figure 1.17** Schematic representation of pH-Responsive mesoporous silica with α -CD.
- Figure 1.18** Schematic representation of enzyme-responsive snap-top mesoporous silica
- Figure 1.19** Schematic representation of light-responsive mesoporous silica based on azobenzene and β -CD
- Figure 1.20** Schematic representation of pH-responsive drug delivery system based on the interaction between negative carboxylic acid modified SBA-15 silica rods with polycations (PDDA)
- Figure 1.21** Schematic representation of pH-responsive drug delivery system based on polyelectrolyte multilayer coated mesoporous silica sphere.
- Figure 1.22** a) Schematic of thermo-responsive polymer poly(N-isopropylacrylamide) response with temperature. b) thermo-responsive release system based on poly(N-isopropylacrylamide) coated mesoporous silica.
- Figure 1.23** Delivery of DNA plasmid pEGP-C1 in cells via a second generation PAMAM-functionalised mesoporous silica.
- Figure 2.1** TEM of (a) Br-MS and (b)PVP-MS
- Figure 2.2** BET nitrogen sorption isotherms and BJH pore size distribution plots (inset) of Br-MS
- Figure 2.3** FTIR(a) and TGA(b) of MCM-41, Br-MS and PVP-MS.
- Figure 2.4** Time course of dye release from PVP-MS at different pHs
- Figure 3.1** TEM of a) MS-Acetal, b) MS-Au and inset in b) Au-COOH

- Figure 3.2** XRD of a) MS-Acetal and MS-Au, b) Au-COOH and MS-Au
- Figure 3.3** BET nitrogen sorption isotherms and BJH pore size distribution plots (inset) of MS-Acetal (red) and MS-Au(green)
- Figure 3.4** Fluorescence spectra of fluorescamine solutions
- Figure 3.5** Time course of dye release from MS-Au at different pHs
- Figure 4.1** FTIR of a) pure silica MCM-41, b) PNAS-MS, c) cross-linked PNAS-MS.
- Figure 4.2** TEM of a) MCM-41, b) PNAS-MS
- Figure 4.3** TGA of a)MCM-41, b)PNAS-MS and c) cross-linked PNAS-MS
- Figure 4.4** XRD of a) PNAS-MS and b) cross-linked PNAS-MS
- Figure 4.5** BET nitrogen sorption isotherms and BJH pore size distribution plots (inset) of a) PNAS-MS and b) cross-linked PNAS-MS
- Figure 4.6** (a) Time course of rhodamine B release from hybrid materials in the presence of DTT concentrations 2.16×10^{-2} M (blue) and 2.16×10^{-4} M (red). (b) The DTT concentration-dependent releases. Released dye concentrations are measured after 2h of the DTT addition.
- Figure 5.1** FTIR of PNAS-MS, Poly-Py-MS, Poly-CD-MS and per-6-thio- β -cyclodextrin
- Figure 5.2** (a)XRD and (b) BET nitrogen sorption isotherms and BJH pore size distribution plots (inset) of Poly-CD-MS
- Figure 5.3** UV-vis spectra of per-6-thio- β -cyclodextrin in DMF (a) before and (b) after the coupling reaction with Poly-Py-MS
- Figure 5.4** Controlled release of calcein from cross-linked Poly-CD-MS (1.0 mg) in 1 mL of PBS solution (100.0 mm, pH 7.4). (a) no noticeable release was observed in the absence of external stimuli. At time 0, triggered by (b)UV, (c) 5mg DTT (after 60min, 5mg more DTT did not induce more release), (d) 5mg α -cd (~ 30 equiv to β -cd of Poly-CD-MS, after 60min, 5mg more α -cd did not induce more release)

- Figure 6.1** TEM of a) MCM-41, b) assembly of MCM-41 with AuNPs and inset in b) AuNPs
- Figure 6.2** BET nitrogen sorption isotherms and BJH pore size distribution plots (inset) of MCM-41
- Figure 6.3** XRD of gold nanoparticles capped MCM-41
- Figure 6.4** ^1H NMR of (a) Cavitand 1, (b) AuNP and (c) AuNP after addition of Cavitand 1 in D₂O. * THF peaks in D₂O
- Figure 6.5** Fluorescence emission spectra of the released fluorescein under a) no additive, b) 1 mg (0.73 μmol) of cavitand 1 and c) 1 mg (6.94 μmol) of sodium benzoate. Blue line: 10 min, red line: 30 min, green line: 60 min.
- Figure 7.1** XRD patterns of OMCs and sulfonated OMCs
- Figure 7.2** SEM of OMC-150(A) and OMC-150-SO₃H(B)
- Figure 7.3** N₂ sorption isotherms and BJH pore size distribution plots (inset) of OMCs and OMC-SO₃Hs
- Figure 7.4** Comparison of catalytic activity for conversion of oleic acid over different catalysts. Reaction condition: acid catalyzed (50 mg catalyst) esterification of oleic acid (0.005 mol) with ethanol (0.05 mol)
- Figure 7.5** Repeating use of OMC-SO₃H-150 and SBA-15-ph-SO₃H for esterification of oleic acid (0.005 mol) with ethanol (0.05 mol) at 80 °C The yields of ethyl oleate produced after reaction for 10 h are shown.

List of Tables

- Table 1.1** Molecular structure and dimensional size of several drugs
- Table 7.1** Textural properties of OMCs and sulfonated ordered mesoporous carbons and catalytic properties of OMC-SO₃Hs

List of Schemes

- Scheme 2.1** pH-controlled release from responsive polymeric nanoshell coated mesoporous silica
- Scheme 3.1** Schematic illustration of pH-responsive nanogated ensemble based on gold-capped mesoporous silica through acid-labile acetal linker
- Scheme 3.2** Schematic outline of synthesis of MS-Aetal and MS-Au.
- Scheme 4.1** Schematic illustration of redox-responsive nanogated ensemble based on polymeric network-capped mesoporous silica.
- Scheme 4.2** Schematic outline of synthesis of PNAS-MS.
- Scheme 5.1** Schematic illustration of multi-responsive nanogated ensemble based on supramolecular polymeric network-capped mesoporous silica.
- Scheme 5.2** Schematic outline of synthesis of Poly-CD-MS
- Scheme 6.1** a) Schematic illustration of the experiment; b) plan view of cavitand 1 and minimized structure of the 1•choline complex (SPARTAN, AM1).
- Scheme 7.1** Functionalization of OMC with sulfonic acid groups.

Chapter One

An Overview of Ordered Mesoporous Materials

1.1 Introduction

According to the IUPAC definition¹, porous materials are classified into three groups on the basis of pore size: microporous materials are porous solids with pore size below 2 nm, mesoporous materials are porous solids with pore size between 2 and 50 nm, and macroporous materials are those with pore size larger than 50 nm. Prior to the 1990s, materials with pore size in the mesoporous range such as silica gels and activated carbons show disordered pore structure with a broad distribution of pore size. In 1992, by using cationic surfactants as template, Mobil scientists prepared a family of ordered mesoporous silicas (denoted M41S) with hexagonal, lamellar phase or cubic symmetry and uniform pore sizes ranging from 2 to 10 nm.² Ever since then, research on ordered mesoporous materials has undergone a rapid growth in the past two decades. Ordered mesoporous materials exhibit unique features, such as tunable pore geometry, high surface area, and large pore volume, which make them potentially suitable for various applications, such as catalysis, separation, sensor and drug delivery.

Here a brief overview of ordered mesoporous materials is given in this chapter, which covers the general synthesis of ordered mesostructures with control of pore structure and surface functionalization and their applications, especially the applications in controlled release and catalysis are discussed.

1.2 Synthesis of ordered mesoporous materials

The synthesis of mesoporous silica by the surfactant-template approach follows the procedure illustrated in Figure 1.1. The formation of surfactant-silica meso-assembly is a result of the cooperative assembly between amphiphilic surfactant molecules and soluble silica precursors. Due to forces such as electrostatic interaction and hydrogen bonding between surfactant molecules and silica precursor molecules, surfactant molecules organize into long-range ordered liquid crystal phases. The condensation and polymerization of silica precursors within the hydrophilic aqueous domain of liquid crystals give rise to mesostructured silica with topology defined by the liquid crystal templates. The final mesoporous silica is obtained by removal of templating surfactant molecules through either calcinations or solvent extraction.

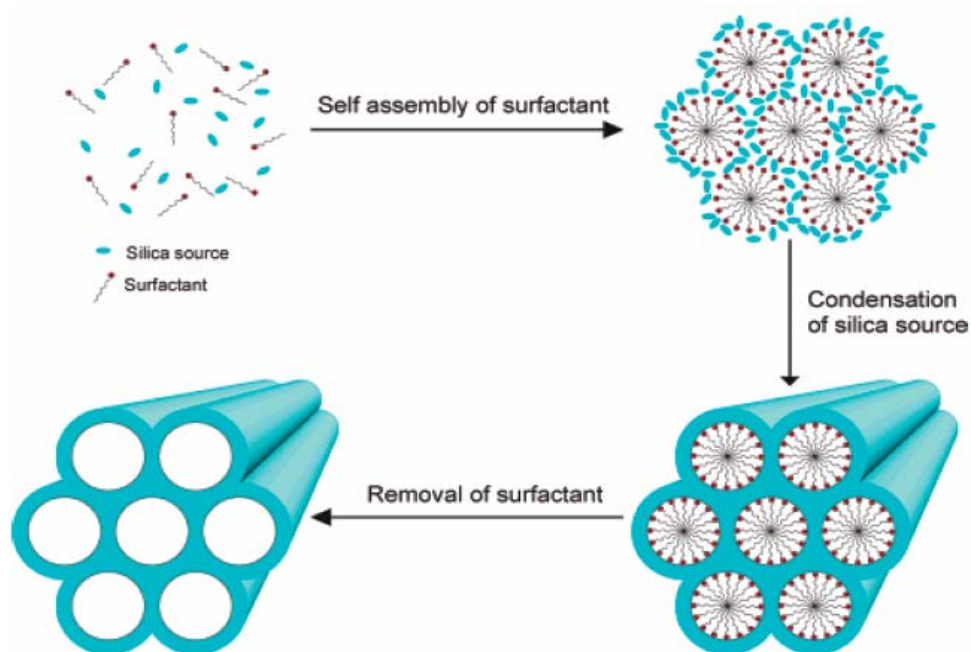


Figure 1.1 Schematic representation of the synthesis of ordered mesoporous silica (Reproduced with permission from ref. 3. copyright 2005 American Chemical Society)

The first reported ordered mesoporous silica are M41s family by Mobil scientists in 1992.² The templates used in the hydrothermal synthesis are cationic surfactants with 8 to 22 carbon alkyl chains. Four different phases have been discovered by using different shapes of templates: a hexagonal phase MCM-41,² cubic phase MCM-48,⁴ lamellar phase MCM-50,⁵ and a cubic octamer [(CTMA)SiO_{2.5}]₈. The widely used MCM-41 possesses honeycomb arrays of nonintersecting uniformly sized channels with diameters ranging from 1.5 to 10 nm. In 1998, highly ordered pore mesoporous silica SBA-15 with larger pore (from 8 to 30 nm) and thicker pore walls (ca. 3 nm) have been reported.⁶ SBA-15 possesses two-dimensional channel structure consisting of a hexagonal array of mesopores interconnected by micropores. The relatively cheap amphiphilic triblock copolymer EO₂₀PO₇₀EO₂₀ (poly(ethylene oxide)-block-polypropylene oxide-block-poly(ethylene oxide), trade name Pluronic 123) is employed as the structure-directing agent in highly acidic media.

The synthesized ordered mesoporous silica described above can be used as hard templates to synthesize carbon mesoporous materials. This work was pioneered by Ryoo's group in 1999: ordered mesoporous carbon CMK-1 was prepared using MCM-48 as a template and sucrose as the carbon source.⁷ Similarly, SBA-15 can also be used as hard template.⁸ The principle procedure is shown in Figure 1.2. Ordered mesoporous silica are impregnated with carbon precursor such as sucrose, furfuryl alcohol, resorcinol-formaldehyde, or vinylbenzene. Cross-linking and carbonization of the organic precursors, followed by dissolution of the silica template lead to the

formation of mesoporous carbon. It was rather surprising that 2D hexagonal SBA-15 leads to the stable carbon replica. This may be caused by the micropores connecting the mesoporous channels of SBA-15.⁹ Since the connecting micropores are also filled with carbon precursor, they form structure-supporting links between the carbon rods to stabilize carbon replica. In addition to the hard template method, Zhao *et al.* reported a direct method for ordered mesoporous polymers and carbons through organic-organic self-assembly of triblock copolymers (e.g., P123 and F127) with resols (phenol/formaldehyde).¹⁰ By this way, the obtained mesostructures include 2D hexagonal ($p6m$), cubic ($Ia-3d$), 3D caged cubic ($Im-3m$), and lamellar frameworks by simply adjusting the mass ratio of the polymer precursors and amphiphilic surfactants.

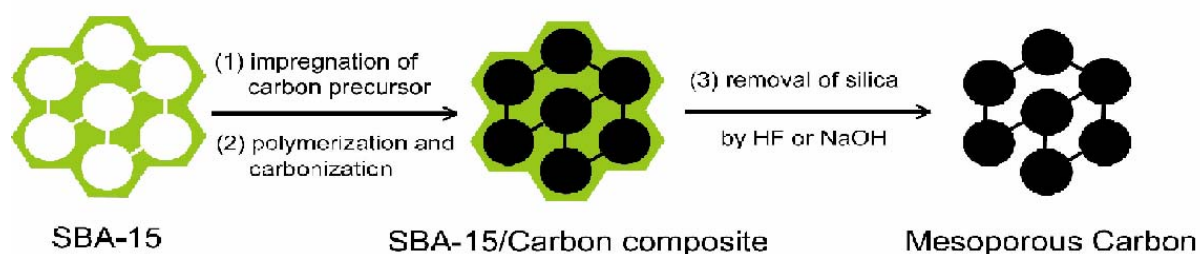


Figure 1.2 Schematic representation of preparation of ordered mesoporous carbon using ordered mesoporous silica (e.g., SBA-15) as the template.

1.3 Control of structure and surface property

1.3.1 Pore geometry

Mesophase geometry affects molecular diffusion and chemical reactivity. By tuning synthetic parameters, it is possible to control the topological features of resulting

mesophases. Huo *et al* examined how the molecular shapes of covalent organosilanes, quaternary ammonium surfactants, and mixed surfactants in various reaction conditions can be used to synthesize silica-based mesophase configurations.¹¹ They found that the structural function of surfactants in mesophase formation can to a first approximation be related to that of classical surfactants in water or other solvents with parallel roles for organic additives. In classical micelle chemistry, micellar organization is related to the local effective surfactant packing parameter, $g = V/a_0l$, where V is the total volume of the hydrophobic chains, a_0 is the effective headgroup area at the micelle surface, and l is the kinetic surfactant tail length. The expected mesophase depends on the value of g . Huo *et al* applied this concept to explain and predict product structure and phase transition.¹¹ Typical mesophase geometries and corresponding materials are listed in Figure 1.3.

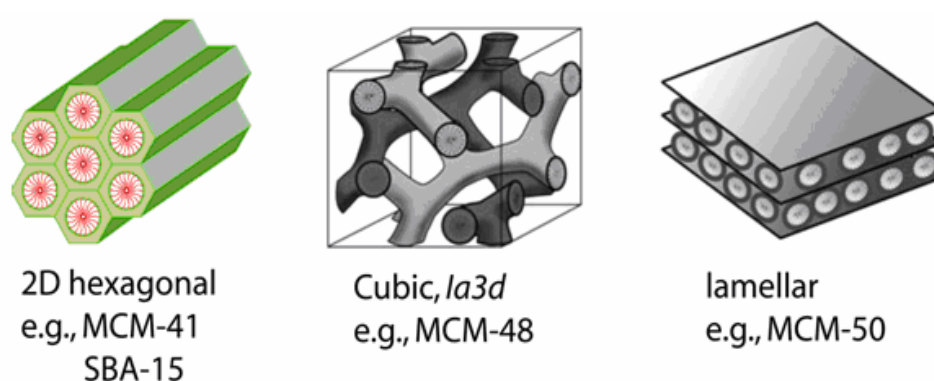


Figure 1.3 Typical mesophases and corresponding mesoporous materials

1.3.2 Morphology

Although the original synthetic methods yield irregular bulk or powder forms, the process can be applied to create various forms, including thin films, nanoparticles, or monoliths. Thin films of mesoporous silica can be prepared from a solution at room temperature by a process called “evaporation-induced self-assembly”.¹² This process employs one-pot sol comprised of templating agents and silica precursors in aqueous ethanol. The cooperatively self-assembly at the surface of the substrate is triggered during evaporation of the ethanol. Condensation of the silica monomers around the surfactant micelles eventually leads to the formation of mesostructured silica films. Free-standing films can be grown at liquid-vapor (e.g. water-air)¹³ and liquid-liquid (e.g. oil-water)¹⁴ interface.

Lin *et al* developed several methods to tune the nanoparticle morphology of mesoporous silica materials. The first method involved the use of a series of antimicrobial room-temperature ionic liquids (RTIL's) with various alkyl chain lengths as templates for the synthesis of mesoporous silica. Spheres, ellipsoids, rods, and tubes were successfully synthesized by using 1-alkyl-3-methylimidazolium with different alkyl chains.¹⁵ The second method was based on a co-condensation reaction with tetraethoxysilane (TEOS) and different organoalkoxysilanes. Lin *et al*¹⁶ found that the presence of organoalkoxysilane precursors during the base catalyzed condensation greatly influenced the final particle shape. By changing the precursor or its concentration, the particle morphology was tuned to various shapes, including

spheres, tubes, and rods of various dimensions.

Transparent and rigid monoliths are of great interest in optics. Feng *et al*¹⁷ prepared monolithic mesoporous silica templated by microemulsion liquid crystal. Zhao *et al*¹⁸ used a liquid paraffin medium assisted solvent evaporation method to yield transparent and crack-free mesostructured silica monoliths

1.3.3 Pore size

The pore size of mesoporous silica can be tuned by synthetic parameters. For example, the pore size generally increases with the increase of chain length of surfactants. Thus it is possible to control the pore size by using different surfactants. A large variety of surfactant molecules are available, including cationic ammonium salts (e.g. $C_{16}H_{33}(CH_3)_3N^+$) and block copolymers (e.g. polyethylene oxide-polypropylene oxide triblock surfactant, $(EO)_m(PO)_n(EO)_m$). With different surfactants, the pore size of the mesoporous materials can be tuned from 2 to about 20nm. It is worth noting that together with other synthetic parameters such as silica to surfactant ratios, the use of different surfactants also allows the synthesis of mesoporous silica with different topologies.

Another effective method to increase the pore size is through the addition of swelling agents. For example, 1,3,5-trimethylbenzene (TMB) can be used as swelling agent to increase the pore size of mesoporous materials.² By adjusting the oil to surfactant ratios, the pore size of mesoporous silica can be continuously adjusted (e.g., from 2 to 10nm). Other aromatic hydrocarbons, alkanes, and amines have also been

used as pore expanders.¹⁹

The pore size of ordered carbon materials synthesized through hard template is primarily determined by the pore wall thickness of the porous silica, which can be tailored by the synthetic conditions. Ryoo *et al* systematically synthesized a series of SBA-15-type ordered silica with tailored pore wall thicknesses of 1.4 – 2.2 nm by controlling the ratio of hexadecyltrimethylammonium bromide (HTAB) to the poly(oxyethylene hexadecyl ether) surfactants (C₁₆EO₈) in the surfactant mixture. With these silica templates, they synthesized CMK-3 materials with a tailored mesopore size of 2.2 – 3.3 nm.²⁰

1.3.4 Surface functionalization

The properties of internal surfaces (chemical functionality, domain sizes of hydrophilicity and hydrophobicity) of mesoporous silica can be controlled using methods illustrated in Figure 1.4. The first method is the post-synthesis grafting of functional groups onto the internal surface of pre-formed mesoporous silica. This method is the easiest and the most frequently used for modification of mesoporous silicas because mesostructures remain unchanged after grafting. Thus diverse functionalized silica-based materials have been generated.²¹ The second method involves the co-condensation of two different silica precursors, one of which contains organic functional groups. By this method, distribution of functional groups is found more homogeneous than the grafting method.²² However, due to the decreasing interactions between surfactants and silica species with an increase in the molar

fraction of organosilanes used for synthesis, the content of organic groups does not exceed 25 % in order to keep the high structural order. The third method is to prepare periodic mesoporous organosilicas (PMO). PMO contains organic groups as an integral component of silica-based framework.²³ The synthesis of PMO involves the hydrolysis and condensation of tailor-made bridged organosilica precursor $((R'O)_3Si)_nR$ ($n = 2$ or 3 , $R' =$ methyl or ethyl) in the presence of surfactant assemblies. Advantages of PMOs include homogeneous distribution of bridged organic groups with high and tunable concentrations, large free void space, and consequently easily accessible functional groups.

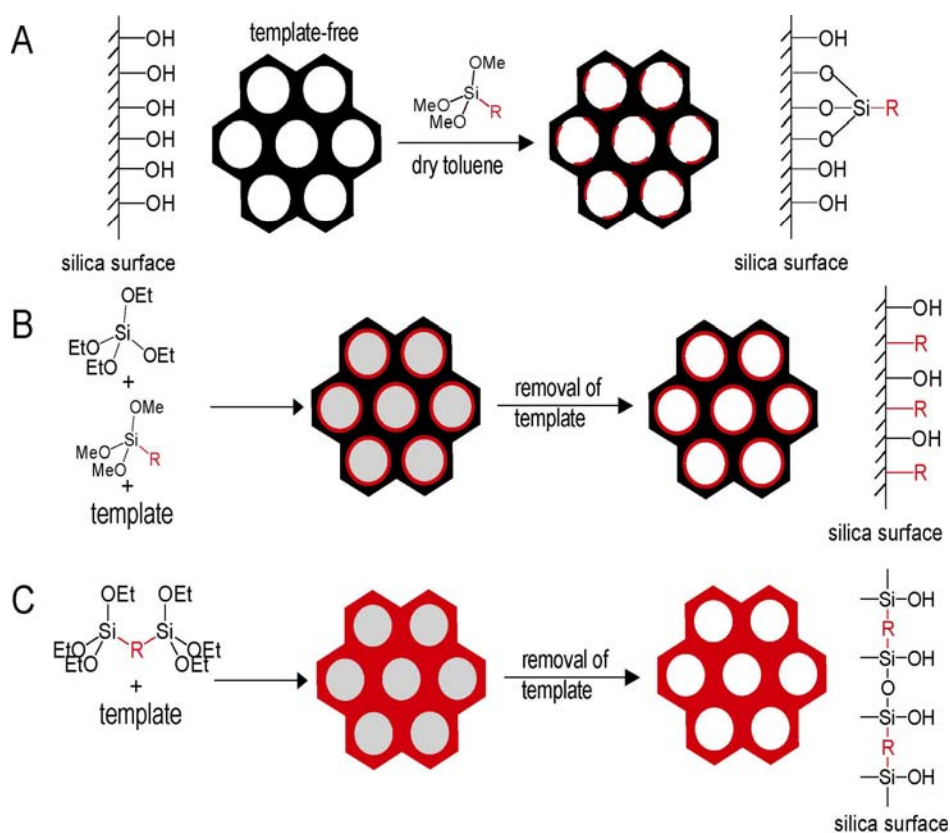


Figure 1.4 Functionalization of ordered mesoporous silicas by (A) post-synthesis grafting and (B) co-condensation methods, and (C) the formation of periodic mesoporous organosilicas (PMOs).

Dai *et al* functionalized ordered mesoporous carbon materials by using a solvent-free technique,²⁴ in which diazonium compounds were generated in situ and reacted with carbon surfaces.²⁵ Aryl groups substituted at the 4-position (ArR, R=Cl, CO₂R', alkyl) were covalently grafted onto the surface of ordered mesoporous carbon materials. The same group also reported the fluorination of ordered mesoporous carbon material, in which ordered mesoporous carbon was treated in diluted fluorine gas (4 vol% in helium) for 4 days at room temperature or moderately elevated temperatures.²⁶

1.4 Ordered mesoporous silica in drug delivery and controlled release

As outlined in Lin's review paper,²⁷ several prerequisites need to be incorporated into a material in order to serve as an efficient drug delivery system:

- a). The carrier material should be biocompatible.*
- b). High loading/encapsulation of desired drug molecules.*
- c). Zero premature release, i.e., no leaking, of drug molecules.*
- d). Cell type or tissue specificity and site directing ability.*
- e). Controlled release of drug molecules with a proper rate of release to achieve an effective local concentration.*

Among many structurally stable materials, mesoporous materials are regarded as excellent candidates for controlled drug-delivery systems due to the unique features (e.g. biocompatible, ordered pore network, high pore volume, high surface area,

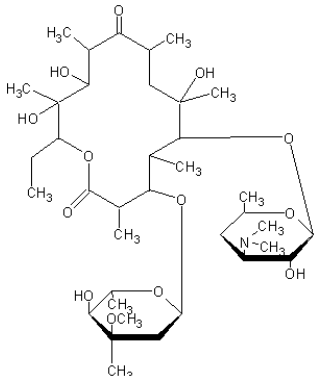
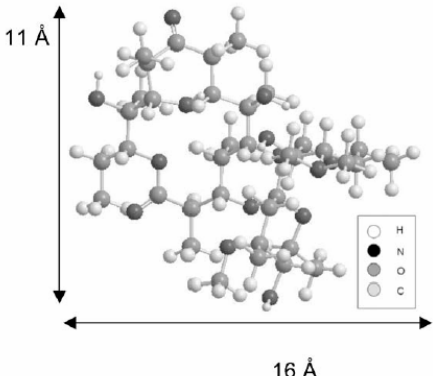
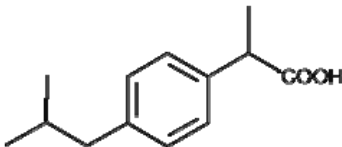
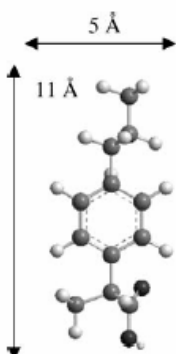
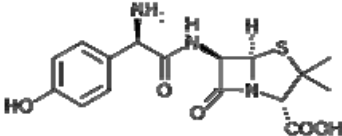
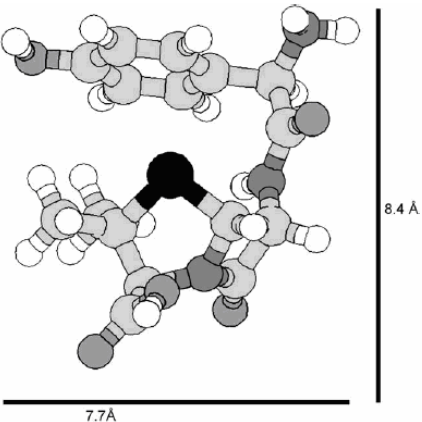
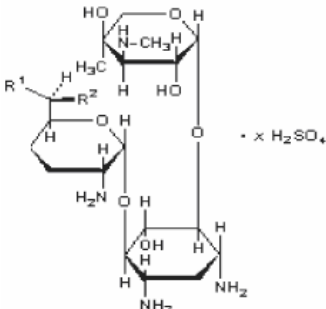
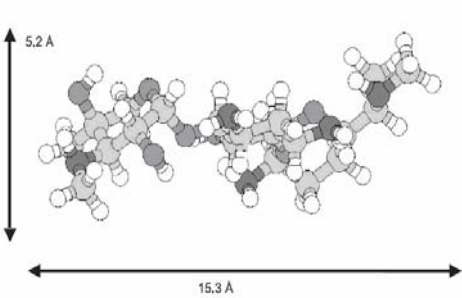
functionalized surface) and intensive research has been carried out on this topic.

1.4.1 Sustained release system

MCM-41 was first used as adsorption matrix to test its drug delivery property by Vallet-Regí *et al* in 2001.²⁸ The loading of ibuprofen (IBU) in MCM-41 reached as high as 30% and completely released in a simulated body fluid after 3 days. After this pioneering work, pore size, pore volume, surface area and functionality have been extensively studied in drug adsorption and release.

The adsorption of drug into mesoporous silica is determined by the pore size. Since most drugs used in clinical practice fall into the nanometer scale, they can easily be trapped into the mesopore ranging from 1.5nm to several tens of nanometers. Table 1 summarized several drugs that have been used in mesoporous silica based drug delivery systems and their molecular structure and dimensional size. Pore size not only works as molecule-sieve for adsorption but also controls the release rate. For example, a series of MCM-41 with different pore size ranging from 2.5 nm to 3.6 nm have been synthesized by using different length surfactants. The delivery rate of ibuprofen in simulated body fluid (SBF) solution increases as the pore size increases.³³

Table 1.1 Molecular structure and dimensional size of several drugs

| | | | |
|---------------------|--|---|------|
| Erythromycin |  <p>The chemical structure of Erythromycin is a large macrolide antibiotic. It features a 14-membered macrolide ring with a methyl group at C4, a methyl ester at C3, and a trimethylammonium group at C2. It is linked to a 14-membered tetraene ring with methyl groups at C11 and C12, and a trimethylammonium group at C13. A 14-membered tetraene ring is also attached to the second ring, with methyl groups at C11 and C12, and a trimethylammonium group at C13.</p> |  <p>A 3D ball-and-stick model of Erythromycin. The legend indicates: H (white), N (black), O (grey), C (light grey). The dimensions are 11 Å in height and 16 Å in width.</p> | [29] |
| Ibuprofen |  <p>The chemical structure of Ibuprofen is a propionic acid derivative. It consists of a central benzene ring with a 4-isobutylphenyl group at the para position and a propionic acid group at the other para position.</p> |  <p>A 3D ball-and-stick model of Ibuprofen. The dimensions are 5 Å in width and 11 Å in height.</p> | [30] |
| Amoxicillin |  <p>The chemical structure of Amoxicillin is a penicillin derivative. It features a beta-lactam ring fused to a thiazolidine ring, with a propionic acid group at C2 and a p-hydroxyphenylacetamido group at C6.</p> |  <p>A 3D ball-and-stick model of Amoxicillin. The dimensions are 7.7 Å in width and 8.4 Å in height.</p> | [31] |
| Gentamicin |  <p>The chemical structure of Gentamicin is an aminoglycoside. It consists of a 2-deoxystreptamine core with two 2-deoxyribose rings attached to the C2 and C3 positions. The structure is shown as a salt with four sulfate groups (x 4 H₂SO₄).</p> |  <p>A 3D ball-and-stick model of Gentamicin. The dimensions are 5.2 Å in height and 15.3 Å in width.</p> | [32] |

As long as pore size allows the diffusion of drug into the mesopore, surface becomes the most determining factor on the amount of adsorbed drug. The influence of surface area can be seen when loading alendronate into MCM-41 and SBA-15.³⁴ Both MCM-41 and SBA-15 have 2D hexagonal structure with BET surface area of 1157 and 719 m² /g, respectively. The maximum loads of alendronate were 139 and 83 mg/g for MCM-41 and SBA-15, respectively when both mesoporous materials were loaded with alendronate under the same conditions.

Surface property of mesoporous silica can be tuned by functionalizing the mesopore silica walls with functional groups to modify the silica/drug affinity. Vallet-Regí *et al*³⁵ and Song *et al*³⁶ used amine functionalized MCM-41 and SBA-15 to control IBU release. NMR analysis revealed that IBU molecules are tightly linked at the surface because the drug-surface ionic interactions are stronger than the IBU dimer hydrogen bonds. The ionic interaction between the carboxylic groups in IBU and the amino groups on silica surface allows the release rate of IBU from amino-functionalized mesoporous silica to be effectively controlled. Vallet-Regí *et al*³⁷ also used amino-functionalized MCM-41 and SBA-15 as alendronate delivery vehicle for bone repair or regeneration (Figure 1.5). The amount of alendronate loaded into amino-modified mesoporous matrices was almost three fold that of unmodified materials. High adsorption is believed coming from the different chemical interaction between the phosphonate groups in alendronate with the silica surface. As shown in Figure 1.5, under the loading conditions (pH 4.8), the interaction between

the amino and the phosphonate groups is stronger than that between the silanol group and the phosphonate. At physiological pH (pH 7.4), the differences in polarity between the silica surface and the bisphosphonate, or between the NH_2 -modified surface and the bisphosphonate, induce weakening of the adsorbed molecules, which are then slowly released to the media.

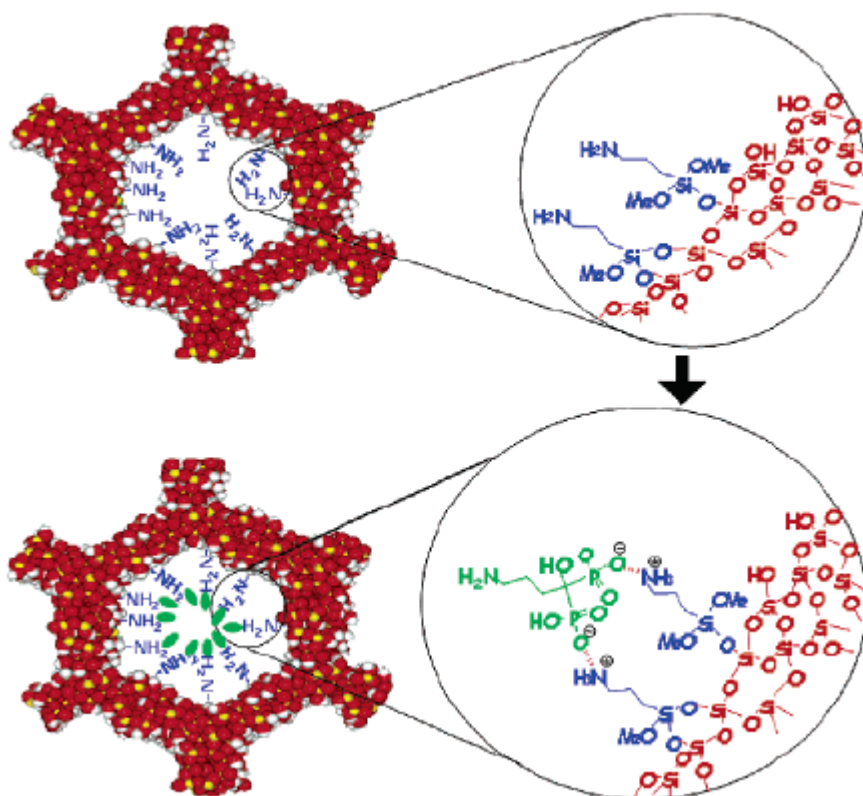


Figure 1.5 Alendronate adsorption on hexagonally ordered mesoporous silica functionalized with propylamine groups. (Reproduced with permission from ref. 37 copyright 2006 American Chemical Society)

The second strategy in surface modification to control drug release is functionalization of the surface with hydrophobic species. In this case, drug transport out of the matrix is impeded because the aqueous delivery solution does not penetrate

inside the pores easily. Controlled release of erythromycin, an antibiotic that belongs to the macrolide family, from SBA-15 was achieved by modifying SBA-15 with trimethoxyoctylsilane and trimethoxyoctadecylsilane, respectively.³⁸ The consequent decrease of pore size and surface wettability by aqueous solutions could effectively control the release rate of erythromycin. For example, the octadecyl-functionalized sample exhibited a release rate one order of magnitude lower than that of non-functionalized SBA-15. Release rate of captopril³⁹ and ibuprofen⁴⁰ from MCM-41 can also be controlled by tailoring the surface chemical properties with hydrophobic methyl group

1.4.2 Stimuli-responsive release system

As mentioned above, the ability to release drugs at will, i.e. precise control over the location and timing of the release is highly desirable in site-specific delivery applications. The gatekeeping effect of mesoporous silica-based stimuli-responsive drug delivery system can fulfill the desirable properties to achieve the controlled release of the cargo in a suitable concentration at the desired target in a determined amount of time. A variety of chemical entities (e.g. nanoparticles, organic molecules, supramolecular assemblies, or polymer) have been used as photochemical, pH responsive, and redox active “gatekeepers”.

1.4.2.1 Nanoparticles as gatekeepers

Lin *et al* first used CdS nanoparticles to cap the pores of mesoporous silica for the

controlled release of cargo molecules (Figure 1.6a).⁴¹ CdS nanoparticles were covalently attached on the silica surface through the amidation reaction between mercaptoacetic acid-functionalized CdS nanoparticles and mesoporous silica containing 2-(propyl)disulfanyl ethylamine. The stimuli-responsive release of vancomycin and adenosine triphosphate (ATP) from mesoporous silica was observed when using disulfide bond-reducing molecules, such as dithiothreitol (DTT) and mercaptoethanol (ME). Instead of CdS, the same group later used magnetic Fe₃O₄ nanoparticles to cap mesoporous entrance.⁴² The disulfide bonds between the silica particle and the Fe₃O₄ nanoparticles can also be cleaved with disulfide reducing agents such as dithiothreitol (DTT) and dihydrolipoic acid (DHLA). The presence of external magnetic field can specifically delivery the drug carrier to target site.

Lin *et al*⁴³ and Martinez-Manez *et al*⁴⁴ have also reported the use of gold nanoparticles (AuNP) to block the pore of mesoporous silica. Lin *et al*⁴³ functionalized the surface of the gold nanoparticle with a photo-responsive linker

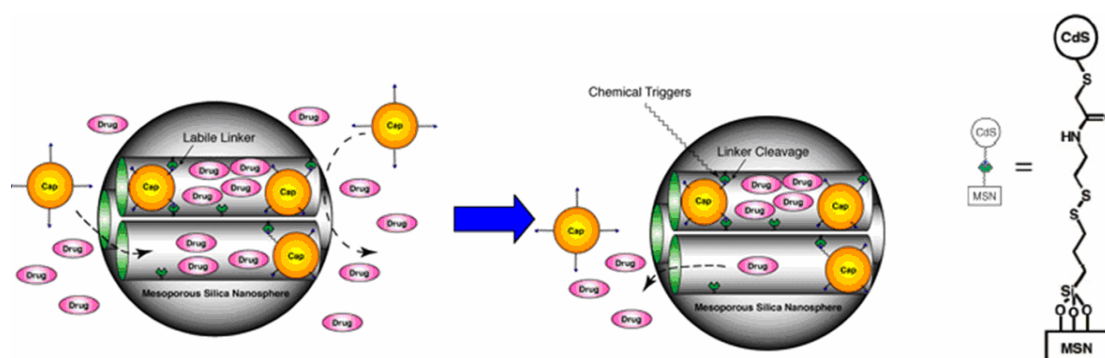


Figure 1.6 Schematic representation of the CdS nanoparticle-capped mesoporous silica based drug/neurotransmitter delivery system (Reproduced with permission from ref. 41 copyright 2003 American Chemical Society).

(thioundecyl-tetraethyleneglycolester-onitrobenzylethyldimethyl ammonium bromide, TUNA) to endow the Au surface positively charged. AuNP can incorporate onto the surface of MCM-41 by electrostatic interaction with the negatively charged surface of the silica. Upon photo-irradiation, the photo-labile linker covalently attached to the surface of AuNPs would be cleaved, resulting in the formation of the negatively charged thioundecyltetraethyleneglycolcarboxylate (TUEC)-functionalized AuNPs. The charge repulsion between the AuNPs and MSN would then uncap the mesopores and allowed the release of guest molecules (Figure1.7). Martinez-Manez *et al*⁴⁴ functionalized a saccharide derivative capable of interacting with boronic acid functionalized gold nanoparticles acting as nanoscopic caps. The gating mechanism involves the reversible reaction between polyalcohols and boronic acids to form boronate esters. The hydrolysis of the boroester bond takes place at pH 3, which results in rapid delivery of the safranin cargo from the pore voids into the aqueous solution. The plasmonic heating at 1064 nm also results in the cleavage of the boronic ester linkage that anchors the nanoparticles to the surface of the mesoporous silica-based material, allowing the release of the entrapped guests. (Figure1.8)

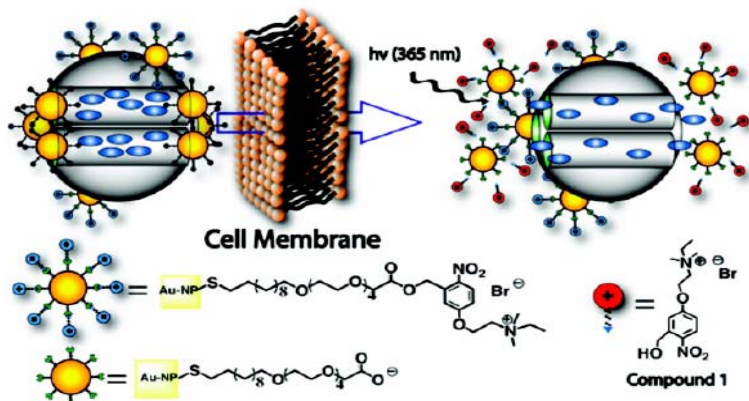


Figure 1.7 Schematic representation of gold nanoparticle-capped mesoporous silica through photocleavable linker. (Reproduced with permission from ref. 43 copyright 2009 American Chemical Society).

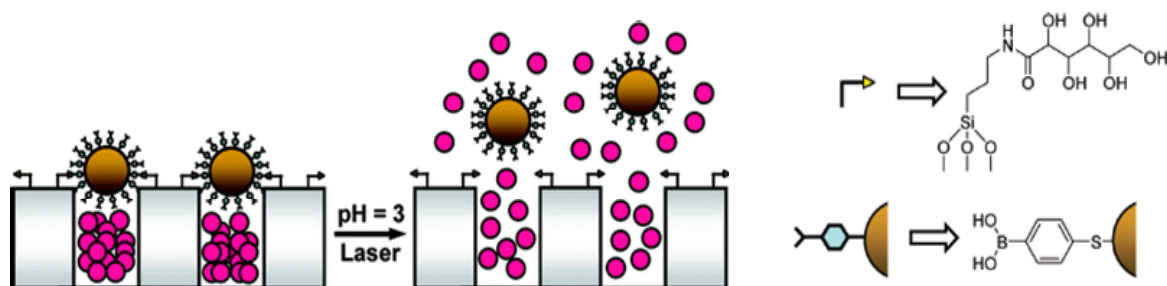


Figure 1.8 Schematic representation of pH and laser light triggered release system. (Reproduced with permission from ref. 44 copyright 2009 American Chemical Society).

1.4.2.2 Organic molecule and biomolecule as gatekeepers

In addition to solid nanoparticles, flexible organic molecules have also been used as capping agent for mesoporous silica. Tanaka et al 45 modified MCM-41 with 7-[(3-triethoxysilyl)propoxy]coumarin. Dimerization of this coumarinic under longer wavelength UV light yielded a cyclobutane, coumarin dimer, which was large enough to close the mesoporous opening of MCM-41. The irradiation to the dimerized-coumarin-modified MCM-41 with shorter wavelength UV light around 250 nm regenerates the coumarin monomer derivative by the photocleavage of

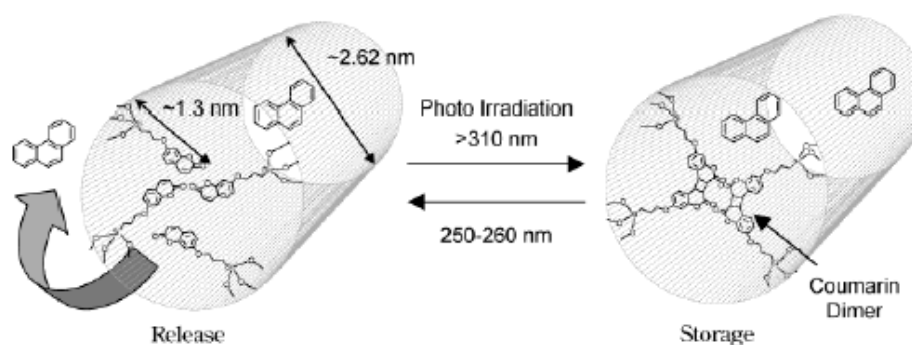


Figure 1.9 Photo-responsive delivery system based on coumarin modified mesoporous silica. (Reproduced with permission from ref. 45b copyright 2003 American Chemical Society).

cyclobutane dimer, and guest molecules included inside are released from the pore void (Figure 1. 9).

In addition to coumarin, photo-sensitive *o*-nitrobenzyl ester was also used in the construction of photo-responsive systems. For example, cyclodextrin(CD) was utilized by Kim *et al*⁴⁶ as cap to develop a CD-covered nanocontainer system with photocleavable *o*-nitrobenzyl ester linkers. Exposure of the hybrid materials to 350 nm UV light results in the photocleavage of *o*-nitrobenzyl and the release of the cargo. Later, same group found that the cyclodextrin gatekeepers on the surface of mesoporous silica can be hydrolyzed by α -amylase to release guest molecules from the porous reservoir (Figure 1.10).⁴⁷ The ester linkage in the stalk part of the cyclodextrin gatekeeper can also be cleaved by lipase to release guests from the channel. Combining the previous photo-sensitivity, the synergistic responsiveness in the controlled release of guest molecules by dual stimuli of enzyme and UV irradiation was demonstrated. Since CD has reversible supramolecular host-guest

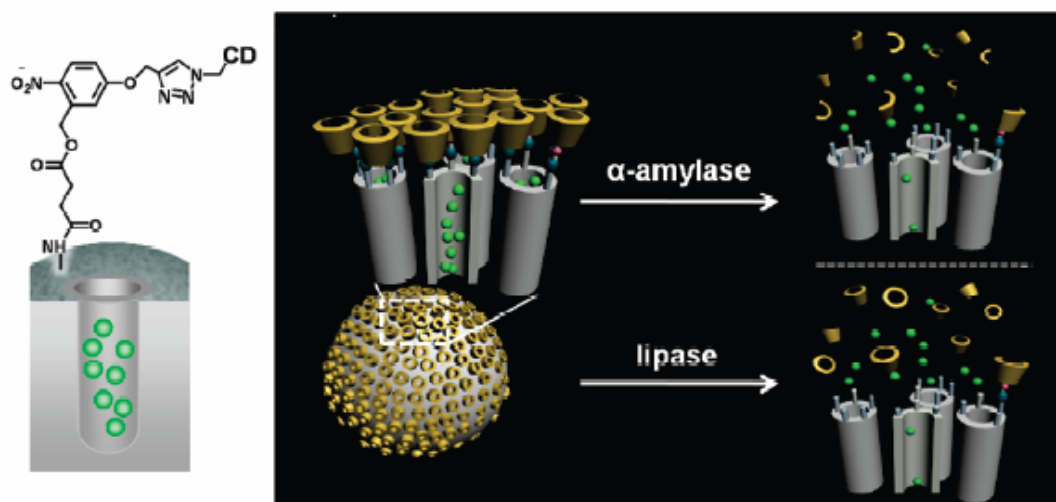
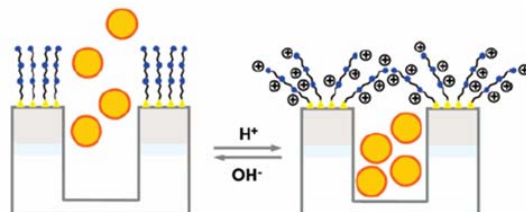


Figure 1.10 Schematic representation of dual responsive system based on CD-covered mesoporous silica through enzyme- and photo-cleavable linker. (Reproduced with permission from ref. 47 copyright 2009 American Chemical Society).

interaction⁴⁸, it can also be used as capping agent through supramolecular assembly, which will be discussed in next section.

Martinez-Manez *et al* developed a pH- and anion -controlled gate-like system by attaching oligoamine onto the surface of mesoporous silica to control the release of cargo molecules (Figure 1.11).⁴⁹ The pH-controlled “open-close” mechanism would arise from hydrogen-bonding interactions between amines (open-gate) and coulombic repulsion between ammonium groups (closed-gate). When protonated, the open-chain oligoamine in the external surface would adopt a rigid like conformation and would be pushed away toward the pore openings, leading to pore blockage that inhibits (complete or partially) the release of trapped molecules. The anion-controlled release was studied by monitoring the dye released from the pore voids at a certain pH in the

pH-control



Anion-control

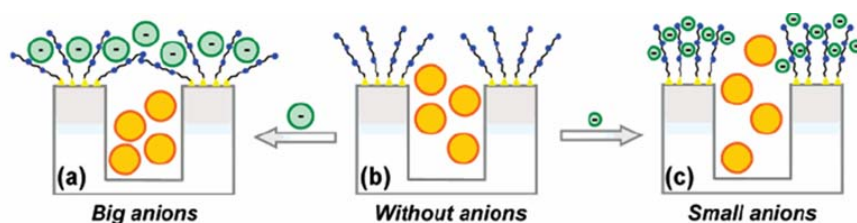


Figure 1.11 pH- and anion-controlled gate-like system by attaching oligoamine onto the surface of mesoporous silica. (Reproduced with permission from ref. 49 copyright 2008 American Chemical Society).

presence of a range of anions with different structural dimensions and charges, including chloride, sulfate, phosphate, and ATP. The choice of a certain anionic guest results in a different gate-like ensemble behavior, ranging from basically no action (chloride) to complete (ATP) or partial pore blockage, depending on the pH (sulfate and phosphate). The remarkable anion-controllable response of the gate-like ensemble can be explained in terms of anion complex formation with the tethered polyamines

In addition to organic molecules, Martinez-Manez *et al*⁵⁰ anchored hapten 4-(4-aminobenzenesulfonylamino) benzoic acid on the outer surface of the mesoporous support, which can be capped with a polyclonal antibody through suitable interaction between hapten and antibody. The opening protocol and delivery of the

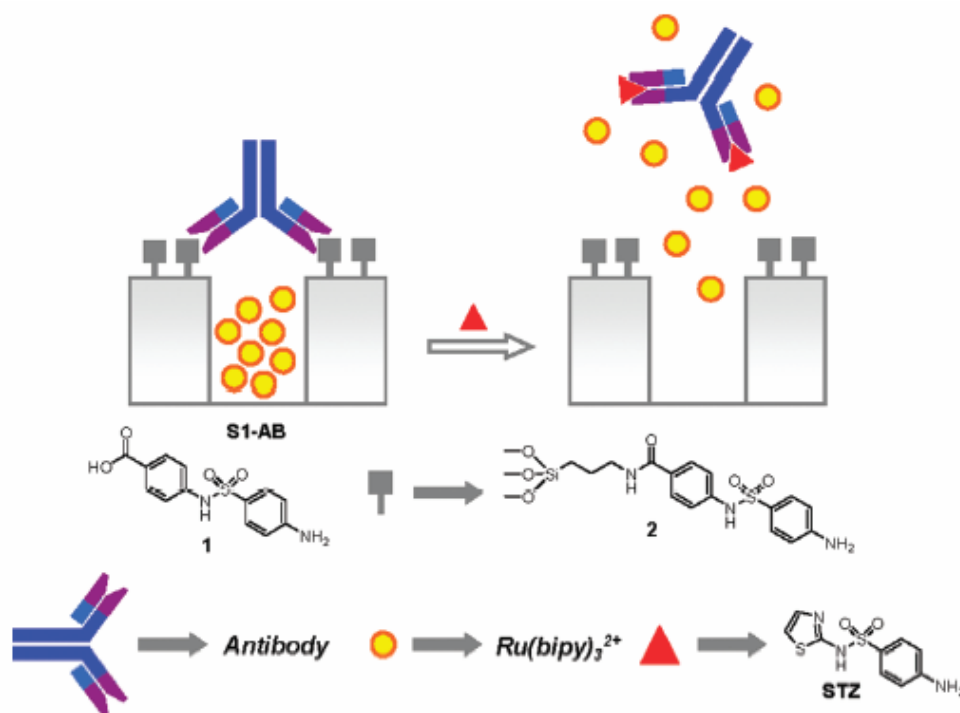


Figure 1.12 Antigen-responsive gate-like system by attaching antibody onto the surface of mesoporous silica. (Reproduced with permission from ref. 50 copyright 2009 American Chemical Society).

entrapped guest is related by a displacement reaction involving the presence in antigen to which the antibody is selective (Figure 1.12). They also synthesized lactose-capped mesoporous silica that is selectively uncapped using β -D-galactosidase by the rupture of a glycosidic bond.⁵¹ Cargo delivery is inhibited owing to the formation of a network of disaccharides linked by hydrogen bonding interactions around the pore outlets. Addition of β -D-galactosidase would result in the enzymatic hydrolysis of the glycosidic bond in the anchored lactose that induces a release of the galactose fragment, leaving only a glucose derivative anchored to the surface. The decrease in the size of the appended group would allow delivery of the entrapped dye.

Bein *et al*⁵² attached avidin to the outer surface of biotin-covered mesoporous silica

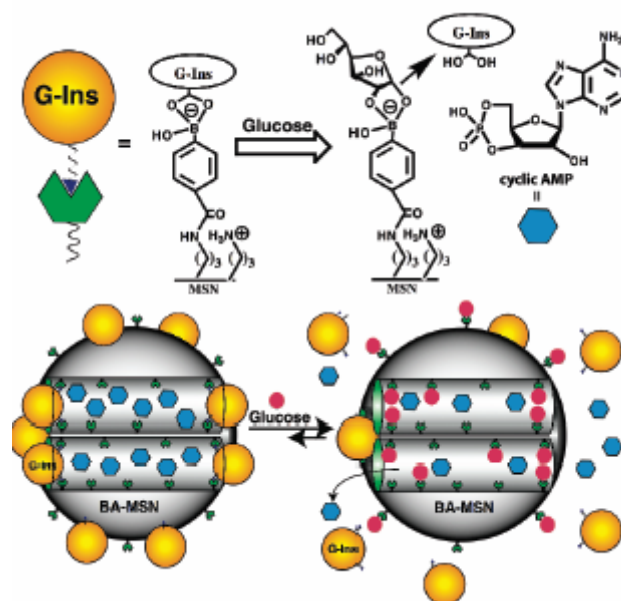


Figure 1.13 Schematic representation of the glucose-responsive mesoporous silica based delivery system for controlled release of bioactive G-Ins and cAMP (Reproduced with permission from ref. 53 copyright 2009 American Chemical Society)

through avidin-biotin interaction to prevent the uncontrolled leaching of incorporated guest molecules. Pore can be reopened based on the controlled enzymatic hydrolysis of the attached protein avidin. Lin *et al*⁵³ has also developed a dual-drug delivery system that is capable of delivering insulin and cyclic adenosine monophosphate (cyclic AMP), sequentially. Insulin is used to cap the pores of MCM-41 and is removed upon the introduction of glucose or other saccharides, through which process both insulin and cyclic AMP) are released (Figure1. 13).

1.4.2.3 Supramolecular assemblies as gatekeepers

A novel type of organic/inorganic hybrid materials with improved functionalities have been developed by combination of mesoporous silica materials as solid supports

and supramolecular assemblies as gatekeepers. Stoddart and Zink groups have successfully produced a series of mechanized mesoporous silica gel nanoparticles. Their seminal report consists of redox-controlled pseudorotaxanes attached to mesoporous silica, which can be switched on and off.⁵⁴ As shown in Figure 1.14, 1,5-dioxynaphthalene derivative (DNP) containing stalks attached to the silica surface, on which cyclobis-(paraquat-p-phenylene) (CBPQT⁴⁺) rings were threaded to prevent the trapped molecules from escaping. Upon the addition of an external reducing agent (NaBH₃CN), the CBPQT⁴⁺ rings are reduced and dissociated from the stalks. Following the same redox-controlled release approach, the authors improved their system by developing a reversible nanovalve (Figure 1.15).⁵⁵ The system consists of a stalk containing two electron-rich stations dioxynaphthalene and tetrathiafulvalene (DNP and TTF) and encircled by an electron-deficient ring (CBPQT⁴⁺). The higher interaction energy make the ring preferentially reside on the TTF station, which is located further away from the pore entrance. Upon oxidation with Fe(ClO₄)₃, the TTF station becomes positively charged, and the tetracationic CBPQT⁴⁺ ring migrates to the DNP station. As a result, the valve “closes”. The TTF²⁺ dication can then be reduced with ascorbic acid and re-encircled by the CBPQT⁴⁺ ring, and the trapped molecules can be released at will.

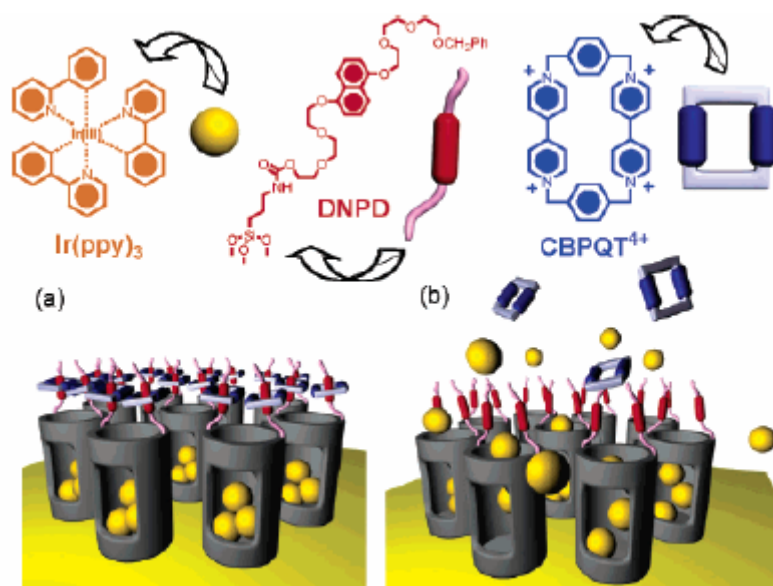


Figure 1.14 Schematic representation of redox-responsive supramolecular nanovalve. (Reproduced with permission from ref. 54 copyright 2004 American Chemical Society)

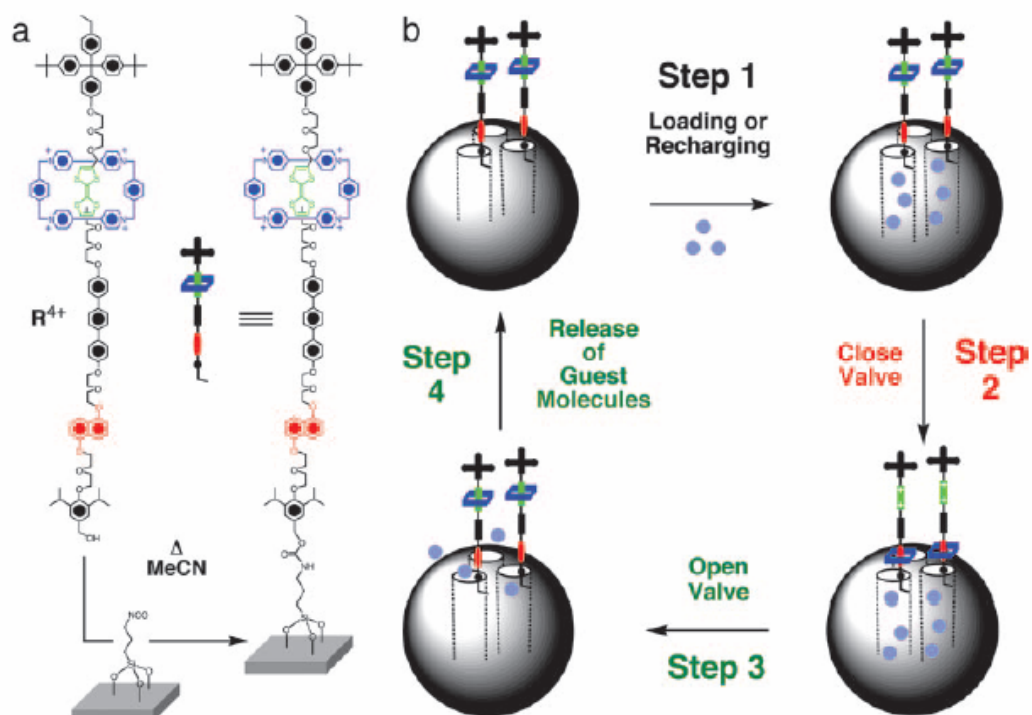


Figure 1.15 Schematic representation of reversible supramolecular nanovalve⁵⁵

Several pH-controlled nanovalves based on supramolecular assemblies have also been reported. For example, as shown in Figure 1.16, naphthalene-containing dialkylammonium threads were tethered to the MCM-41, followed by loading with coumarin 460 and capping with dibenzo[24]crown-8(DB24C8). DB24C8 is a sufficiently large macrocyclic polyether to be able to encircle dialkylammonium ion centers ($-\text{CH}_2\text{NH}_2^+\text{CH}_2-$), thus forming [2]pseudorotaxanes. The noncovalent bonding, $[\text{N}-\text{H}\cdots\text{O}]^+$ hydrogen bond, is responsible for the formation of these 1:1 complexes, which can be made to dissociate in solution on addition of base. Controlled release of coumarin 460 from the pores of MCM-41 was demonstrated using different bases.⁵⁶ Acid-sensitive nanovalve is prepared by anchoring stalk containing anilino group onto the pore entrance.⁵⁷ When the α -CD ring is complexed with the stalk at neutral pH, the bulky cyclic component is located near the pore openings, thereby blocking departure of cargo molecules that were loaded in the nanopores and hollow interior of the particle. Protonation of the nitrogen atoms at lower pH causes the binding affinity to decrease, releasing the α -CD and allowing the cargo molecules to escape (Figure 1.17). Kim *et al.* reported one novel pH-responsive pseudorotaxane-based MSNP system, which consists of polyethyleneimine (PEI) modified mesoporous silica and CD.⁵⁸ Guest molecules entrapped in the nanopores of mesoporous can be blocked by the surface-grafted pH-responsive PEI/CD polypseudorotaxanes. PEI polymer threads itself through α -CD or γ -CD and the formed complex inhibits the cargo transport from the nanopores as long as the PEI

polymer remains deprotonated (pH 11). By lowering the pH, the CDs can de-thread as a result of the weak interaction between the protonated PEI chain with the hydrophobic cavity of the CDs. β -CD does not show pH-responsive ability because PEI and β -CD did not form a stable polyseudorotaxane.

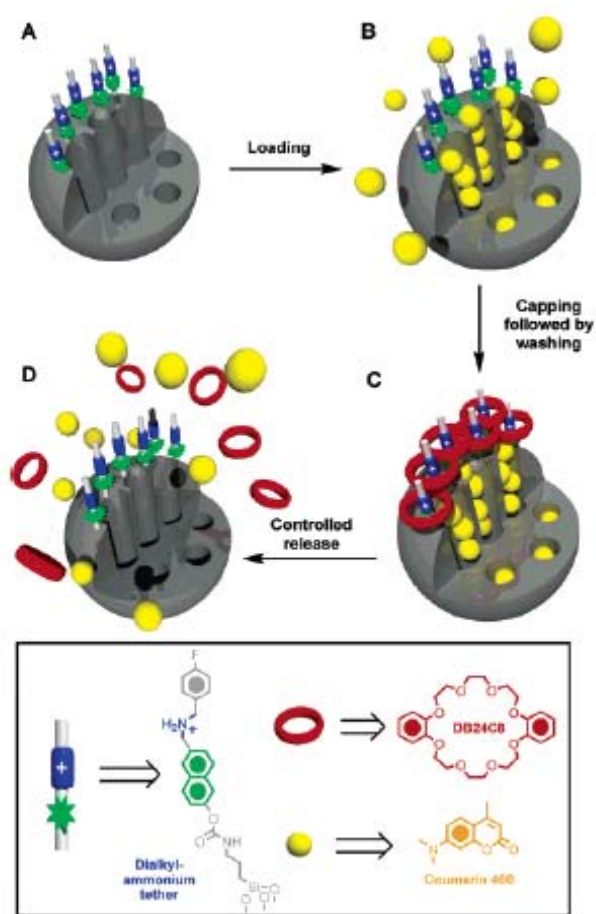


Figure 1.16 Schematic representation of pH-Responsive mesoporous silica with dibenzo[24]crown-8. (Reproduced with permission from ref. 56 copyright 2006 American Chemical Society)

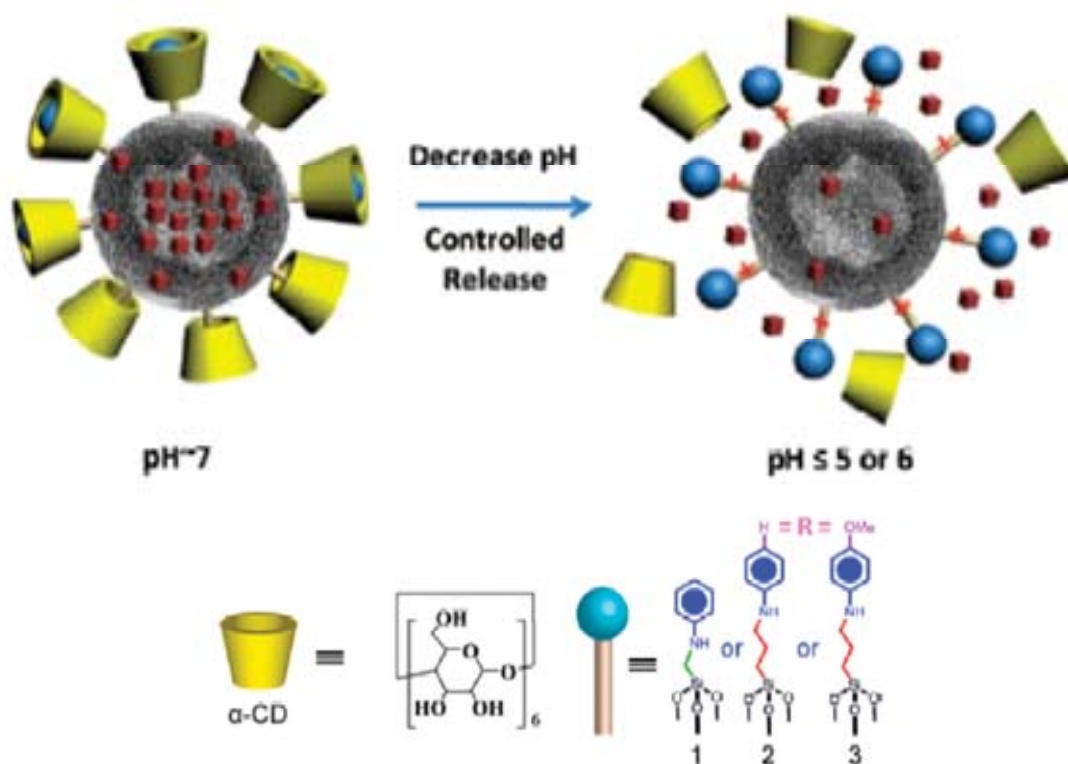


Figure 1.17 Schematic representation of pH-Responsive mesoporous silica with α -CD. (Reproduced with permission from ref. 57 copyright 2009 American Chemical Society)

Enzyme-responsive nanovalve in Figure 1. 18 shows that porcine liver esterase (PLE) catalyses the hydrolysis of adamantyl ester stoppers, resulting in de-threading of the α -CD rings, leading to the release of the cargo molecules from the nanopores.⁵⁹ As a control, no release is observed using adamantyl amide stopper, which does not undergo hydrolysis by PLE. Remote activation of stopper has been achieved by taking advantage of the high affinity of β -CD for *trans*-azobenzene. Irradiation of the azobenzene stalks with 351 nm light induces isomerisation from the *trans* to *cis* geometry, of which binding ability is significantly reduced, caused the β -CD caps to de-thread from the stalks and, as a result, the cargo is released from nanopores (Figure 1. 19).⁶⁰

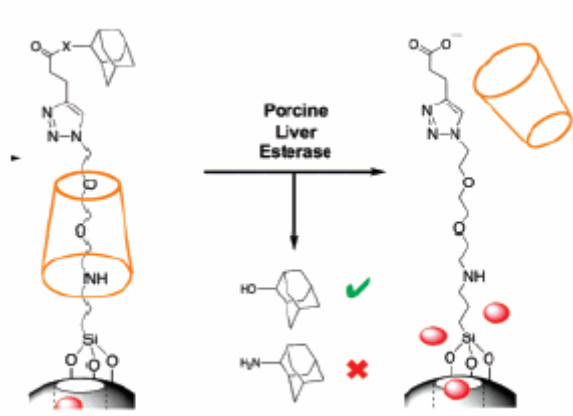


Figure 1.18 Schematic representation of enzyme-responsive snap-top mesoporous silica (Reproduced with permission from ref. 59 copyright 2008 American Chemical Society)

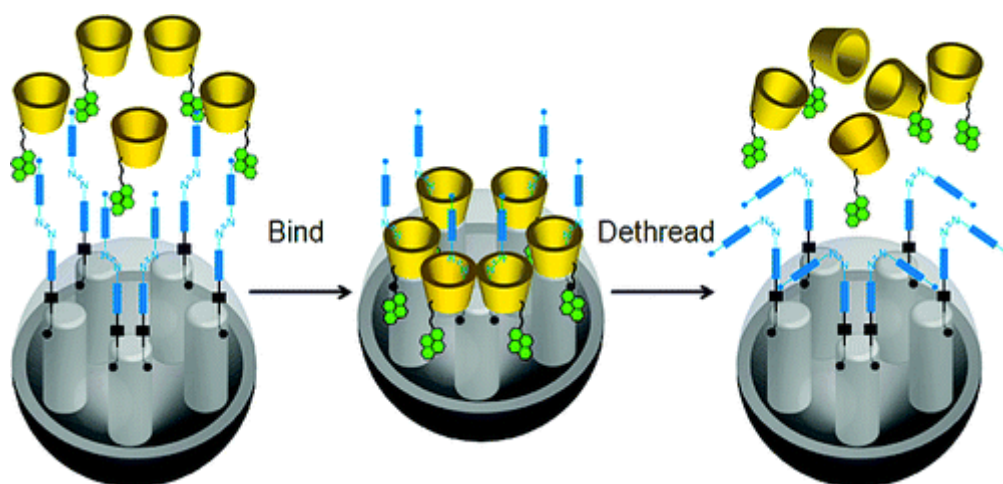


Figure 1.19 Schematic representation of light-responsive mesoporous silica based on azobenzene and β -CD. (Reproduced with permission from ref. 60 copyright 2009 American Chemical Society)

1.4.2.4 Polymer and dendrimer as gatekeepers

Xiao *et al*⁶¹ designed a pH-responsive carrier by oppositely charged ionic interaction between carboxylic acid modified SBA-15 and polycation (poly(dimethyldiallylammonium chloride)). Active molecules such as vancomycin can be stored at neutral pH and release from the pore voids of SBA-15 at acidic pH, in

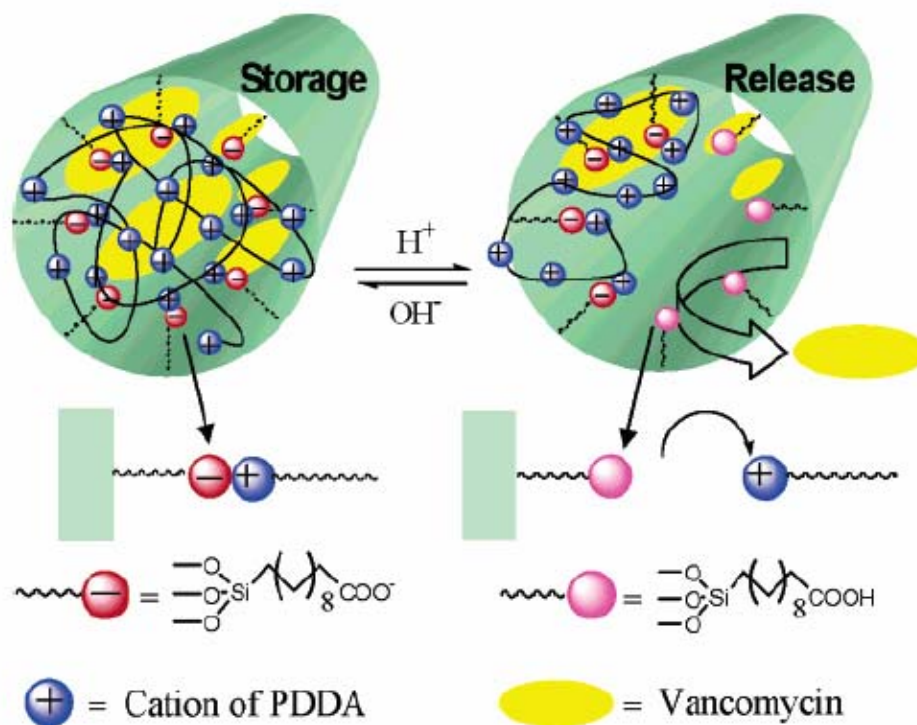


Figure 1.20 Schematic representation of pH-responsive drug delivery system based on the interaction between negative carboxylic acid modified SBA-15 silica rods with polycations (PDDA) (Reproduced with permission from ref. 61 copyright 2005 American Chemical Society)

which ionized carboxylic acid groups are protonated and the polycations are detached from the surface (Figure 1. 20).

Shi *et al*⁶² proposed a strategy to combine the advantages of mesoporous silica spheres with a 3D pore network and polyelectrolyte multilayers with a stimuli-responsive property. The system consists of mesoporous silica spheres with an average sphere diameter of 300-400 nm and polyelectrolyte multilayer coatings (sodium polystyrene sulfonate (PSS) and the polycation poly(allylamine hydrochloride) (PAH)) (PAH/PSS) with an average thickness of 14 nm. A simple sustained-release pattern was observed in the system without polyelectrolyte

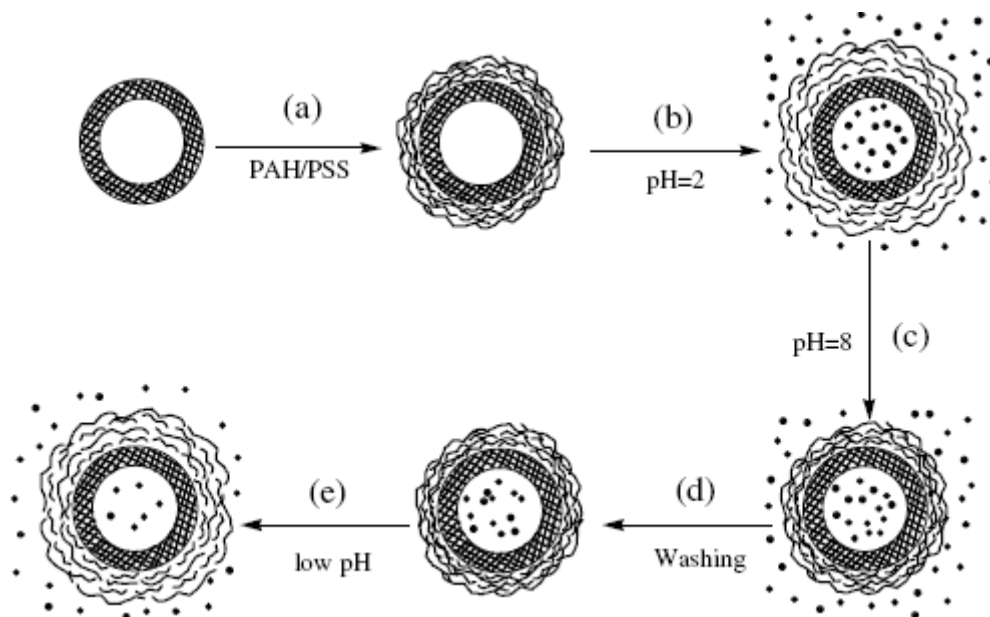


Figure 1.21 Schematic representation of pH-responsive drug delivery system based on polyelectrolyte multilayer coated mesoporous silica sphere (Reproduced with permission from ref. 62b copyright 2007 Elsevier).

multilayer coating while stimuli-responsive controlled-release was observed in polyelectrolyte multilayer coated system and drug release rate from the hybrid system can be well-controlled by changing the pH value (or the salt concentration) of the release medium (Figure 1. 21).

Poly(*N*-isopropylacrylamide) (PNIPAm) can undergo a conformational change in response to variations in temperature.⁶³ When heated in water above 33°C, it undergoes a reversible lower critical solution temperature (LCST) phase transition from a swollen hydrated state to a shrunken dehydrated state. (Figure 1.22a) Lopez *et al*⁶⁴ prepared hybrids PNIPAM-mesoporous silica by atom transfer radical polymerization (ATRP) of the NIPAM monomer from the surface of calcined MCM-41. Thermo-responsive polymers are encapsulated within the pores of

MCM-41, acting to reduce small molecule diffusion when in the open coil configuration below LCST while facilitating diffusion in the globule conformation by effectively retreating to the pore walls above LCST. Later, Brock *et al*⁶⁵ grafted poly(*N*-isopropylacrylamide) onto the external surface of MCM-41. In their system, above LCST, the polymer forms “stoppers” that prevent uptake and release, whereas below this temperature, the random coil conformation permits diffusion into and out of the pores (Figure 1.22b).

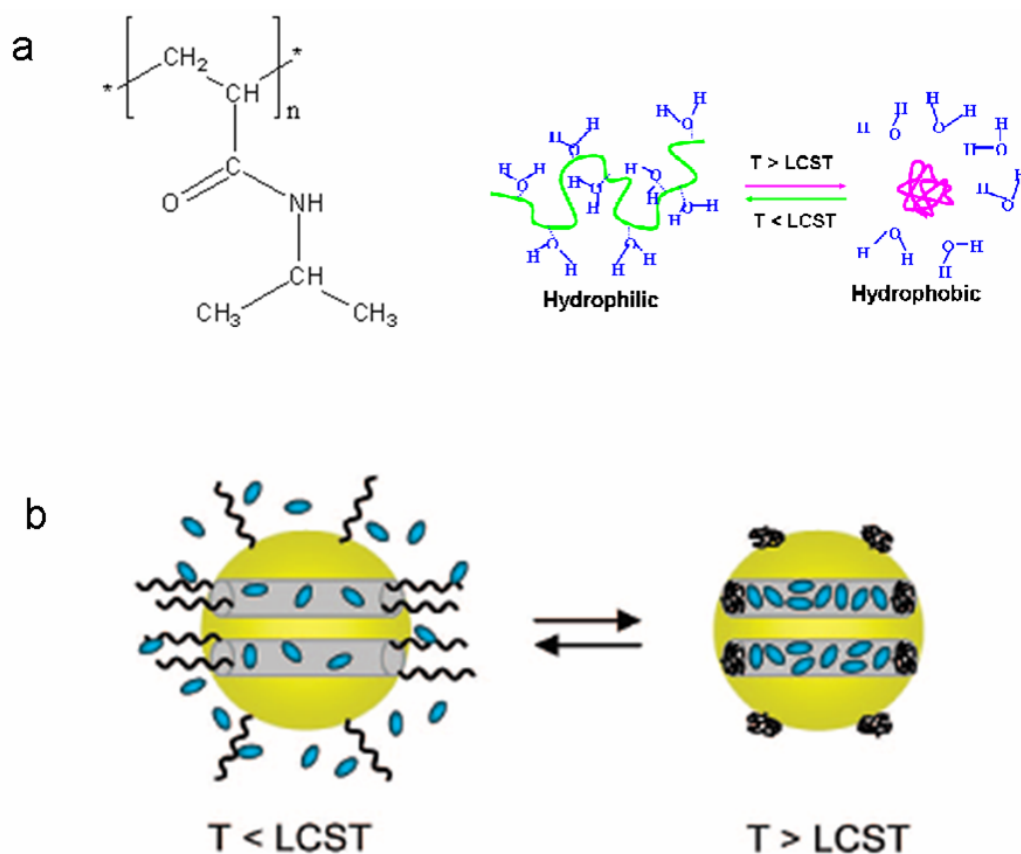


Figure 1.22 a) Schematic of thermo-responsive polymer poly(*N*-isopropylacrylamide) response with temperature. b) thermo-responsive release system based on poly(*N*-isopropylacrylamide) coated mesoporous silica. (Reproduced with permission from ref. 65 copyright 2008 American Chemical Society)

Pan *et al* anchored poly(acrylic acid) and poly(2-(diethylamino)ethyl methacrylate) onto the exterior surface of mesoporous silica by reversible addition-fragmentation chain transfer(RAFT) polymerization and atom transfer radical polymerization (ATRP), respectively.^{66,67} The obtained two hybrid materials show different pH-responsive property based on charge ability and conformation state at different pHs.

Dendrimer-capped mesoporous silica gene transfection system has been synthesized using a generation 2 poly(amidoamine) dendrimer (G2-PAMAM). This system could be used as both drug delivery and gene transfection agent(Figure 1.23).⁶⁸ G2-PAMAM onto mesoporous silica alter the surface charge property to be positive and bind electrostatically to a plasmid DNA vector encoding for enhanced green fluorescence protein (EGFP). G2-PAMAM–MSN protects efficiently the plasmid DNA against the digestion and successful delivery the plasmid to the cell nucleus.

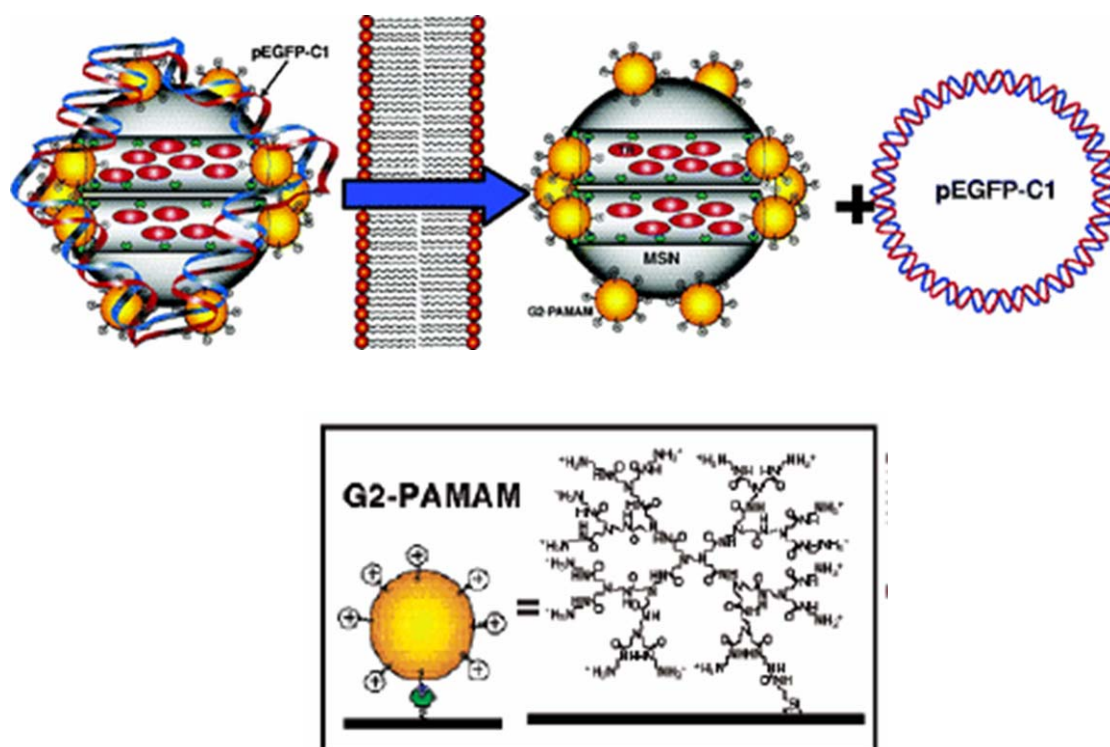


Figure 1.23 Delivery of DNA plasmid pEGFP-C1 in cells *via* a second generation PAMAM-functionalised mesoporous silica. (Reproduced with permission from ref. 68 copyright 2004 American Chemical Society)

1.5 Ordered mesoporous materials in catalysis

Since Mobil scientists prepared a family of ordered mesoporous silicas (OMS) in 1992, mesoporous materials have been the focus of great interest due to their high surface areas, tunable pore sizes and surface property are among the desirable properties that made OMS highly attractive in catalysis, separation, adsorption and sensing. For catalytic applications, a large variety of materials have been prepared by introducing catalytically active species into mesoporous silica, either incorporated into the framework or supported on the surface. For example, the acidity can be generated by atomic substitution⁶⁹ or by grafting organic functional groups onto the

surface of mesoporous solids⁷⁰. Metal, metal oxide or metal cluster can also be encapsulated into the pore of OMS by ion-exchange, impregnation, adsorption and post-synthesis⁷¹. All these materials are widely studied in catalytic applications such as alkylation, polymerization or biocatalysis.⁷¹

Combining chemical inertness, biocompatibility, and thermal stability, mesoporous carbon materials are thus suitable for many different applications. In addition to silica mesoporous materials, functionalized mesoporous carbons have also been examined as heterogeneous catalysts in the past decade. Ordered mesoporous carbon(OMC) containing molecular-level dispersed Pd clusters in the carbon walls was synthesized by Schüth *et al.*⁷² They coated the wall of SBA-15 with polyacrylonitrile, which provided anchoring sites for the adsorption of Pd cations, followed by carbonization of the composite and removal of silica. Confined/stabilized by the carbon framework and the silica walls, Pd clusters do not grow during pyrolysis. In the oxidation of various alcohols to aldehydes, the obtained Pd-OMC show the selectivity to the corresponding aldehyde higher than 99% and a high activity was maintained over multiple runs.

An alternate method of forming metal nanoparticles within mesoporous carbon channels involves a surfactant-assisted microwave synthesis. A small amount of cationic surfactant, cetyltrimethylammonium bromide(CTAB) could greatly improve the wettability of mesoporous carbon support as well as the dispersion of Pt nanoparticles. The highly dispersed Pt nanoparticles exhibited a high catalytic activity

for hydrogen electro-oxidation.⁷³

Pt catalysts supported on mesoporous carbons (CMK-1 and CMK-3) significantly outperform their counterparts supported on activated carbon in biphasic conversion of nitrobenzene to p-aminophenol. These enhancements in activity are believed to be a consequence of an increased metal dispersion and a concurrent reduction in pore diffusion resistance in the mesoporous structure of CMK-1 and CMK-3.⁷⁴

In addition to being an efficient metal-catalyst support, mesoporous carbon can be a useful support for organic acid catalysis. For example, mesoporous carbon was synthesized after pyrolysis of expanded starch and subsequently functionalized with sulfonated groups, providing highly active and reusable materials in various acid catalyzed reactions, including esterification of diacids, liquid phase acylation of alcohols, and alkylation of aromatic substrates.⁷⁵

1. 6 Summary and Outlook

Due to the unique structural features, such as different compositions, controllable pore geometry and pore size, and tunable surface functionalities, ordered mesoporous materials have attracted extensive research attention in the past two decades. The combination of ordered mesoporous materials with the extensive experience gathered in other research areas would allow the design of various advanced materials for diverse applications.

1.7 References

1. Sing, K. S. W.; Everett, D. H.; Haul, R. A. W.; Moscou, L.; Pierotti, R. A.; Rouquerol, J.; Siemieniewska, R. *Pure Appl. Chem.* **1985**, *57*, 603.
2. (a) Kresge, C. T.; Lonowicz, M. E.; Roth, W. J.; Vartuli, J. C.; Beck, J. S. *Nature* **1992**, *359*, 710. (b) Beck, J. S.; Vartuli, J. C.; Roth, W. J.; Lonowicz, M. E.; Kresge, C. T.; Schmitt, K. T.; Chu, C. T.-W.; Olson, D. H.; Sheppard, E. W.; McCullen, S. B.; Higgins, J. B.; Schlenker, J. L. *J. Am. Chem. Soc.* **1992**, *114*, 10834.
3. Hatton, B., Landskron, K., Whitnall, W., Perovic, D., and Ozin, G. A. *Acc. Chem. Res.* **2005**, *38*, 305.
4. Vartuli, J. C.; Schmitt, K. D.; Kresge, C. T. *Chem. Mater.* **1994**, *6*, 2317.
5. Dubois, M.; Gulik-Krzywicki, T. H.; Cabane, B. *Langmuir* **1993**, *9*, 673.
6. (a) Zhao, D.; Huo, Q.; Feng, J.; Chmelka, B. F.; Stucky, G. D. *J. Am. Chem. Soc.* **1998**, *120*, 6024. (b) Zhao, D.; Feng, J.; Huo, Q.; Melosh, N.; Fredrikson, G.; Chmelka, B.; Stucky, G. D. *Science* **1998**, *279*, 548.
7. Ryoo, R.; Joo, S. H.; Jun, S. *J. Phys. Chem. B* **1999**, *103*, 7743.
8. Ju, S.; Joo, S. H.; Ryoo, R.; Kruk, M.; Jaroniec, M.; Liu, Z.; Ohsuna, T.; Terasaki, O. *J. Am. Chem. Soc.* **2000**, *122*, 10712.
9. (a) Kruk, M.; Jaroniec, M.; Koo, C. H.; Ryoo, R. *Chem. Mater.* **2000**, *12*, 1961. (b) Göltner, C. G.; Smarsly, B.; Berton, B.; Antonietti, M. *Chem. Mater.* **2001**, *13*, 1617. c) Hartmann, M.; Vinu, A. *Langmuir* **2002**, *18*, 8010.
10. (a) Zhang, F. Q.; Meng, Y.; Gu, D.; Yan, Y.; Yu, C. Z.; Tu, B.; Zhao, D. Y. *J. Am. Chem. Soc.* **2005**, *127*, 13508. (b) Meng, Y.; Gu, D.; Zhang, F. Q.; Shi, Y. F.; Yang, H. F.; Li, Z.; Yu, C. Z.; Tu, B.; Zhao, D. Y. *Angew. Chem., Int. Ed.* **2005**, *44*, 7053.
11. (a) Huo, Q.; Leon, R.; Petroff, P. M.; Stucky, G. D. *Science* **1995**, *268*, 1324. (b) Huo, Q.; Margolese, D. I.; Stucky, G. D. *Chem. Mater.* **1996**, *8*, 1147.
12. (a) Lu, Y.; Ganguli, R.; Drewien, C. A.; Anderson, M. T.; Brinker, C. J.; Gong, W.; Guo, Y.; Soyez, H.; Dunn, B.; Huang, M. H.; Zink, J. I. *Nature* **1997**, *389*, 364. (b) Brinker, C. J.; Lu, Y.; Sellinger, A.; Fan, H. *Adv. Mater.* **1999**, *11*, 579. (c) Grosso,

- D.; Cagnol, F.; Soler-Illia, G. J. A. A.; Crepaldi, E. L.; Amenitsch, H.; Brunet-Bruneau, A.; Bourgeois, A.; Sanchez, C. *Adv. Funct. Mater.* **2004**, 14, 309.
13. (a) Yang, H.; Coombs, N.; Sokolov, I.; Ozin, G. *Nature* **1996**, 381, 589. (b) Brown, A.S.; Holt, S.A.; Dam, T.; Trau, M.; White, J.W. *Langmuir* **1997**, 13, 6363.
14. Schacht, S.; Huo, Q.; Voigt-Martin, I. G.; Stucky, G.D.; Schüth, F. *Science* **1996**, 273, 768.
15. Trewyn, B. G.; Whitman, C. M.; Lin, V. S. Y. *Nano Lett.* **2004**, 4, 2139.
16. (a) Huh, S.; Wiench, J. W.; Yoo, J.-C.; Pruski, M.; Lin, V. S. Y. *Chem. Mater.* 2003, 15, 4247. (b) Huh, S.; Wiench, J. W.; Trewyn, B. G.; Song, S.; Pruski, M.; Lin, V. S. Y. *Chem. Commun.* **2003**, 18, 2364.
17. Feng, P.; Bu, H.; Stucky, G. D.; Pine, D. J. *J. Am. Chem. Soc.* **2000**, 122, 994.
18. Yang, H. F.; Shi, Q. H.; Tian, B. Z.; Xie, S. H.; Zhang, F. Q.; Yan, Y.; Tu, B.; Zhao, D. Y. *Chem. Mater.* **2003**, 15, 536.
19. (a) Blin, J.; Su, B. *Langmuir* **2002**, 18, 5303. (b) Sun, J.; Zhang, H.; Ma, D. Chen, Y. Bao, X. Klein-Hoffmann, A. Pfänder, N.; Su, D. S. *Chem. Commun.* **2005**, 5343.
20. Lee, J. S.; Joo, S. H.; Ryoo, R. *J. Am. Chem. Soc.* **2002**, 124, 1156.
21. (a) Vinu, A.; Hossain, K. Z.; Ariga, K. *J. Nanosci. Nanotech.* **2005**, 5, 347. (b) Luan, Z.; Fournier, J. A.; Wooten, J. B.; Miser, D. E. *Micropor. Mesopor. Mater.* **2005**, 83, 150. (c) Anwender, R. *Chem. Mater.* **2001**, 13, 4419. (d) Yokoi, T.; Yoshitake, H.; Tatsumi, T. *J. Mater. Chem.* **2004**, 14, 951.
22. (a) Wang, X.; Lin, K. S. K.; Chan, J. C. C.; Cheng, S. *J. Phys. Chem. B* **2005**, 109, 1763. (b) Wang, Y. Q.; Yang, C. M.; Zibrowius, B.; Spliethoff, B.; Linden, M.; Schuth, F. *Chem. Mater.* **2003**, 15, 5029. (c) Wang, Y. Q. Zibrowius, B. Yang, C. M. Spliethoff, B. Schuth, F. *Chem. Commun.* **2004**, 15, 46.
23. (a) Asefa, T.; MacLachlan, M. J.; Coombs, N.; Ozin, G. A. *Nature* **1999**, 402, 867. (b) Inagaki, S.; Guan, S.; Fukushima, Y.; Ohsuna, T.; Terasaki, O. *J. Am. Chem. Soc.* **1999**, 121, 9611. (c) Melde, B. J.; Holland, B. T.; Blanford, C. F.; Stein, A. *Chem. Mater.* **1999**, 11, 3302.
24. (a) Price, B. K.; Hudson, J. L.; Tour, J. M. *J. Am. Chem. Soc.* **2005**, 127, 14867. (b)

- Dyke, C. A.; Stewart, M. P.; Maya, F.; Tour, J. M. *Synlett* **2004**, 155. (c) Dyke, C. A.; Tour, J. M. *J. Am. Chem. Soc.* **2003**, 125, 1156. (d) Bahr, J. L.; Yang, J. P.; Kosynkin, D. V.; Bronikowski, M. J.; Smalley, R. E.; Tour, J. M. *J. Am. Chem. Soc.* **2001**, 123, 6536.
25. (a) Li, Z. J.; Yan, W. F.; Dai, S. *Langmuir* **2005**, 21, 11999. (b) Li, Z. J.; Dai, S. *Chem. Mater.* **2005**, 17, 1717.
26. Li, Z. J.; Del Cul, G. D.; Yan, W. F.; Liang, C. D.; Dai, S. *J. Am. Chem. Soc.* **2004**, 126, 12782.
27. Slowing, I. I.; Vivero-Escoto, J. L.; Wu, C.-W.; Lin, V. S.-Y. *Adv. Drug Delivery Rev.* **2008**, 60, 1278.
28. Vallet-Regí, M.; Rámila, A.; del Real, R. P.; Pérez-Pariente, J. *Chem. Mater.* **2001**;13, 308.
29. Doadrio, J. C.; Sousa, E. M. B.; Izquierdo-Barba, I.; Doadrio, A. L.; Perez-Pariente, J.; Vallet-Regí, M. *J. Mater. Chem.* **2006**,16, 462.
30. Izquierdo-Barba, I., Martinez, A., Doadrio, A. L., Perez-Pariente, J.; Vallet-Regí, M. *Eur. J. Pharm. Sci.* **2005**, 26, 365.
31. Vallet-Regí, M., Doadrio, J. C., Doadrio, A. L., Izquierdo-Barba, I., and Perez-Pariente, *J. Solid State Ionics* **2004**, 172, 435.
32. Doadrio, A. L., Sousa, E. M. B., Doadrio, J. C., Pariente, J. P., Izquierdo-Barba, I., and Vallet-Regí, M. *J. Controlled Release* **2004**, 97, 125.
33. Horcajada, P.; Rámila, A.; Perez-Pariente, J.; Vallet-Regí, M. *Micropor. Mesopor. Mater.* **2004**, 68, 105.
34. Vallet-Regí, M.; Balas, F.; Colilla, M.; Manzano, M. *Drug Metab.Lett.* **2007**, 1, 37.
35. Munoz, B.; Rámila, A.; Perez-Pariente, J.; Dí az, I.; Vallet-Regí, M. *Chem. Mater.* **2003**, 15, 500.
36. Song, S. W.; Hidajat, K.; Kawi, S. *Langmuir* **2005**, 21, 9568.
37. Balas, F.; Manzano, M.; Horcajada, P.; Vallet-Regí, M. *J. Am. Chem. Soc.* **2006**, 128, 8116.

38. Doadrio, J. C.; Sousa, E. M. B.; Izquierdo-Barba, I.; Doadrio, A. L. Perez-Pariente, J. Vallet-Regí, M. *J. Mater. Chem.* **2006**, 16, 462.
39. Qu, F.; Zhu, G.; Huang, S.; Li, S.; Qiu, S. *ChemPhysChem* **2006**, 7, 400.
40. Tang, Q.; Xu, Y.; Wu, D.; Sun, Y. *Chem. Lett.* **2006**, 35, 474.
41. Lai, C.-Y.; Trewyn, B. G.; Jeftinija, D. M.; Jeftinija, K.; Xu, S.; Jeftinija, S.; Lin, V. S. Y. *J. Am. Chem. Soc.* **2003**, 125, 4451.
42. Giri, S.; Trewyn, B. G.; Stellmaker, M. P.; Lin, V. S. Y. *Angew. Chem., Int. Ed.* **2005**, 44, 5038.
43. Vivero-Escoto, J. L.; Slowing, I. I.; Wu, C.; Lin, V. S.-Y. *J. Am. Chem. Soc.* **2009**, 131, 3462.
44. Aznar, E.; Marcos, M. D.; Martinez-Manez, R.; Sancenon, F.; Soto, J.; Amoro, P.; Guillem, P. *J. Am. Chem. Soc.* **2009**, 131, 6833.
45. (a) Mal, N. K.; Fujiwara, M.; Tanaka, Y. *Nature* **2003**, 421, 350. (b) Mal, N. K. Fujiwara, M.; Tanaka, Y.; Taguchi, T.; Matsukata, M. *Chem. Mater.* 2003, 15, 3385.
46. Park, C.; Lee, K.; Kim, C. *Angew. Chem., Int. Ed.* **2009**, 48, 1275.
47. Park, C.; Kim, H.; Kim, S.; Kim, C. *J. Am. Chem. Soc.* **2009**, 131, 16614.
48. Harada, A. *Acc. Chem. Res.*, **2001**, 34, 456.
49. Casaus, R.; Climent, E.; Marcos, M. D.; Martinez-Manez, R.; Sancenon, F.; Soto, J.; Amoros, P.; Cano, J.; Ruiz, E. *J. Am. Chem. Soc.* **2008**, 130, 1903.
50. Climent, E.; Bernardos, A.; Martinez-Manez, R.; Maquieira, A.; Marcos, M. D.; Pastor-Navarro, N.; Puchades, R.; Sancenon, F.; Soto, J.; Amoros, P. *J. Am. Chem. Soc.* **2009**, 131, 14075.
51. Bernardos, A.; Aznar, E.; Marcos, M. D.; Martinez-Manez, R.; Sancenon, F.; Soto, J.; Barat, J. M.; Amoros, P. *Angew. Chem., Int. Ed.* **2009**, 48, 5884.
52. Schlossbauer, A.; Kecht, J.; Bein, T. *Angew. Chem., Int. Ed.* **2009**, 48, 3092.
53. Zhao, Y.; Trewyn, B. G.; Slowing, I. I.; Lin, V. S. Y. *J. Am. Chem.*

- Soc.* **2009**, 131, 8398.
54. Hernandez, R.; Tseng, H.-R.; Wong, J. W.; Stoddart, J. F.; Zink, J. I. *J. Am. Chem. Soc.* **2004**, 126, 3370.
55. Nguyen, T. D.; Tseng, H.-R.; Celestre, P. C.; Flood, A. H.; Liu, Y.; Stoddart, J. F.; Zink, J. I. *Proc. Natl. Acad. Sci. U.S.A.* **2005**, 102, 10029.
56. Nguyen, T. D.; Leung, K. C. F.; Liong, M.; Pentecost, C. D.; Stoddart, J. F.; Zink, J. I. *Org. Lett.* **2006**, 8, 3363.
57. Du, L., Liao, S., Khatib, H. A., Stoddart, J. F., and Zink, J. I. *J. Am. Chem. Soc.* **2009**, 131, 15136.
58. Park, C.; Oh, K.; Lee, S.; Kim, C. *Angew. Chem., Int. Ed.* **2007**, 46, 1455.
59. Patel, K.; Angelos, S.; Dichtel, W. R.; Coskun, A.; Yang, Y.-W.; Zink, J. I.; Stoddart, J. F. *J. Am. Chem. Soc.* **2008**, 130, 2382.
60. Ferris, D. P.; Zhao, Y.; Khashab, N. M.; Khatib, H. A.; Stoddart, J. F.; Zink, J. I. *J. Am. Chem. Soc.* **2009**, 131, 1686.
61. Yang, Q., Wang, S., Fan, P., Wang, L., Di, Y., Lin, K.; Xiao, F.-S. *Chem. Mater.* **2005**, 17, 5999.
62. (a) Zhu, Y.; Shi, J.; Shen, W.; Dong, X.; Feng, J.; Ruan, M.; Li, Y. *Angew. Chem., Int. Ed.* **2005**, 44, 5083. (b) Zhu, Y.; Shi, J. *Micropor. Mesopor. Mater.* **2007**, 103, 243.
63. Alarcon, C. D. H.; Pennadam, S.; Alexander, C. *Chem. Soc. Rev.* **2005**, 34, 276.
64. Fu, Q.; Rao, G. V. R.; Ista, L. K.; Wu, Y.; Andrzejewski, B. P.; Sklar, L. A.; Ward, T. L.; Lopez, G. P. *Adv. Mater.* **2003**, 15, 1262.
65. You, Y. Z.; Kalebaila, K. K.; Brock, S. L.; Oupicky, D. *Chem. Mater.* **2008**, 20, 3354.
66. Hong, C.-Y.; Li, X.; Pan, C.-Y. *J. Mater. Chem.* **2009**, 19, 5155.
67. Sun, J.-T.; Hong, C.-Y.; Pan, C.-Y. *J. Phys. Chem. C* **2010**, 114, 1248.
68. Radu, D. R.; Lai, C.-Y.; Jeftinija, S.; Lin, V. S.-Y. *J. Am. Chem.*

- Soc.* **2004**, 126, 13216.
69. Sayari, A. *Chem. Mater.* **1996**, 8, 1840.
70. Van Rhijin, W. M.; De Vos, D. E.; Sels, B. F.; Bossaert, W. D.; Jacobs, P. A. *Chem. Commun.* **1998**, 317.
71. Trong On, D.; Desplantier-Giscard, D.; Danumah, C.; Kaliaguine, S. *Appl. Catal. A.* **2001**, 222, 299.
72. Lu, A.-H.; Li, W.-C.; Hou, Z.; Schüth, F. *Chem. Commun.* **2007**, 1038.
73. Zhou, J. H.; He, J. P.; Ji, Y. J.; Dang, W. J.; Liu, X. L.; Zhao, G. W.; Zhang, C. X.; Zhao, J. S.; Fu, Q. B.; Hu, H. P. *Electrochim. Acta* **2007**, 52, 4691.
74. Min, K.-I.; Choi, J.-S.; Chung, Y.-M.; Ahn, W.-S.; Ryoo, R.; Lim, P. K. *Appl. Catal. A* **2008**, 337, 97.
75. Budarin, V. L.; Clark, J. H.; Luque, R.; Macquarrie, D. J. *Chem. Commun.* **2007**, 634.

Chapter Two

Responsive Polymer Coated Mesoporous Silica as pH-sensitive Nanocarrier for Controlled Release

2.1 Introduction

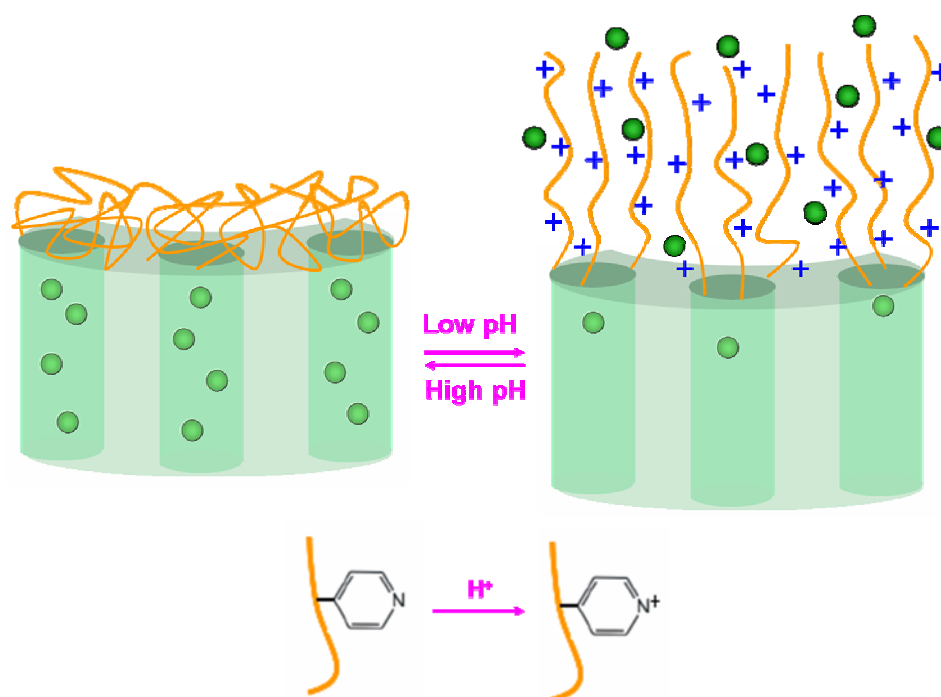
The ability to trap and release molecules from mesoporous silica nanoparticles holds promise in sensor and drug delivery applications.¹ The great diversity in surface functionalization of mesoporous silica offers a unique advantage in construction of nanogates responsive to different stimuli. Various types of nanoparticles², organic molecules³ and biomolecules⁴ have been used as capping agents to block molecule transport from silica mesopore and to unlock the entrance for triggered release under specific external stimuli. Combination of mesoporous silica with functional polymers generates a novel type of hybrid nano-switch that takes advantage of the unique features of polymers and porous materials. Thermosensitive Poly(*N*-isopropylacrylamide) was coated on mesoporous silica by atom transfer radical polymerization(ATRP) and can control the molecule release at different temperatures.⁵ Poly(acrylic acid) was grafted onto the exterior surface of mesoporous silica by reversible addition-fragmentation chain transfer(RAFT) polymerization and works as a smart nanovalve sensitive to pH changes.⁶ Poly(2-(diethylamino)ethyl methacrylate) was also anchored on mesoporous silica by ATRP for pH-controlled release.⁷ Our group introduced cross-linkable polymer into mesoporous silica release system and prepared a new type of versatile responsive system.⁸ The pore of guest

molecules loaded silica materials are blocked by the addition of cystamine, a disulfide-based bifunctional primary amine, which allows polymer chains around the silica surface to be cross-linked. The polymeric network thus formed around the pore opening can be reopened by cleaving the disulfide bond of cystamine in the presence of disulfide reducing agents such as dithiothreitol (DTT), leading to the redox-controlled release.^{8(a)} The cyclodextrins are further introduced into the polymer network and expand responsive diversity by photoirradiation, redox signal, and competitive supramolecular binding.^{8(b)}

Most reported polymer-mesoporous silica hybrid materials use “grafting from” method and involve complicated polymerization on surface. Here, we use a simple “grafting to” method to facilely modify silica surface with responsive polymer to fabricate a novel type of pH-sensitive controlled release materials. The responsive polymer used here is commercially available poly(4-vinyl pyridine) (PVP). PVP has been widely used in the construction of responsive colloid and surface systems due to its pH-triggered switching ability. For example, PVP-brush-functionalized ITO electrode allowed the reversible transition of the electrode interface between the active and inactive states due to the reversible restructuring of the polymer brush induced by the local interfacial pH changes.⁹ PVP has also been used to direct reversible formation of nanoparticle aggregates by tuning the pH of the particles aqueous suspensions.¹⁰ In our system, we anchor PVP on mesoporous silica by simply grafting PVP with Bromo-functionalized silica surface. As shown in Scheme 1, at

high pH, the deprotonation of the polymer produces hydrophobic shrunken state and inhibits the release of trapped molecules. The swollen state of the protonated PVP at low pH is permeable to molecule transport, leading to the pH-controlled release.

Scheme 2. 1 pH-controlled release from responsive polymeric nanoshell coated mesoporous silica



2.2 Experimental Section

MCM-41-Type mesoporous silica particles: MCM-41 was synthesized according to literature procedures:^{2(a)} *n*-Cetyl-trimethylammonium bromide (CTAB, 1.0 g) was dissolved in 480 mL of distilled water. NaOH (aq) (2.00 M, 3.50 mL) was added to CTAB solution, and the solution temperature was adjusted to 80 °C. Triethoxysilane (5.00 mL) was added drop-wise to the solution, and the mixture allowed to stir for 2 h at 80 °C. The resultant white precipitate was isolated by filtration. The silica particles were then calcined at 550 °C for 5 h to remove the template.

Poly(4-vinyl pyridine) functionalized mesoporous silica (PVP-MS) 50 mg MCM-41 was reacted with 0.05ml bromomethyldimethylchlorosilane in 5ml toluene for 20min at 70°C to give Bromo-functionalized mesoporous silica(Br-MS). Short reaction time makes the attachment of functional group to the pore outlets rather than their inside walls.¹¹ 5mg Br-MS was reacted with 15mg Poly(4-vinyl pyridine) (PVP, MW 60,000 g³ mole⁻¹, Sigma-Aldrich) in 1ml nitromethane at 50 °C for 60 h. The solid was repeatedly washed by nitromethane and water and give rise to PVP-MS.

Loading, capping and release experiments: Br-MS (5mg) was stirred in 1 ml of 0.1mg/ml [Ru(bipy)₃]Cl₂ solution in nitromethane at room temperature for 60h. Then PVP (15mg) was added to the suspension. The mixture was stirred at 50 °C for another 60h. The precipitate was centrifuged, washed extensively with nitromethane and water. The final absorbance is 18%. To investigate the pH-responsive properties, dye-loaded particle (1.0mg) was dispersed in 1 ml water at a certain pH. The release

of dye from the pore was monitored via the spin-allowed d- π metal-to-ligand charge-transfer transition band of the $[\text{Ru}(\text{bipy})_3]\text{Cl}_2$ dye centered at 454 nm.³ The control experiments were carried out by soaking 5mg Br-MS in 1 ml of 0.1mg/ml $[\text{Ru}(\text{bipy})_3]\text{Cl}_2$ solution in nitromethane at room temperature for 60h before the precipitate was centrifuged and washed extensively with water, then 1mg particle was dispersed in 1ml water at different pHs to test release property.

2.3 Results and Discussion

Mesoporous silica MCM-41 are synthesized according to reported method.^{2(a)} The obtained MCM-41 was then reacted with bromomethyldimethylchlorosilane to yield a Bromo-functionalized mesoporous silica (Br-MS).⁹ The honeycomb-like structure of Br-MS was confirmed by TEM (Figure 2.1a) with BET surface area of 640 m²/g and average pore diameter of 2.5 nm from N₂ sorption analysis(Figure 2.2). PVP was grafted to the functionalized silica surface through quaternized pyridine groups,⁹ yielding tethered polymer layers on the exterior surface of MCM-41 (denoted as PVP-MS, see synthesis pathway in Scheme 2.2). The successful grafting

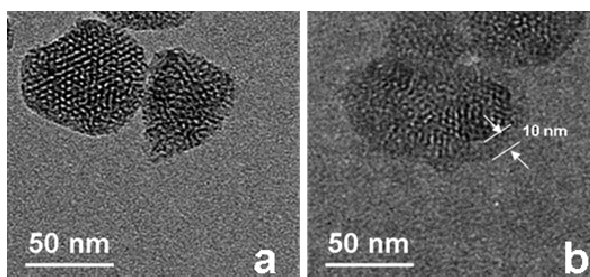


Figure 2.1 TEM of (a) Br-MS and (b)PVP-MS

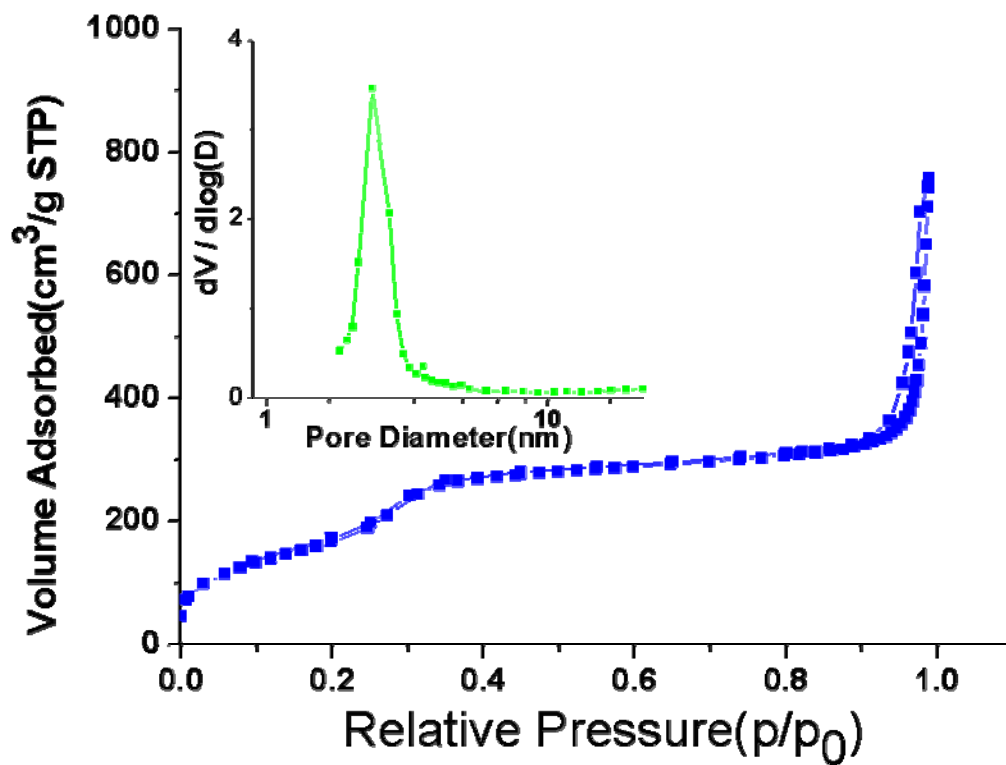
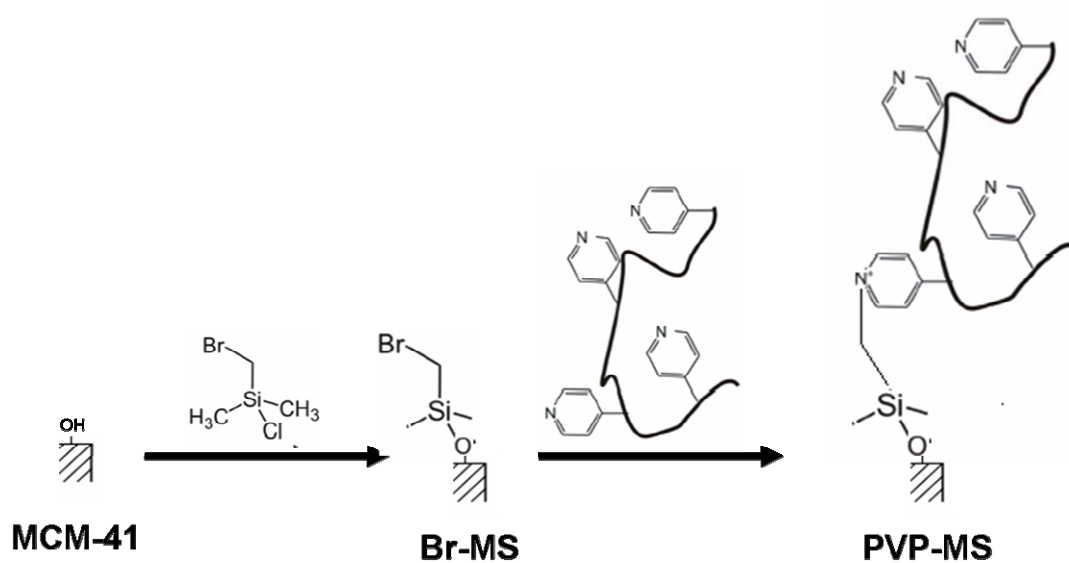


Figure 2.2 BET nitrogen sorption isotherms and BJH pore size distribution plots (inset) of Br-MS

Scheme 2. 2 Schematic outline of synthesis of PVP-MS



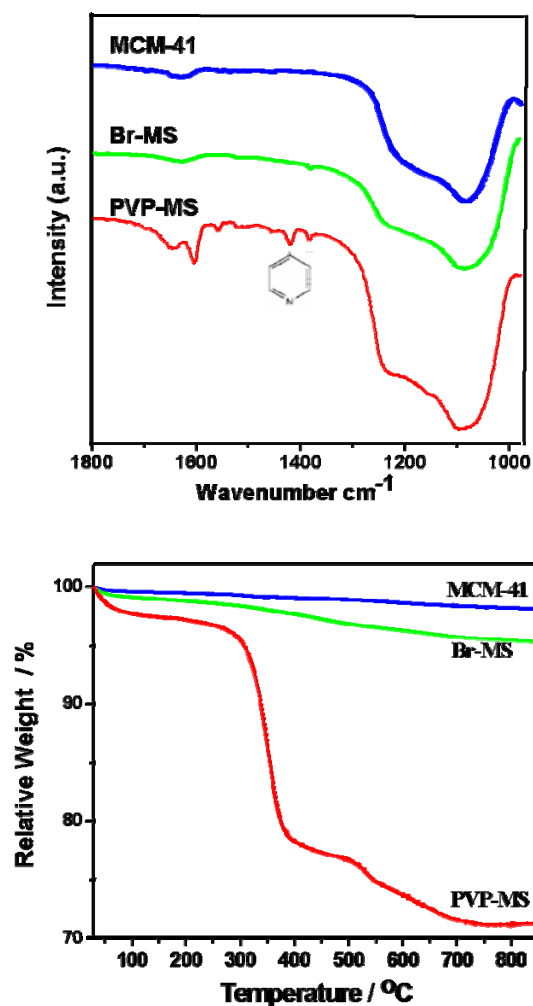


Figure 2.3 FTIR(a) and TGA(b) of MCM-41, Br-MS and PVP-MS

of polymer onto mesoporous silica was confirmed by the appearance of band at 1414 cm^{-1} in the FT-IR spectroscopy (Figure 2.3a), which is characteristic of pyridine group of PVP. Thermogravimetric analysis (TGA) of PVP-MS yielded about 30% weight loss from the grafted polymer when heating in N_2 atmosphere to 800°C while 4% weight loss was observed for Br-MS and almost no weight loss for pure MCM-41 in the same temperature range (Figure 2.3b). TEM in Figure 2.1b showed that PVP-MS

remained the honeycomb-like pore structure as Br-MS and a 10 nm dense polymer coating was observed around the silica particle after grafting.

To investigate the pH-responsive gating behavior of the hybrid nanomaterials, dye $[\text{Ru}(\text{bipy})_3]\text{Cl}_2$ (bipy:2,2-bipyridine), as a guest, was first loaded by soaking Br-MS in $[\text{Ru}(\text{bipy})_3]\text{Cl}_2$ nitromethane solution. Then, PVP was added into the mixture to coat the mesoporous silica. The excessive dye was removed by centrifugation and repeated washing with nitromethane and water. The resulting particles were then dispersed in water at different pHs to test their controlled release property. At pH 7.4, slow release of dye was observed and it needs 14h to reach 70% release, indicating the capping effect of the coated polymeric barrier. The pH 5.5 environment induced the fast release of dye molecules and the release profile in Figure 3 exhibited that the release reached 70% at 6h and no more release was observed after that. The release profile in Figure 3 exhibited fastest molecular transport at pH 4.0, in which 100% release is obtained within 1h. The effect of pH value on the releasing property is strongly related to the protonation degree of pyridine groups of PVP at different pHs. At pH 7.4, neutral shrunken hydrophobic polymer works as collapsed monolayer and does not allow the fast molecule penetration. The decrease of pH induces polymer swelling associated with the ionized pyridine groups. The stretched swollen layer starts to be permeable for trapped molecule. Since the apparent $\text{p}K_a$ of 4-vinyl pyridine is 5.39,¹² the pyridine groups become fully protonated at pH 4. The fully positively charged and swollen hydrophilic state of surface-tethered polymer layer

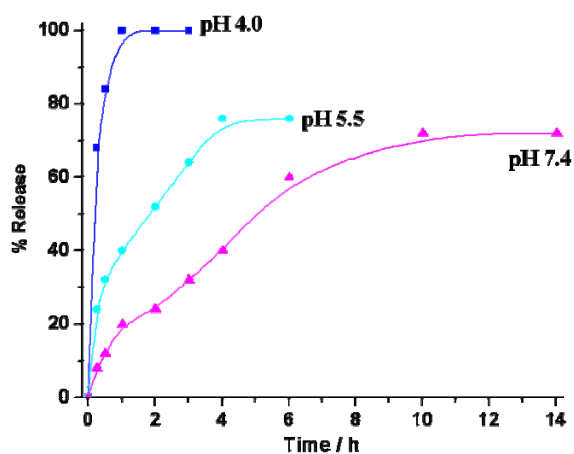


Figure 2.4 Time course of dye release from PVP-MS at different pHs

allows quick transportation of dye from mesoporous silica and leads to the fastest release at pH 4. To further demonstrate the capping effect of pH-dependent coated PVP, control experiment was carried out. Br-MS was used as nanocontainer to trap the dye molecules without further capping PVP. No molecule was released in both cases at pH 7.4, 5.5 and 4.0 because the absorbed molecules escaped from unguarded pores or external surface during the extensive washing steps, which again confirm that the pH-responsive capping ability comes from responsive polymer.

2.4 Conclusion

In conclusion, we report here the controlled release of guest molecules from mesoporous silica particles by using poly(4-vinyl pyridine) as pH-responsive capping nanoshell. We use simple “grafting to” method to tether poly(4-vinyl pyridine) onto

mesoporous silica surface and surface-tethered polymer layer works as permission barrier of molecule transport from mesopore at neutral pH. Lower pH induces quick release because protonation polymer becomes swollen and permeable to the trapped molecule. The releasing kinetics is dependent on the protonation degree of poly(4-vinyl pyridine) at different pHs. The results make the system reported here promising candidates in the formulation of pH-sensitive vehicle in *in vivo* delivery of therapeutic contents to low pH tissues, such as tumors and inflammatory sites. This approach could also provide a general route to graft other sensitive polymer onto the surface of silica particles for a wide range of different applications.

2.5 References

1. (a) Trewyn, B. G.; Slowing, I. I.; Giri, S.; Chen, H.; Lin, V. S.-Y. *Acc. Chem. Res.* **2007**, *40*, 846. (b) Slowing, I. I.; Trewyn, B. G.; Giri, S.; Lin, V. S.-Y. *Adv. Func. Mater.* **2007**, *17*, 1225. (c) Trewyn, B. G.; Giri, S.; Slowing, I. I.; Lin, V. S.-Y. *Chem. Comm.* **2007**, 3236. (d) Vallet-Regi, M.; Balas, F.; Acros, D. *Angew. Chem., Int. Ed.* **2007**, *46*, 7548.
2. (a) Lai, C.-Y.; Trewyn, B. G.; Jeftinija, D. M.; Jeftinija, K.; Xu, S.; Jeftinija, S.; Lin, V. S.-Y. *J. Am. Chem. Soc.* **2003**, *125*, 4451. (b) Giri, S.; Trewyn, B. G.; Stellmaker, M. P.; Lin, V. S.-Y. *Angew. Chem., Int. Ed.* **2005**, *44*, 5038. (c) Vivero-Escoto, J. L.; Slowing, I. I.; Wu, C. W.; Lin, V. S. Y. *J. Am. Chem. Soc.* **2009**, *131*, 3462. (d) Torney, F.; Trewyn, B. G.; Lin, V. S. Y.; Wang, K. *Nat. Nanotechnol.* **2007**, *2*, 295. (e) Lee, J. E.; Lee, N.; Kim, H.; Kim, J.; Choi, S. H.; Kim, J. H.; Kim, T.; Song, I. C.; Park, S. P.; Moon, K. M.; Hyeon, T. *J. Am. Chem. Soc.* **2010**, *132*, 552. (f) Liu, R.; Zhang, Y.; Zhao, X.; Agarwal, A.; Muller, L. J.; Feng, P. *J. Am. Chem. Soc.* **2010**, *132*, 1500. (g) Aznar, E.; Marcos, M. D.; Martinez-Manez, R.; Sancenon, F.; Soto, J.; Amoros, P.; Guillem, C. *J. Am. Chem. Soc.* **2009**, *131*, 6833.
3. (a) Hernandez, R.; Tseng, H.-R.; Wong, J. W.; Stoddart, J. F.; Zink, J. I. *J. Am. Chem. Soc.* **2004**, *126*, 3370. (b) Nguyen, T. D.; Tseng, H.-R.; Celestre, P. C.;

- Flood, A. H.; Liu, Y.; Stoddart, J. F.; Zink, J. I. *Proc. Natl. Acad. Sci. U.S.A.* **2005**, 102, 10029. (c) Nguyen, T. D.; Liu, Y.; Saha, S.; Leung, K. C.-F.; Stoddart, J. F.; Zink, J. I. *J. Am. Chem. Soc.* **2007**, 129, 626. (d) Nguyen, T. D.; Leung, K. C.-F.; Liong, M.; Pentecost, C. D.; Stoddart, J. F.; Zink, J. I. *Org. Lett.* **2006**, 8, 3363. (e) Angelos, S.; Yang, Y.-W.; Patel, K.; Stoddart, J. F.; Zink, J. I. *Angew. Chem., Int. Ed.* **2008**, 47, 2222. (f) Leung, K. C.-F.; Nguyen, T. D.; Stoddart, J. F.; Zink, J. I. *Chem. Mater.* **2006**, 18, 5919. (g) Nguyen, T. D. K.; Leung, C. F.; Liong, M.; Liu, Y.; Stoddart, J. F.; Zink, J. I. *Adv. Funct. Mater.* **2007**, 17, 2101. (h) Patel, K.; Angelos, S.; Dichtel, W. R. Coskun, A.; Yang, Y.-W.; Zink, J. I.; Stoddart, J. F. *J. Am. Chem. Soc.* **2008**, 130, 2382.
4. (a) Schlossbauer, A.; Kecht, J.; Bein, T. *Angew. Chem., Int. Ed.* **2009**, 48, 3092. (b) Climent, E.; Bernardos, A.; Martinez-Manez, R.; Maquieira, A.; Marcos, M. D.; Pastor-Navarro, N.; Puchades, R.; Sancenon, F.; Soto, J.; Amoros, P. *J. Am. Chem. Soc.* **2009**, 131, 14075. (c) Bernardos, A.; Aznar, E.; Marcos, M. D.; Martinez-Manez, R.; Sancenon, F.; Soto, J.; Barat, J. M.; Amoros, P. *Angew. Chem., Int. Ed.* **2009**, 48, 5884.
 5. Fu, Q.; Rao, G. V. R.; Ista, L. K.; Wu, Y.; Andrzejewski, B. P.; Sklar, L. A.; Ward, T. L.; Lopez, G. P. *Adv. Mater.* **2003**, 15, 1262.
 6. Hong, C.-Y.; Li, X.; Pan, C.-Y. *J. Mater. Chem.*, **2009**, 19, 5155.
 7. Sun, J.-T.; Hong, C.-Y.; Pan, C.-Y. *J. Phys. Chem. C.* **2010**, 114, 12481.
 8. (a) Liu, R.; Zhao, X.; Wu, T.; Feng, P. *J. Am. Chem. Soc.* **2008**, 130, 14418. (b) Liu, R.; Zhang, Y.; Feng, P. *J. Am. Chem. Soc.* **2009**, 131, 15128.
 9. Tam, T. K.; Pita, M.; Trotsenko, O.; Motornov, M.; Tokarev, I.; Halamek, J.; Minko, S.; Katz, E. *Langmuir* **2010**, 26, 4506.
 10. Motornov, M.; Sheparovych, R.; Lupitsky, R.; MacWilliams, E.; Minko, S. *J. Colloid Interface Sci.*, **2007**, 310, 481.
 11. Yang, Q.; Wang, S.; Fan, P.; Wang, L.; Di, Y.; Lin, K.; Xiao, F.-S. *Chem. Mater.* **2005**, 17, 5999.
 12. (a) Pinkrah, V. T.; Snowden, M. J.; Mitchell, J. C.; Seidel, J.; Chowdhry, B. Z.; Fern, G. R. *Langmuir* **2003**, 19, 585; (b) Kuang, M.; Wang, D. Y.; Bao, H. B.; Gao, M. Y.; Möhwald, H.; Jiang, M. *Adv. Mater.* **2005**, 17, 267.

Chapter Three

pH-Responsive Nanogated Ensemble Based on Gold-Capped Mesoporous Silica through an Acid-Labile Acetal Linker*

3.1 Introduction

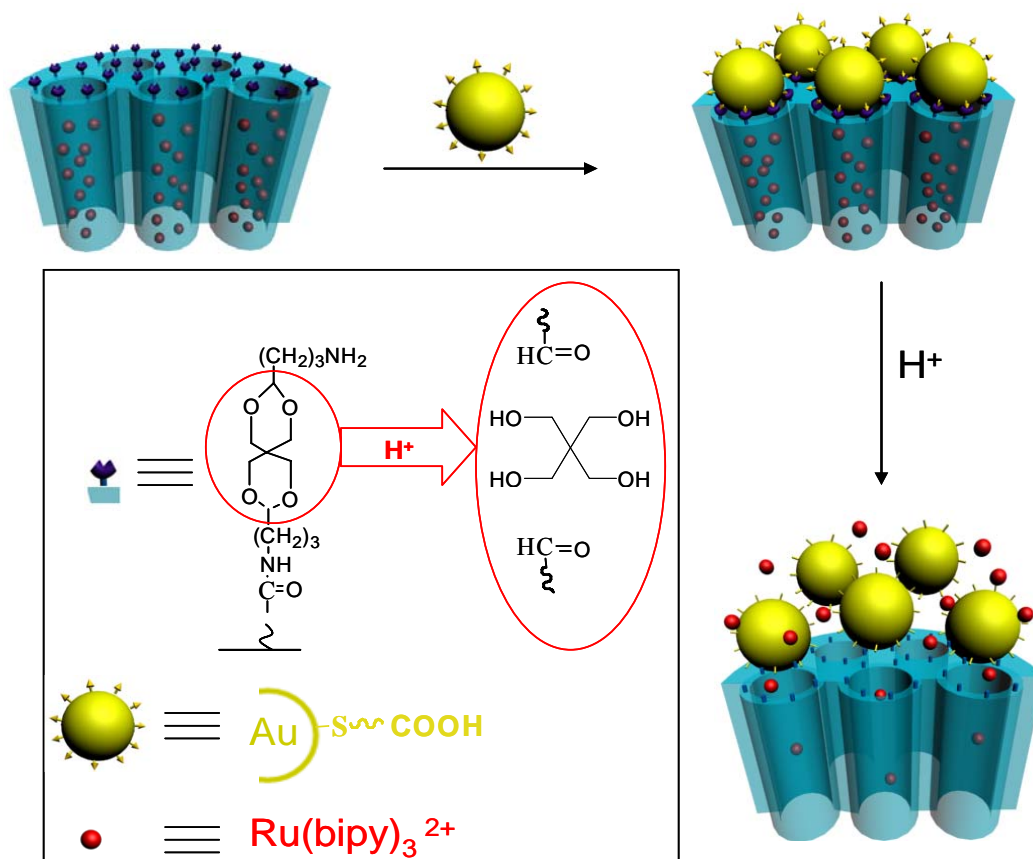
Due to their high surface area, uniform and tunable pore structure, and diversity in surface functionalization, mesoporous silica (MS) have been widely used as versatile solid supports to construct hybrid materials for catalysis, enzyme immobilization, drug delivery, and imaging.¹ A series of MS based controlled release systems have been developed that are responsive to distinct external stimuli. For example, a photocontrolled release system based on coumarin functionalized mesoporous materials was demonstrated.² Polyamines anchored on the pore outlets of mesoporous materials for use as a dual pH- and anion-driven gated ensemble have also been reported.³ A series of supramolecular nanovalves using redox^{4a,b,c}, pH^{4d,e,f}, competitive binding^{4g}, light^{4h,i} and enzyme^{4j} as actuators have also been demonstrated. We recently reported cross-linkable polymer modified mesoporous silica as a new type of versatile responsive system.⁵ Nanoparticles are another type of widely used capping agent in MS release systems. CdS and Fe₃O₄ nanoparticles were first used as capping agents to control the opening and closing of pore entrance of mesostructured materials through redox-dependent S-S bond cleavage.⁶ Recently, gold nanoparticles

* Reproduced with permission from *J. Am. Chem. Soc.* **2010**, 132, 1500. copyright 2010 American Chemical Society

were used as blocking caps to control the transport of cargo from mesoporous silica either through reversible pH-dependent boronate ester bond^{7a} or photo-controlled electrostatic interaction^{7b}.

Acid sensitive drug delivery vehicles are highly desired in the treatment of acidic targets, such as tumors and inflammatory tissues. Several acid degradable linkers have been used in the construction of prodrug conjugate, lipid, polymeric micelles and nanogels to deliver therapeutic contents in acidic pH environments. For example, hydrazone or cis-aconityl linkers have been reported in the construction of polymer-Doxorubicin (DOX) conjugates to control the release of attached anticancer drug DOX at physiological and acidic environment.⁸ pH-sensitive polyethylene glycol (PEG) lipids containing orthoester linkage demonstrated their pH-dependent degradation and showed potential use in gene delivery.⁹ Polymeric micelles with anticancer drug, adriamycin (ARD), attached to the core via an hydrazone bond are stable at physiological pH but degrade and release ARD at lower pH.¹⁰ The protein-loaded hydrogels or microgel based on acetal cross-linkers release encapsulated protein at pH 5.0 while the release is inhibited at pH 7.4.¹¹ Here, we introduce acid cleavable linker into MS-based controlled release system and report a new pH-responsive nanogated ensemble by capping the gold nanoparticle onto the mesoporous silica through an acid-labile acetal linker. As shown in Scheme 3.1, at neutral pH, the linker remains intact and pores are blocked with gold nanoparticles to strongly inhibit the molecule diffusion from the pores. At acidic pHs, the hydrolysis

Scheme 3. 1 Schematic illustration of pH-responsive nanogated ensemble based on gold-capped mesoporous silica through acid-labile acetal linker



of the acetal group will remove the gold cap and allow escape of the entrapped molecules in a pH-dependent controlled release.

3.2 Experimental Section

Materials: Tetraethylorthosilicate (TEOS) and 3-aminopropyltriethoxysilane (APTES) were purchased from Gelest. Mercaptosuccinic acid (MSA), hydrogen tetrachloroaurate(III) (HAuCl_4), succinic anhydride, 1-ethyl-3-(3-dimethylaminopropyl)carbodiimide-HCl (EDC)

N-hydroxysuccinimide (NHS) were purchased from Sigma-Aldrich. Sodium borohydride and tris(2,2'-bipyridine)dichlororuthenium(II) hexahydrate were purchased from Alfa Aesar. 3,9-Bis(3-aminopropyl)-2,4,8,10-tetraoxaspiro[5.5]undecane was purchased from TCI.

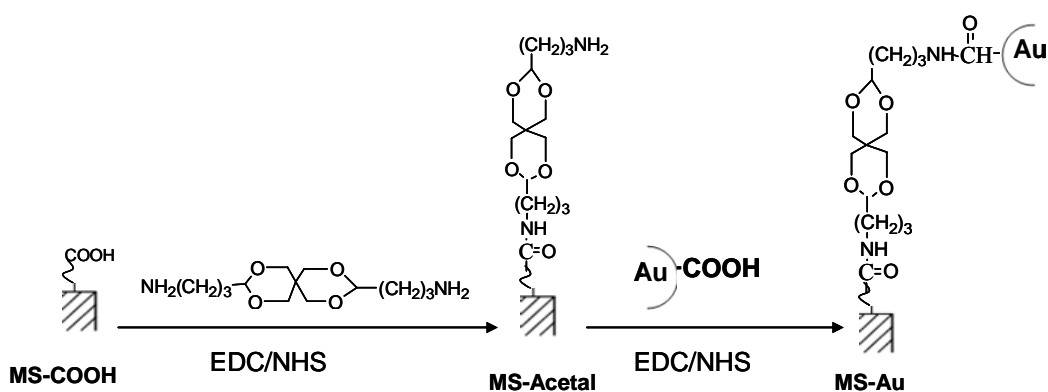
Synthesis of carboxylic acid modified gold nanoparticle(Au-COOH): Following a literature procedure¹², 4.1 mL of aqueous solution containing 0.5 mmol of HAuCl₄ and 0.5 mmol of MSA were mixed in 100 mL of deoxygenated methanol (100 mL). Then 25 mL of 0.2 M aqueous NaBH₄ solution was added at a rate of 7 mL/min under vigorous stirring. A dark-brown precipitate was produced and separated by centrifugation. The precipitate was repeatedly washed with a water/ethanol (V/V, 1/4) and ethanol to remove any impurities. Finally, the precipitate was dried under vacuum to get Au-COOH. FTIR of obtained Au-COOH matched the reported spectra¹² and confirmed the presence of COOH group.

Synthesis of carboxylic acid-functionalized mesoporous silica (MS-COOH): MCM-41-type mesoporous silica(MS) nanosphere was synthesized using reported method^{6a} with mean diameter ~140 nm. MS-COOH was synthesized using reported method^{4f} with slight modification. MCM-41 as-synthesized (1.6 g) was suspended in a solution containing 20 mL of dry toluene and 0.50 g of APTES under stirring at ambient temperature for 15 min. Toluene was evaporated by a rotary evaporator at 80°C for 2 h. to obtain amine-functionalized MS. 90 mg of amine-functionalized MS

was added into 5mL DMSO solution containing succinic anhydride (40mg) and triethylamine (40mg) and stirred at 40 °C for 48 h. The particle was recovered by centrifugation and washed with ethanol to obtain MS-COOH.

Synthesis of acetal linker containing mesoporous silica (MS-Acetal): 80 mg of MS-COOH was well suspended in 3mL H₂O containing 50mg EDC and 20mg NHS, then 130mg of 3,9-Bis(3-aminopropyl)-2,4,8,10-tetraoxaspiro[5.5]undecane added and stirred at room temperature for 8h. The obtained particles were refluxed in hot acetone for 48h to remove template CTAB¹³ and gave rise to MS-Acetal. Gold nanoparticles capped onto mesoporous silica (MS-Au) was obtained by reaction 15mg of MS-Acetal with 5mg of Au-COOH in the presence of 10mg EDC and 5mg NHS for 8h.(see Scheme 3.2).

Scheme 3.2 Schematic outline of synthesis of MS-Acetal and MS-Au



Characterization: Powder X-ray diffraction (XRD) patterns were recorded on a Bruker D8 Advance diffractometer with Cu K α radiation (40 kV, 40 mA). N₂ sorption analysis was performed on a Micromeritics ASAP2010 volumetric adsorption analyzer at 77 K. Fluorescence were taken using Spex Fluorolog Tau-3 fluorescence spectrophotometer TEM images were recorded on a Philips Tecnai 12 transmission electron microscope.

Loading, capping and release experiments: MS-Acetal (15mg) was stirred in 1 ml of 0.67 mM [Ru(bipy)₃]Cl₂ aqueous solution (pH 7.0) at room temperature for 12h. Then Au-COOH (5mg) was added to the suspension, followed by addition of 10mg EDC and 5mg NHS. The mixture was stirred for another 8h. The precipitate was centrifuged, washed extensively with pH 7.0 water. The final absorbance is 0.045mmol dye/g silica To investigate the pH-responsive properties, dye-loaded particle (2.0mg) in dialysis tubing was dispersed in 2 ml water at a certain pH. The release of the Ru(bipy)₃²⁺ dye from the pore was monitored via the spin-allowed d- π metal-to-ligand charge-transfer transition band of the Ru(bipy)₃²⁺ dye centered at 454 nm³. The control experiments were carried out by soaking 15mg MS-Acetal or MS-Au in 1 ml of 0.67 mM [Ru(bipy)₃]Cl₂ aqueous solution (pH 7.0) at room temperature for 20h before the precipitate was centrifuged and washed extensively with pH 7.0 water, then 2mg particles in dialysis tubing were dispersed in 2ml water at different pHs to test release property.

3.3 Results and Discussion

To create this nanogated ensemble, carboxylic acid groups were first introduced onto the outlet of mesoporous silica (denoted as MS-COOH) using an established method^{4f}. Then, the acetal containing linker was grafted on by the reaction of excess 3,9-bis(3-aminopropyl)-2,4,8,10-tetraoxaspiro[5.5]undecane with the

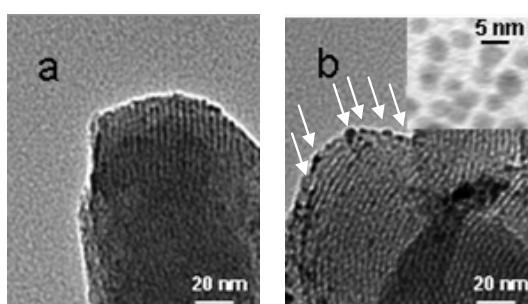


Figure 3.1. TEM of a) MS-Acetal, b) MS-Au and inset in b) Au-COOH

carboxylic acid modified MS, followed by the removal of the surfactant template by acetone extraction¹³ to produce MS-Acetal. The TEM in Figure 3.1a, XRD in Figure 3.2a and N₂ sorption measurement in Figure 3.3 demonstrate a typical hexagonal mesopore channel for MS-Acetal. A fluorescamine test (Figure 3.4) confirmed the presence of free amine from the attached acetal linker whereas no amine was detected on MS-COOH. The free amine groups were then coupled with COOH groups on the carboxylic acid modified gold nanoparticle (Au-COOH¹²) to cap the gold nanoparticles onto the mesoporous silica (MS-Au). The successful capping was confirmed by various spectroscopic methods. Powder X-ray diffraction (XRD) (Figure 3.2a) in $2^\circ < 2\theta < 8^\circ$ showed that MS-Au remained mesoporous despite of

lower intensity of XRD peaks that may be ascribed to the pore-filling effect induced by gold nanoparticle capping.⁶ XRD in the $30^\circ < 2\theta < 70^\circ$ range (Figure 3.2b) showed similar (111), (200) and (220) diffraction peaks to those observed for Au-COOH, supporting the presence of gold nanoparticles on MS-Au. N₂ sorption measurement of MS-Acetal exhibited the typical type IV isotherms of mesoporous

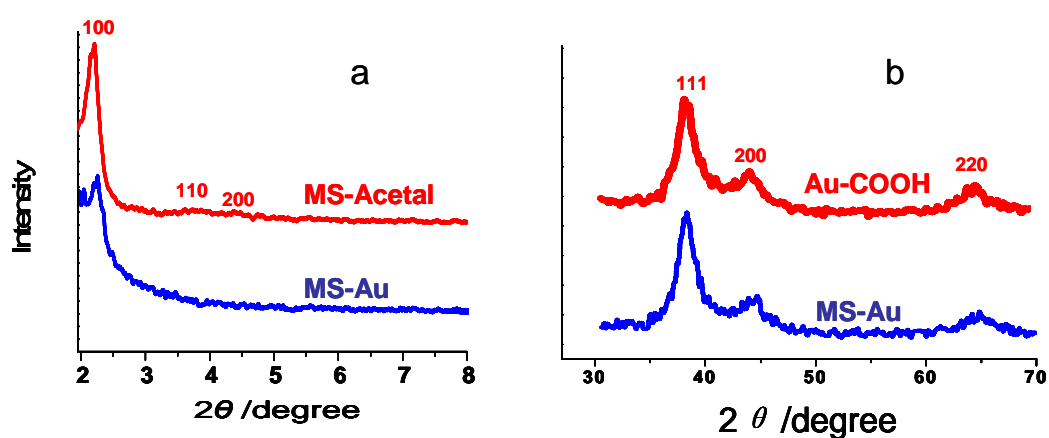


Figure 3.2 XRD of a) MS-Acetal and MS-Au, b) Au-COOH and MS-Au

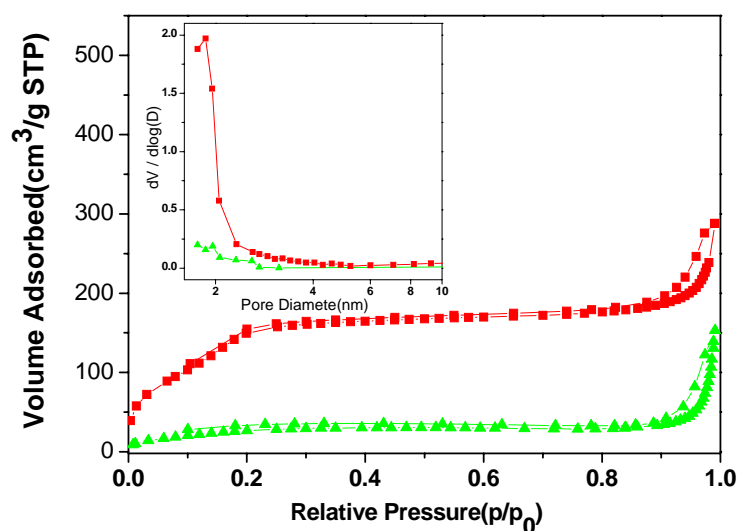


Figure 3.3 BET nitrogen sorption isotherms and BJH pore size distribution plots (inset) of MS-Acetal (red) and MS-Au (green)

materials while MS-Au showed an isotherm characteristic of nonporous materials (Figure 3.3). The change of sorption type, together with a decrease of surface area and pore size distribution is expected due to the capping effect of the nanoparticles.⁶ TEM showed that Au nanoparticles are clearly visible as dark spot on the outside of the

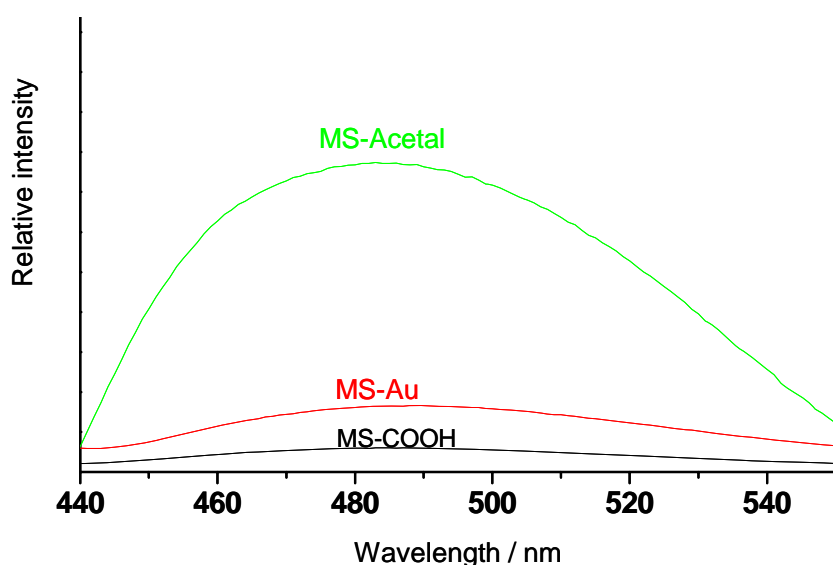


Figure 3.4 Fluorescence spectra of fluorescamine solutions (with excitation wavelength at 420 nm after reacting with MS-COOH, MS-Acetal and MS-Au. (Reaction condition: 2.5mg of particles were mixed thoroughly for 5min with 0.5ml of 5mM fluorescamine in MeOH)

mesopores (indicated in the Figure 3.1b by arrows) while characteristic mesoporous channels remain. The largely decreased amount of free amino groups on MS-Au in the fluorescamine test (Figure 3.4) demonstrates that Au nanoparticles are indeed coupled through amide bond.

To investigate the pH-responsive gating behavior of the hybrid nanomaterials, [Ru(bipy)₃]Cl₂ (bipy=2,2'-bipyridine) dye was loaded as a guest by soaking MS-Acetal in aqueous solution (pH 7.0) of [Ru(bipy)₃]Cl₂. Then, Au-COOH was

added into the mixture to cap the mesoporous silica in the presence of EDC/NHS. The excessive dye was removed by centrifugation and repeated washing with water. The resulting particles were then dispersed in water at different pHs to test their controlled release property. At pH 7.0, no free dye was observed, indicating an efficient capping

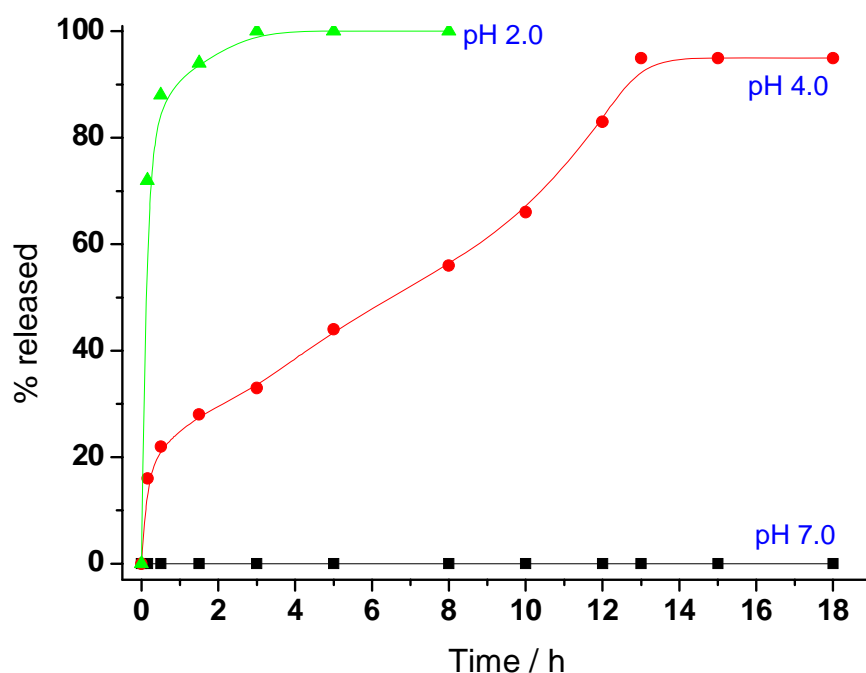


Figure 3.5 Time course of dye release from MS-Au at different pHs

of the agent. pH 4.0 solution, however, induced the release of dye molecules with the profile shown in Figure 3.5 that reaches 100% release at 13h. At pH 2.0, faster molecular transport was observed with 90% release in 30mins and equilibrium in 2h with final concentration 0.0014mM. The effect of pH on the releasing tracks the degradation rates of acetal groups at different pHs. It has been reported that while the acetal linker is stable from pH 6~8.2, it is completely hydrolyzed in 30mins at pH 2.0

and in 12 hrs at pH 4.0.¹⁴ The release profile at different pHs herein matches well with the reported degradation profile of acetal group. Two additional controlled studies were carried out. In the first, we used MS-Acetal as a nanocontainer to trap the dye molecules without further capping by the gold nanoparticle. In the second, we used already capped MS-Au to adsorb the dye molecules mainly at the external surface. After the same washing procedure, no molecule release was observed at any pH because the absorbed molecules escaped from unguarded pores or external surface during the washing steps, which again confirms the previously observed release due to dye molecules trapped within the pH-responsive gold-capped nanogated vessel.

3.4 Conclusion

In conclusion, we report here the controlled release of guest molecules from mesoporous silica particles by using acid-labile acetal group linked gold nanoparticles as pH-responsive capping agent. The guest molecules were blocked from the hybrid materials at neutral pH and released at lower pH. The releasing profile is strongly dependent on the cleavage of acetal linker at different pHs. The results make the system reported here a promising candidate in the formulation of pH-sensitive vehicle for in vivo delivery of therapeutic agents to low pH tissues, such as tumors and inflammatory sites. This approach could also provide a general route to graft other sensitive linkers onto the surface of silica particles for a wide range of applications.

3.5 References

1. (a) Kesanli, B.; Lin, W. *Chem. Commun.* **2004**, 2284. (b) Mihalcik, DJ; Lin, W. *Angew. Chem., Int. Ed.* **2008**, *47*, 6229.(c) Zhu, H.; Liang, C.; Yan, W.; Overbury, S. H.; Dai, S. *J. Phys. Chem. B* **2006**, *110*, 10842. (d) Lei, C.; Shin, Y.; Liu, J.; Ackerman, E. J. *J. Am. Chem. Soc.* **2002**, *124*, 11242. (e) Lei, C.; Shin, Y.; Liu, J.; Ackerman, E. J. *Nano Lett.* **2007**, *7*, 1050. (f) Trewyn, B. G.; Slowing, I. I.; Giri, S.; Chen, H.; Lin, V. S.-Y. *Acc. Chem. Res.* **2007**, *40*, 846. (g) Slowing, I. I.; Trewyn, B. G.; Giri, S.; Lin, V. S.-Y. *Adv. Func. Mater.* **2007**, *17*, 1225. (h) Trewyn, B. G.; Giri, S.; Slowing, I. I.; Lin, V. S.-Y. *Chem. Comm.* **2007**, 3236. (i) Taylor, K. M. L.; Kim, J. S.; Rieter, W. J.; An, H.; Lin, W.; Lin, W. *J. Am. Chem. Soc.* **2008**, *130*, 2154.
2. Mal, N. K.; Fujiwara, M.; Tanaka, Y. *Nature* **2003**, *421*, 350.
3. Casasus, R.; Climent, E.; Marcos, M. D.; Martinez-Manez, R.; Sancenon, F.; Soto, J.; Amoros, P.; Cano, J.; Ruiz, E. *J. Am. Chem. Soc.* **2008**, *130*, 1903.
4. (a) Hernandez, R.; Tseng, H.-R.; Wong, J. W.; Stoddart, J. F.; Zink, J. I. *J. Am. Chem. Soc.* **2004**, *126*, 3370. (b) Nguyen, T. D.; Tseng, H.-R.; Celestre, P. C.; Flood, A. H.; Liu, Y.; Stoddart, J. F.; Zink, J. I. *Proc. Natl. Acad. Sci. U.S.A.* **2005**, *102*, 10029. (c) Nguyen, T. D.; Liu, Y.; Saha, S.; Leung, K. C.-F.; Stoddart, J. F.; Zink, J. I. *J. Am. Chem. Soc.* **2007**, *129*, 626. (d) Nguyen, T. D.; Leung, K. C.-F.; Liong, M.; Pentecost, C. D.; Stoddart, J. F.; Zink, J. I. *Org. Lett.* **2006**, *8*, 3363. (e) Angelos, S.; Yang, Y.-W.; Patel, K.; Stoddart, J. F.; Zink, J. I. *Angew. Chem., Int. Ed.* **2008**, *47*, 2222. (f) Park, C.; Oh, K.; Lee, S.; Kim, C. *Angew. Chem., Int. Ed.* **2007**, *46*, 1455. (g) Leung, K. C.-F.; Nguyen, T. D.; Stoddart, J. F.; Zink, J. I. *Chem. Mater.* **2006**, *18*, 5919. (h) Nguyen, T. D. K.; Leung, C. F.; Liong, M.; Liu, Y.; Stoddart, J. F.; Zink, J. I. *Adv. Funct. Mater.* **2007**, *17*, 2101. (i) Ferris, D. P.; Zhao, Y.; Khashab, N. M.; Khatib, H. A.; Stoddart, J. F.; Zink, J. I. *J. Am. Chem. Soc.* **2009**, *131*, 1686. (j) Patel, K.; Angelos, S.; Dichtel, W. R. Coskun, A.; Yang, Y.-W.; Zink, J. I.; Stoddart, J. F. *J. Am. Chem. Soc.* **2008**, *130*, 2382.
5. (a) Liu, R.; Zhao, X.; Wu, T.; Feng, P. *J. Am. Chem. Soc.* **2008**, *130*, 14418. (b) Liu, R.; Zhang, Y.; Feng, P. *J. Am. Chem. Soc.* **2009**, *131*, 15128.
6. (a) Lai, C.-Y.; Trewyn, B. G.; Jeftinija, D. M.; Jeftinija, K.; Xu, S.; Jeftinija, S.; Lin, V. S.-Y. *J. Am. Chem. Soc.* **2003**, *125*, 4451. (b) Giri, S.; Trewyn, B. G.; Stellmaker, M. P.; Lin, V. S.-Y. *Angew. Chem., Int. Ed.* **2005**, *44*, 5038.
7. (a) Aznar, E.; Marcos, M. D.; Martinez-Manez, R.; Sancenon, F.; Soto, J.; Amoro, P.; Guillem, P. *J. Am. Chem. Soc.* **2009**, *131*, 6833. (b) Vivero-Escoto, J.

- L.; Slowing, I. I.; Wu, C.; Lin, V. S.-Y. *J. Am. Chem. Soc.* **2009**, *131*, 3462.
8. Ulbrich, K.; Etrych, T.; Chytil, P.; Jelinkova, M.; Rihov, B. *J. Control. Release.* **2003**, *87*, 33
 9. Masson, C.; Garinot, M.; Mignet, N.; Wetzler, B.; Mailhe, P.; Scherman, D.; Bessodes M. *J. Control. Release.* **2004**, *99*, 423.
 10. Bae, Y.; Fukushima, S.; Harada, A.; Kataoka, K. *Angew. Chem., Int. Ed.* **2003**, *42*, 4640.
 11. Murthy, N.; Thng, Y. X.; Schuck, S.; Xu, M.C.; Frechet, J M. J. *J. Am. Chem. Soc.* **2002**, *124*, 12398.
 12. Yao, H.; Momozawa, O.; Hamatani, T. Kimura, K. *Chem. Mater.* **2001**, *13*, 4692
 13. Deng, Y.; Qi, D.; Deng, C.; Zhang, X.; Zhao, D. *J. Am. Chem. Soc.* **2008**, *130*, 28.
 14. Zhang, L.; Bernard, J.; Davis, T. P.; Barner-Kowollik, C.; Stenzel, M. H. *Macromol. Rapid Commun.* **2008**, *29*, 123

Chapter Four

Tunable Redox-responsive Hybrid Nanogated Ensembles*

4.1 Introduction

Materials that can trap and release molecules controllably hold promise for sensor and drug delivery applications.¹ The great diversity in surface functionalization of mesoporous silica together with their uniform and tunable pore size and high surface area bestows such materials with unique advantages in the construction of nanocontainers that are responsive to stimulus. Different nanomaterials have been achieved. For example, CdS and Fe₃O₄ nanoparticles have been used as the capping agent to control opening/closing of pore entrance of mesostructured materials.² A photocontrolled release system based on coumarin functionalized mesoporous materials was demonstrated.³ Polyamines anchored on the pore outlets of mesoporous materials as a dual pH- and aniondriven gate-like ensemble have also been demonstrated.⁴ A series of supramolecular nanovalves using redox,^{5a-c} pH,^{5d,e} competitive binding,^{5f} light,^{5g} and enzyme^{5h} as actuators have also been demonstrated.

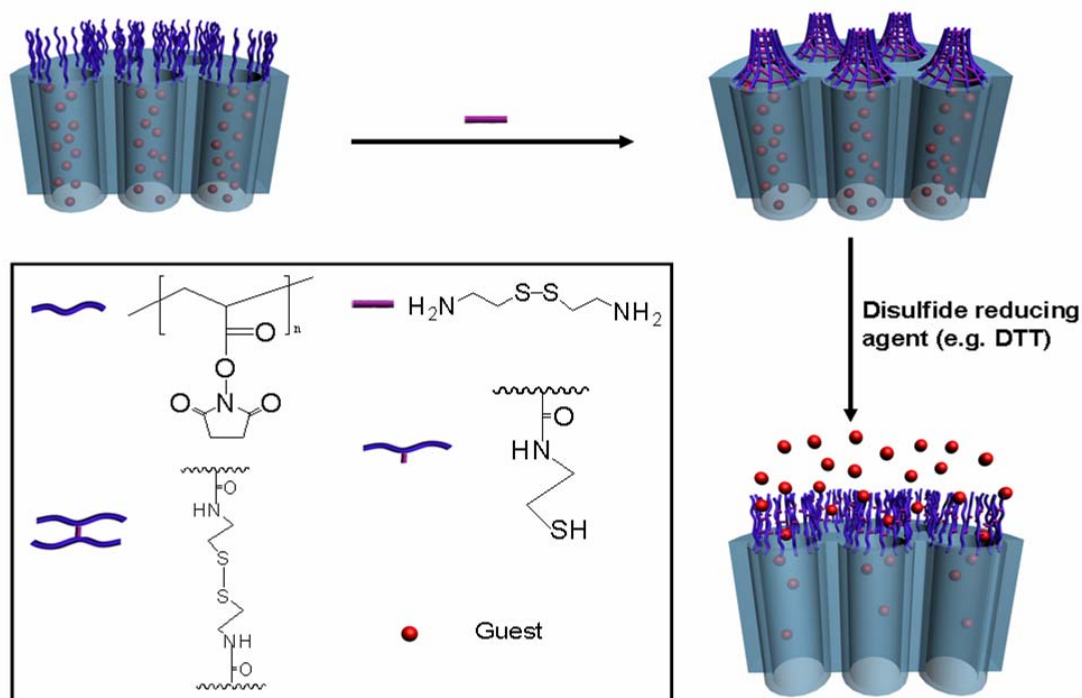
Polymeric micelles, another type of functional nanomaterials, have been extensively studied for their applications as delivery vehicles, molecular imaging agents, and microelectronic devices.⁶ Recent progresses in this area are mainly focused on core or shell cross-linked polymeric micelles, where the cross-linked layers work as a barrier to modulate molecular transport as well as a stabilizer to improve the micellar integrity.⁷ However, these types of organic carrier-based systems suffer from inherent low stability in a biochemical environment or in organic solvents

* Reproduced with permission from *J. Am. Chem. Soc.* **2008**, 130, 14418. copyright 2008 American Chemical Society

used for drug loading. Integration of both polymeric organic and inorganic components into a functional system represents a unique advantage.

Here for the first time, a cross-linked polymeric network is used as a “gatekeeper” on the surface of mesoporous silica-based materials. The gate operation is based on redox reactions in which the cross-linked polymeric network works as an off-on switch in response to redox signals. The system consists of poly(*N*-acryloxysuccinimide)-grafted mesoporous silica (denoted as PNAS-MS), in which the polymers are attached at the pore entrance of MCM-41 particles. The working principle of the system is illustrated in Scheme 4.1. After loading the dye molecules into porous silica particles, the openings of PNAS-MS are blocked by the addition of cystamine, a disulfidebased bifunctional primary amine, which allows polymer chains to be cross-linked through the reaction between cystamine and *N*-oxysuccinimide groups along the polymer chain. The polymeric network thus formed around the pore opening can be reopened by cleaving the disulfide bond of cystamine in the presence of disulfide reducing agents such as dithiothreitol (DTT), leading to the redox controlled release.

Scheme 4.1. Schematic illustration of redox-responsive nanogated ensemble based on polymeric network-capped mesoporous silica



2.2 Experimental Section

MCM-41-Type mesoporous silica particles: MCM-41 is synthesized using a procedure similar to the reported procedure^{2a}: *n*-Cetyltrimethylammonium bromide (CTAB, 1g) was dissolved in 480 mL of distilled water. NaOH(aq) (2.00 M, 3.50 mL) was added to CTAB solution, followed by adjusting the solution temperature to 80°C. TEOS (5.00 mL) was added drop-wise to the solution. The mixture was allowed to stir for 2 h at 80°C, followed by filtration, giving rise to white precipitates (as synthesized MCM-41).

Poly(*N*-acryloxysuccinimide) functionalized mesoporous silica (PNAS-MS)(Scheme 4.2): (1) as-synthesized MCM-41 (1.6g) was suspended in a solution containing 20 mL of dry toluene and 0.50 g of ((chloromethyl) phenylethyl) trimethoxysilane under stirring at ambient temperature for 15 min.

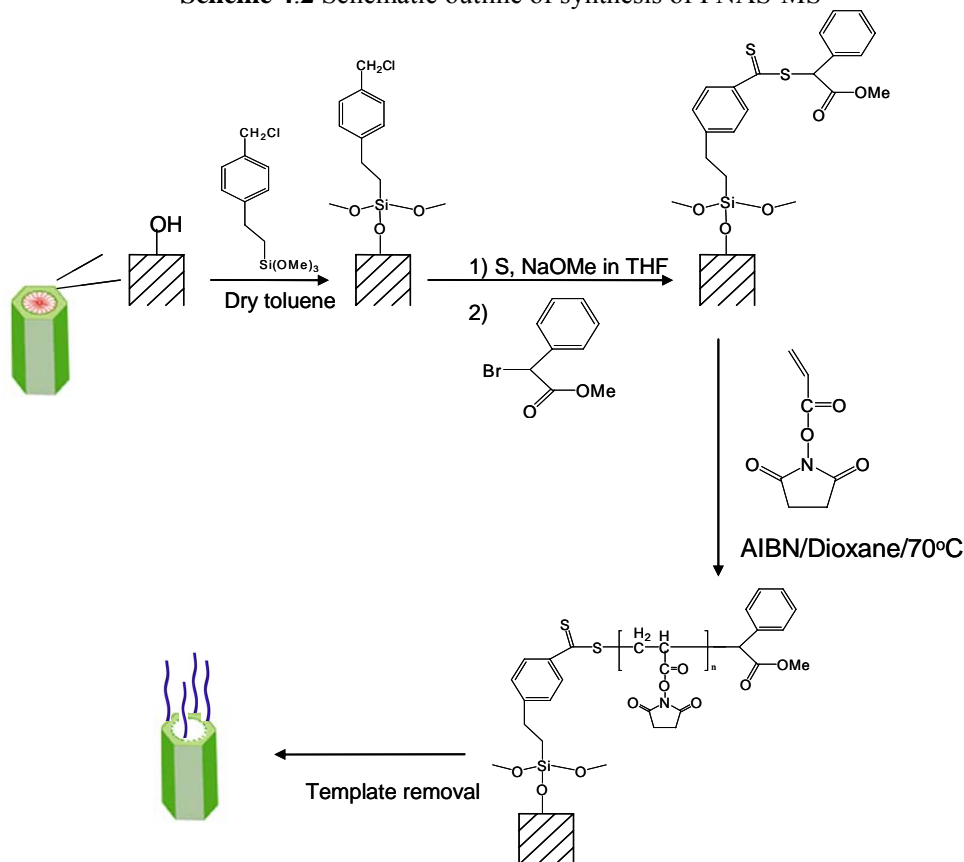
Toluene was evaporated by a rotary evaporator at 80°C for 2 h. Using of as-synthesized MCM-41 and proper reaction time are necessary for the attachment of functional group to the pore outlets rather than their inside walls⁸.(2) Chain transfer agent (CTA) was attached to silica particle according to the reported procedure⁹: The silica particle obtained in step(1) was introduced into 50ml THF containing 0.08 g of elemental sulfur and 0.135g of sodium methoxide, followed by stirring for 8h at 70°C. The substrate was removed and washed with warm toluene, warm THF, methanol, and warm H₂O. The dried substrate was then immersed in a solution containing 0.5 g of methyl- α -bromophenylacetate in 10 mL THF. The mixed solution was refluxed at 70 °C for 12 h. The substrate was removed and washed with toluene, warm THF, a mixture of water and THF (1:1, v:v), warm THF and dichloromethane, denoted as silica-MCPDB (3)RAFT polymerization: 1.0g of NAS and 10mg of AIBN were added to 10ml of *p*-dioxane and degassed for 30min , then 0.5g of silica-MCPDB was introduced and the temperature was raised to 70 °C. The mixture was allowed to stir for 24h at 70 °C. The solid was filtrated and washed in 150ml methanol containing 1ml HCl(37.4%) to give rise to PNAS-MS. Cross-linked PNAS-MS was obtained by reaction 50mg of PNAS-MS with 100mg of cystamine in 5ml PBS buffer(100mM, pH 7.4) at 45°C for 6h.

Characterization: Powder X-ray diffraction (XRD) patterns were recorded on a Bruker D8 Advance diffractometer with Cu K α radiation (40 kV, 40 mA). N₂ sorption analysis was performed on a Micromeritics ASAP2010 volumetric adsorption analyzer at 77 K. Fourier transform infrared (FT-IR) spectra were performed on Bruker Equinox 55 with KBr plates. Thermal gravimetric analysis was carried out on Mettler Toledo TGA/SDTA-851 under flowing N₂ at a heating rate of 10 °C/min.

TEM images were recorded on a Philips Tecnai 12 transmission electron microscope.

Loading, capping and release experiments: PNAS-MS(50mg) was stirred in 5 ml 0.5 mM rhodamine B in PBS solution(100mM, pH 7.4) at room temperature for 6h. Then cystamine (100mg) was added to the suspension, followed by adjusting the temperature to 45°C. The mixture was stirred for another 6h before the precipitate was centrifuged, washed extensively with water. To investigate the redox-responsive properties, dye-loaded silica particle (1.0mg) was dispersed in 3ml PBS solution. Release profiles were obtained by plotting the absorbance intensity of rhodamine B in solution at 555 nm as a function of time. The activation of nanogate was accomplished by adding different amount of DTT.

Scheme 4.2 Schematic outline of synthesis of PNAS-MS



4.3 Results and Discussion

Poly(*N*-acryloxysuccinimide) was anchored to the outlet of silica mesopore through reversible addition-fragmentation chain transfer (RAFT) polymerization (see Scheme 4.2). RAFT polymerization has emerged as a promising living radical polymerization method in functionalization of a solid surface because of its versatility and compatibility with almost all of the conventional radical polymerization monomers. The absence of metal catalyst in RAFT makes it better suited for the bioapplication than ATRP. The successful grafting of polymer onto mesoporous silica was confirmed by the appearance of a band at 1730-1822 cm⁻¹, which is characteristic of ester carbonyl and two cyclic carbonyl group of NAS, in the FTIR spectroscopy (Figure 4.1). TEM (Figure 4.2) showed that PNAS-MS retained the pore structure

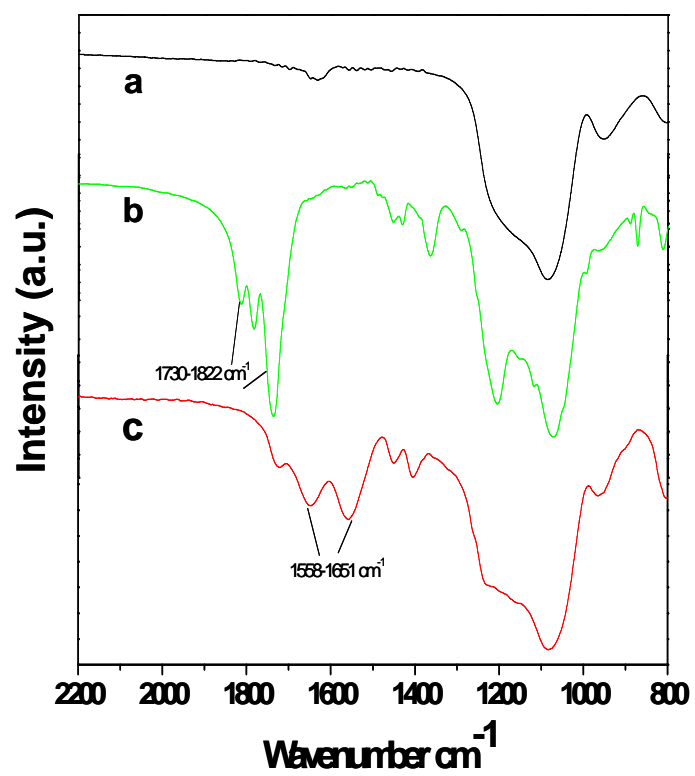


Figure 4.1 FTIR of a) pure silica MCM-41, b) PNAS-MS, c) cross-linked PNAS-MS

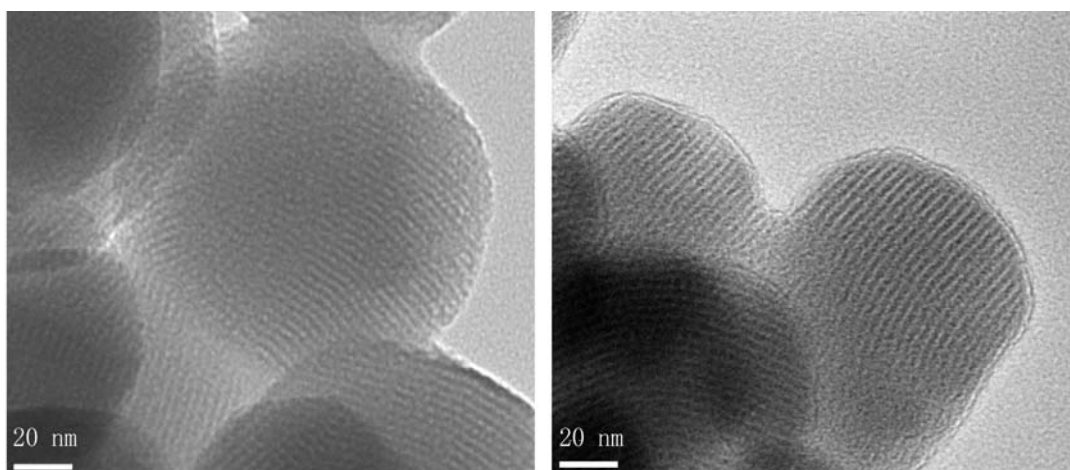


Figure 4.2 TEM of a) MCM-41, b) PNAS-MS

as the parent MCM-41 and a uniform 2nm thick polymer coating was observed around the silica particle after grafting. Thermogravimetric analysis (TGA, Figure 4.3) of the hybrid materials yielded 58% weight loss from the grafted polymer when heated in the N₂ atmosphere to 800 °C while almost no weigh loss was observed for pure MCM-41 in the same temperature range (Figure 4.3). Poly(*N*-acryloxysuccinimide) around the entrance of mesopore can be cross-linked by adding cystamine.^{7e,10} The successful crosslinking of NAS units of PNAS-MS was confirmed by various spectroscopic methods. A decrease in intensity of powder X-ray diffraction (XRD) peaks may be ascribed to the pore-filling effect induced by cross-linking (Figure 4.4).² N₂ sorption measurement of PNAS-MS exhibited the typical type IV isotherms of mesoporous materials while cross-linked PNAS-MS showed an isotherm characteristic of nonporous materials (Figure 4.5). The change of sorption type together with a decrease of surface area and pore size distribution indicated the capping effect of the polymeric network after cross-linking.² The FTIR peaks (Figure 4.1) around 1730-1822 cm⁻¹ disappeared while the absorption peaks of amide groups at around 1558-1651 cm⁻¹ appeared,¹¹ which further confirmed the substitution of *N*-oxysuccimide unit by cystamine. TGA of cross-linked PNSA-MS showed 51% weight loss (Figure 4.3), the lower weight loss compared with PNAS-MS indicated the substitution of *N*-oxysuccimide with cystamine in the molar ratio 2:1 between *N*-oxysuccimide and cystamine, the optimal reaction ratio to form the cross-linked network.(see *Notes* in Figure 4.3)

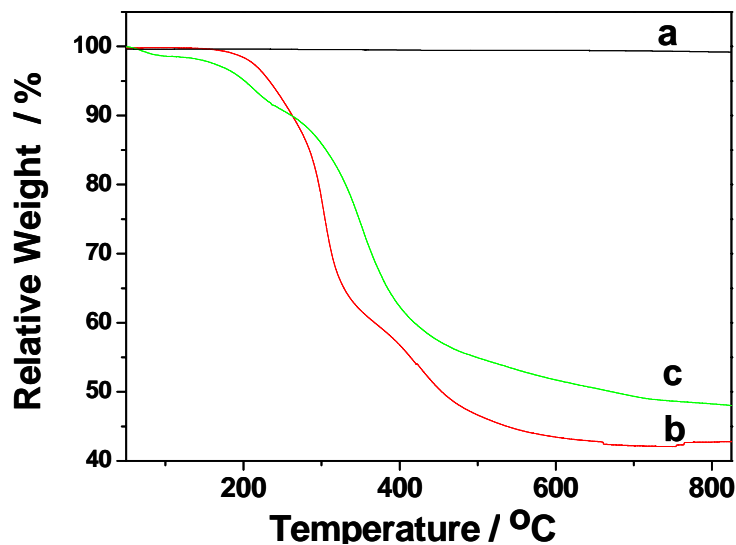
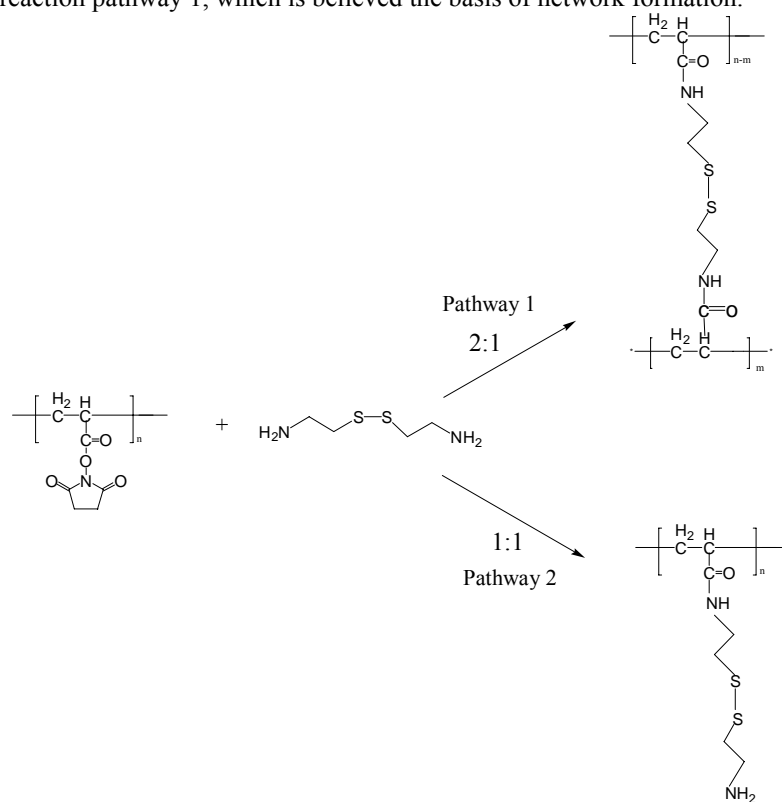


Figure 4.3 TGA of a)MCM-41, b)PNAS-MS and c) cross-linked PNAS-MS

Notes: Weight loss of PNAS-MS compared with pure mesoporous silica MCM-41 indicated that the grafting density of NAS monomer is about 8.27 mmol NAS/g SiO₂. If the reaction is proceeded under complete substitution with ratio of NAS : cystamine 2: 1(pathway 1), the weight loss of substituted PNAS-MS should be 51.8%. If the reaction ratio of NAS : cystamine is 1: 1(pathway 2), the weight loss of substituted PNAS-MS should be 63.0%.The TGA result for cross-linked PNAS-MS(52% loss) supported the reaction pathway 1, which is believed the basis of network formation.



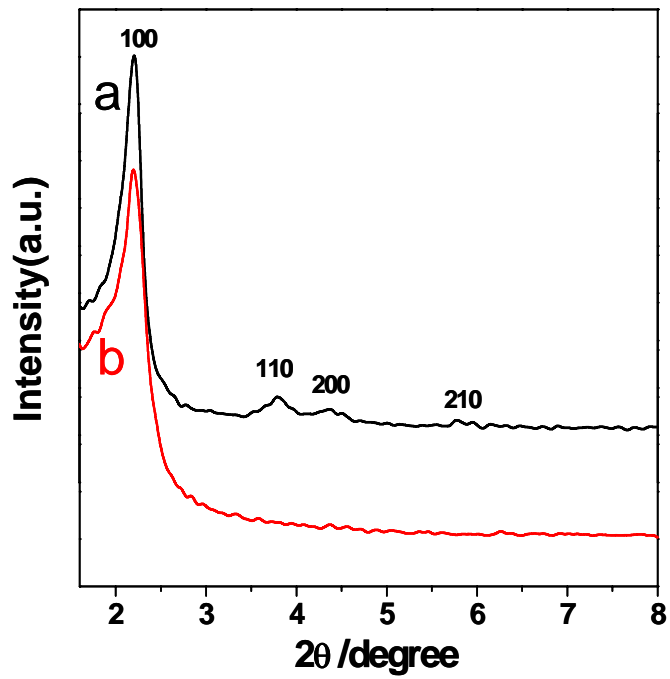


Figure 4.4 XRD of a) PNAS-MS and b) cross-linked PNAS-MS

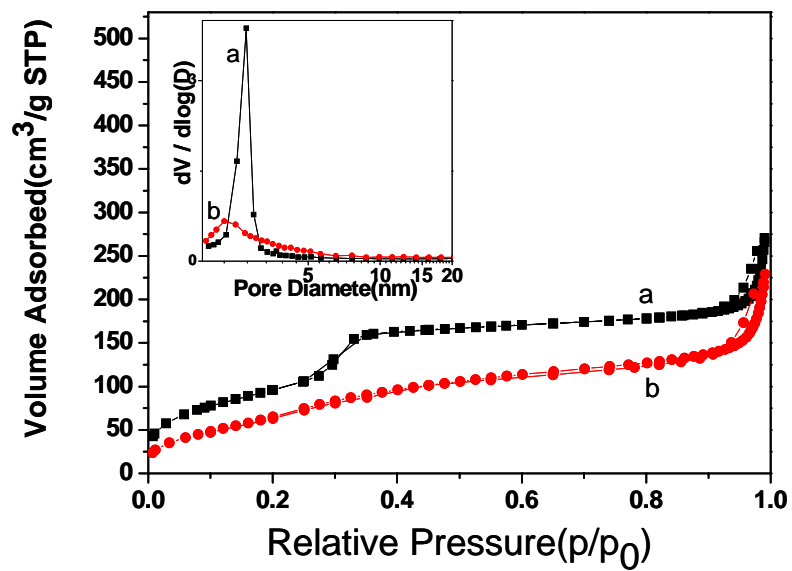


Figure 4.5 BET nitrogen sorption isotherms and BJH pore size distribution plots (inset) of a) PNAS-MS and b) cross-linked PNAS-MS

To investigate the redox-responsive gating behavior of the hybrid nanomaterials, rhodamine B was first loaded by soaking PNAS-MS in a phosphate-buffered saline (PBS) solution (pH 7.4) of rhodamine B. Cystamine was then added into the mixture to crosslink the polymer chain around mesoporous silica. The excessive rhodamine B was removed by centrifugation and repeated washing with water. The resulting particles were then dispersed in the PBS buffer to test their controlled release property. Prior to the addition of DTT, the intensity of rhodamine B is essentially constant, indicating no leakage of the entrapped dye molecules. The addition of DTT induced the release of dye molecules, and the release profile in Figure 4.6a exhibited a rapid molecular transport in the presence of a high concentration of DTT (2.16×10^{-2} M). In comparison, the dye delivery is relatively slow at a low DTT concentration (2.16×10^{-4} M), indicating the gate-like ensemble is ajar. The effect of DTT concentration can be further confirmed in Figure 4.6b as the released dye concentration is positively dependent on the added DTT amount. This behavior can be ascribed to the different degrees of cleavage due to the difference in the concentration of the disulfide reducing agent, which demonstrates the tunable gating effect of the material reported here. In comparison, 1,6-hexadiazine cross-linked ensemble shows no induced release with the addition of DTT.

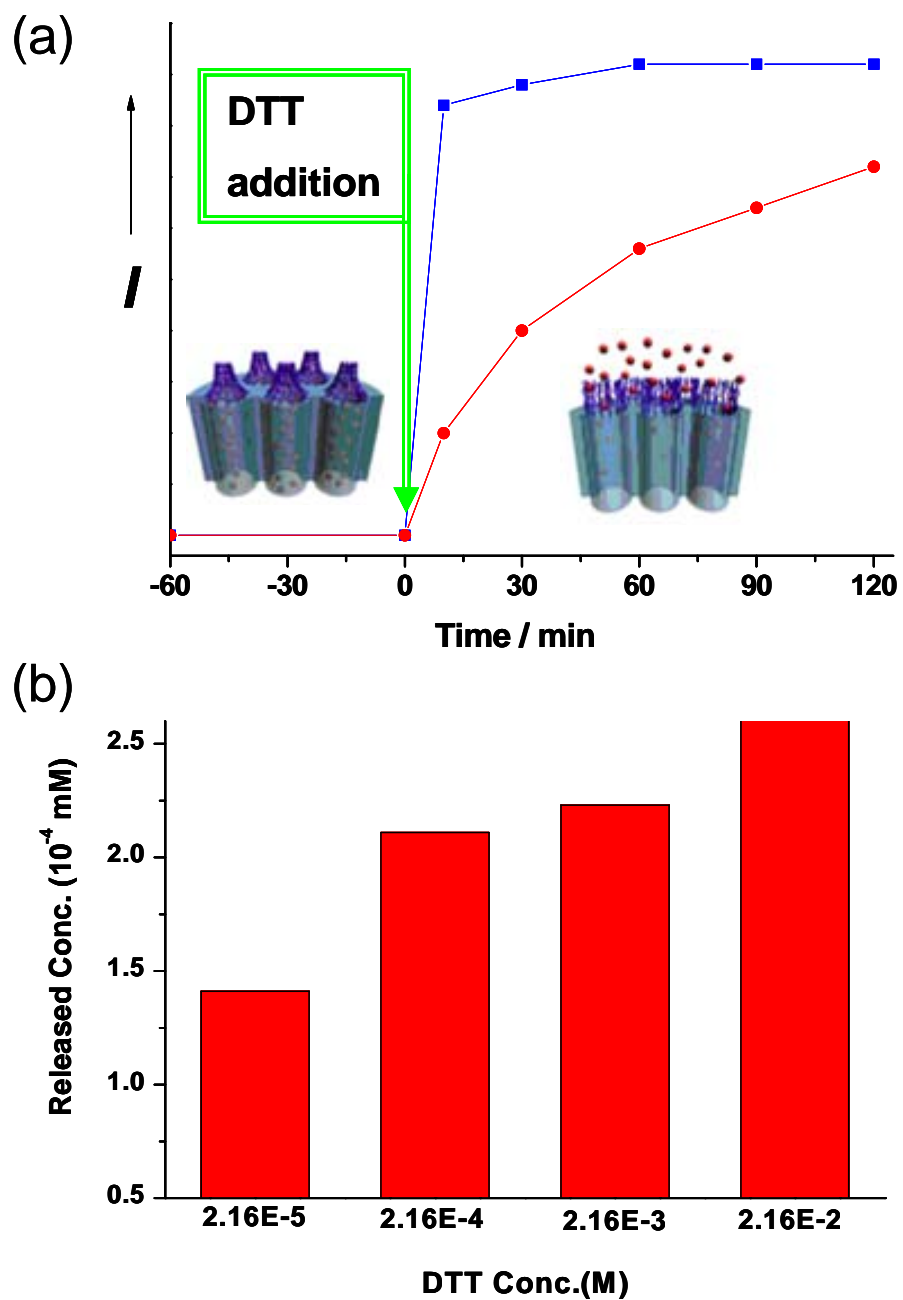


Figure 4.6 (a) Time course of rhodamine B release from hybrid materials in the presence of DTT concentrations 2.16×10^{-2} M (blue) and 2.16×10^{-4} M (red). (b) The DTT concentration-dependent releases. Released dye concentrations are measured after 2h of the DTT addition.

4.4 Conclusion

In conclusion, we report here the controlled release of guest molecules from mesoporous silica particles by using polymer network as a redox-responsive valve. PNAS-MS was filled with guest molecules and then blocked by adding cystamine to crosslink the PNAS chain around the pore opening. The loaded molecules were released from the hybrid materials by the cleavage of the disulfide linker of the polymeric network with the addition of disulfide reducing agents dithiothreitol (DTT). Since disulfide bonds can also be cleaved by using cell-produced antioxidants (e.g., dihydrolipoic acid or glutathione), the system reported here is promising for biosensor and in vivo site-specific drug delivery. This approach could also provide a general route to graft other functional polymers onto the surface of silica particles for various applications.

4.5 References

1. (a) Trewyn, B. G.; Slowing, I. I.; Giri, S.; Chen, H.; Lin, V. S.-Y. *Acc. Chem. Res.* **2007**, *40*, 846. (b) Slowing, I. I.; Trewyn, B. G.; Giri, S.; Lin, V. S.-Y. *Adv. Func. Mater.* **2007**, *17*, 1225. (c) Trewyn, B. G.; Giri, S.; Slowing, I. I.; Lin, V. S.-Y. *Chem. Comm.* **2007**, 3236. (d) Vallet-Regi, M.; Balas, F.; Acros, D. *Angew. Chem., Int. Ed.* **2007**, *46*, 7548.
2. (a) Lai, C.-Y.; Trewyn, B. G.; Jeftinija, D. M.; Jeftinija, K.; Xu, S.; Jeftinija, S.; Lin, V. S.-Y. *J. Am. Chem. Soc.* **2003**, *125*, 4451. (b) Giri, S.; Trewyn, B. G.; Stellmaker, M. P.; Lin, V. S.-Y. *Angew. Chem., Int. Ed.* **2005**, *44*, 5038.
3. (a) Mal, N. K.; Fujiwara, M.; Tanaka, Y. *Nature* **2003**, *421*, 350. (b) Mal, N. K.; Fujiwara, M.; Tanaka, Y.; Taguchi, T.; Matsukata, M. *Chem. Mater.* **2003**, *15*, 3385.
4. Casaus, R.; Climent, E.; Marcos, M. D.; Martinez-Manez, R.; Sancenon, F.; Soto, J.; Amoros, P.; Cano, J.; Ruiz, E. *J. Am. Chem. Soc.* **2008**, *130*, 1903.
5. (a) Hernandez, R.; Tseng, H.-R.; Wong, J. W.; Stoddart, J. F.; Zink, J. I. *J. Am. Chem. Soc.* **2004**, *126*, 3370. (b) Nguyen, T. D.; Tseng, H.-R.; Celestre, P. C.; Flood, A. H.; Liu, Y.; Stoddart, J. F.; Zink, J. I. *Proc. Natl. Acad. Sci. U.S.A.*

- 2005**, *102*, 10029. (c) Nguyen, T. D.; Liu, Y.; Saha, S.; Leung, K. C.-F.; Stoddart, J. F.; Zink, J. I. *J. Am. Chem. Soc.* **2007**, *129*, 626. (d) Nguyen, T. D.; Leung, K. C.-F.; Liong, M.; Pentecost, C. D.; Stoddart, J. F.; Zink, J. I. *Org. Lett.* **2006**, *8*, 3363. (e) Angelos, S.; Yang, Y.-W.; Patel, K.; Stoddart, J. F.; Zink, J. I. *Angew. Chem., Int. Ed.* **2008**, *47*, 2222. (f) Leung, K. C.-F.; Nguyen, T. D.; Stoddart, J. F.; Zink, J. I. *Chem. Mater.* **2006**, *18*, 5919. (g) Nguyen, T. D. K.; Leung, C. F.; Liong, M.; Liu, Y.; Stoddart, J. F.; Zink, J. I. *Adv. Funct. Mater.* **2007**, *17*, 2101. (h) Patel, K.; Angelos, S.; Dichtel, W. R. Coskun, A.; Yang, Y.-W.; Zink, J. I.; Stoddart, J. F. *J. Am. Chem. Soc.* **2008**, *130*, 2382.
- 6 O'Reilly, R. K.; Hawker, C. J.; Wooley, K. L. *Chem. Soc. Rev.* **2006**, *35*, 1068.
7. (a) Kakizawa, Y.; Harada, A.; Kataoka, K. *Biomacromolecules* **2001**, *2*, 491. (b) Tian, L.; Yam, L.; Wang, J.; Tat, H.; Uhrich, K. E. *J. Mater. Chem.* **2004**, *14*, 2317. (c) Bronich, T. K.; Keifer, P. A.; Shlyakhtenko, L. A.; Kabanov, A. V. *J. Am. Chem. Soc.* **2005**, *127*, 8236. (d) Lee, W.-C.; Li, Y.-C.; Chu, I.-M.; *Macro. Biosci.* **2006**, *6*, 846. (e) Li, Y.; Lokitz, B. S.; Armes, S. P.; McCormick, C. L. *Macromolecules* **2006**, *39*, 2726. (f) Hu, F.-Q.; Ren, G.-F.; Yuan, H.; Du, Y.-Z.; Zeng, S. *Colloids Surf. B: Biointerf.* **2006**, *50*, 97. (g) Huo, Q. S.; Liu, J.; Wang, L. Q.; Jiang, Y. B.; Lambert, T. N.; Fang, E. *J. Am. Chem. Soc.* **2006**, *128*, 6447. (h) Jiang, X.; Ge, Z.; Xu, J.; Liu, H.; Liu, S. *Biomacromolecules* **2007**, *8*, 3184.
8. Yang, Q.; Wang, S.; Fan, P.; Wang, L.; Di, Y.; Lin, K.; Xiao, F.-S. *Chem. Mater.* **2005**, *17*, 5999
9. Peng, Q.; Lai, D. M. Y.; Kang, E. T.; Neoh, K. G. *Macromolecules* **2006**, *39*, 5577.
10. Zhang, J.; Jiang, X.; Zhang, Y.; Li, Y.; Liu, S. *Macromolecules* **2007**, *40*, 9125.
11. Hu, Z.; Liu, Y.; Hong, C.; Pan, C. *J. Appl. Polym. Sci.* **2005**, *98*, 189.

Chapter Five

Multiresponsive Supramolecular Nanogated Ensembles*

5.1 Introduction

Supramolecular chemistry has been widely used in the construction of molecular shuttles, motors and nanomachines.¹ Due to the unique features of mesoporous silica (MS), such as uniform and tunable pore structure, and great diversity in surface functionalization, MS have been used as useful and versatile solid supports to construct various hybrid materials in catalysis, enzyme immobilization, drug delivery, and imaging.²

By combining functional supramolecular parts, a series of MS based supramolecular nanovalves for controlled release have been developed that are responsive to distinct external stimuli. Tetracationic cyclophane based rotaxane and pseudorotaxane caps that could undergo conformational changes triggered by redox chemistry were first reported as gatekeeper for mesoporous silica MCM-41.³ The supramolecular nanovalves controlled by pH and competitive binding were later developed.⁴ Cyclodextrin(CD), a well-known and readily available molecular host in supramolecular chemistry, has recently been used as a new functional component for building up MS based stimuli-responsive nanocarriers. CD-based polypseudorotaxanes could work as pH-responsive molecular gate to control the

* Reproduced with permission from *J. Am. Chem. Soc.* **2009**, 131, 15128. copyright 2009 American Chemical Society

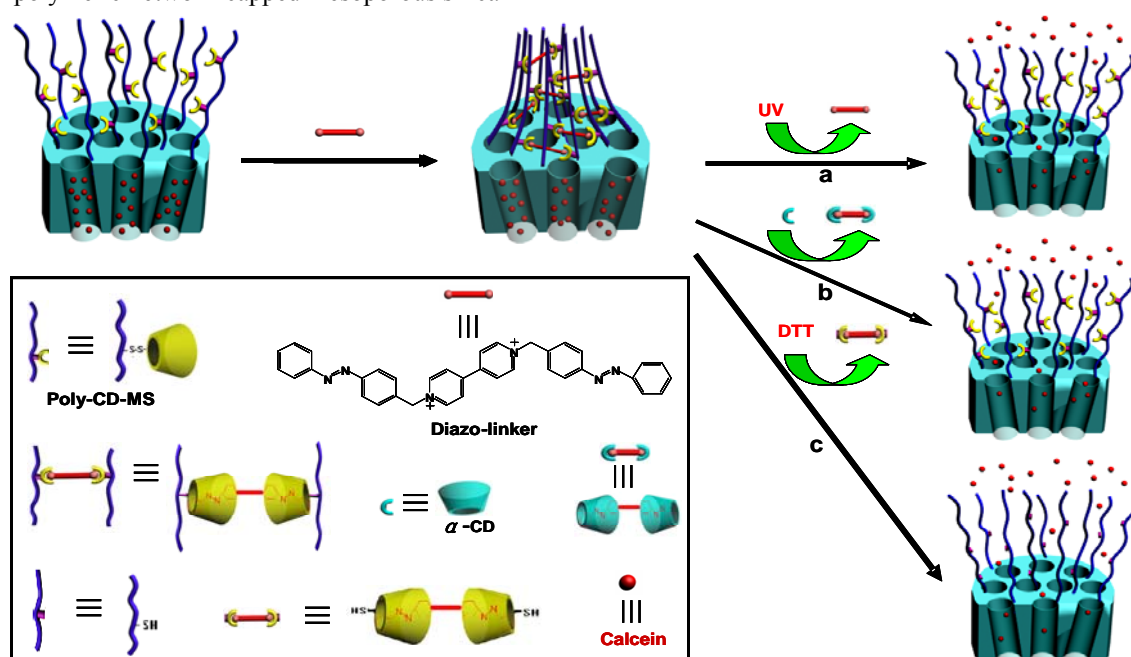
release of molecules from mesopore due to its pH-dependent capability in threading/dethreading the ethyleneimine polymer grafted on MCM-41.⁵ Alternative methods for MS controlled release using enzyme⁶ and light⁷ have also been studied using CD-based rotaxane and pseudorotaxane, respectively.

Responsive polymers are another widely used functional part to construct MS-based controlled release systems, such as thermo-responsive nanocontainer from poly(NIPAAm)-MS hybrid materials.⁸ We recently introduced cross-linkable polymer into mesoporous silica to construct a redox-responsive nanogated system, in which labile polymeric network could work as gatekeeper to control molecules transport.⁹ In this work, we seek to develop a multi-responsive nanogated system by integrating the advantages of polymeric network as capping agent with versatile assembly/disassembly of CD-based supramolecular chemistry. Herein we report a novel supramolecular nanogated material responsive to different stimuli relying on distinct motifs. The system is based on mesoporous silica grafted with β -CD bearing polymer (denoted as Poly-CD-MS). The working principle is illustrated in Scheme 5.1. The polymer around the silica can be cross-linked to form a polymeric network to block the molecule transport by the addition of diazo-linker, a water-soluble ditopic guest molecules with azobenzene group at each end.¹⁰ Such crosslinking is possible because it is well established that the *trans*-azobenzene group has high binding affinity with β -CD. On the other hand, such binding complex disassociates when *trans*-azobenzene is transformed to *cis*-azobenzene upon photoirradiation^{7,11}.

Therefore, the polymeric network that blocks the pore of MS can be opened by cleaving the linkage with UV irradiation, leading to light-controlled release (Pathway a).

The disassociation of supramolecular complex and the release of entrapped molecules can also be realized by addition of competitive host α -CD which favors the formation of inclusion complexes with azobenzene group more than β -CD does^{10, 11b,12}(Pathway b). Furthermore, since β -CD is linked to the polymer main chains through the S-S bond, the polymeric network can also be opened by cleaving the disulfide bond in the presence of disulfide reducing agents such as dithiothreitol (DTT), leading to the redox-controlled release (Pathway c).

Scheme 5.1 Schematic illustration of multi-responsive nanogated ensemble based on supramolecular polymeric network-capped mesoporous silica



5.2 Experimental Section

S-(2-Aminoethylthio)-2-thiopyridine Hydrochloride was synthesized following the reported procedure¹³ : 8.82g of aldrithiol-2 was dissolved in 40 mL of methanol and 1.2 mL of acetic acid, in which 18ml of methanol containing 2.28g of 2-aminoethylthiol hydrochloride added dropwise over 0.5h.. The reaction mixture was stirred for another 48 h and was concentrated under reduced pressure to give yellow oil. The product was washed with 100 mL of diethyl ether and dissolved in 10 mL of methanol, and then was precipitated by addition of 600 mL of cold anhydrous diethyl ether as white power. ¹H NMR(400 MHz, CDCl₃): 8.6 (d, 1H), 7.6 (t, 1H), 7.3 (d, 1H), 7.2(t, 1H), 3.4 (t, 2H) and 3.3 (t, 2H).

Per-6-thio-β-cyclodextrin was prepared from β-CD according to previous method reported by Stoddart¹⁴. Triphenylphosphine (20.2 g) and I₂ (20.25 g) were dissolved with stirring in dry DMF (80 ml). β-CD (5.8 g) was then added and was stirred at 70 °C under N₂ atmosphere for 18 h. The reaction solution was concentrated under the reduced pressure to half volume and the solution was adjusted to pH 9–10 by addition 30ml of 3M sodium methoxide in methanol with simultaneous cooling to room temperature. The solution was kept at room temperature for 30 min, then poured into 400mL of methanol to form a precipitate. The precipitate was filtered and was washed with methanol and Soxhlet extracted with methanol without discoloration. The product was dried under vacuum to give *per-6-iodo-β-cyclodextrin*. 0.965g of

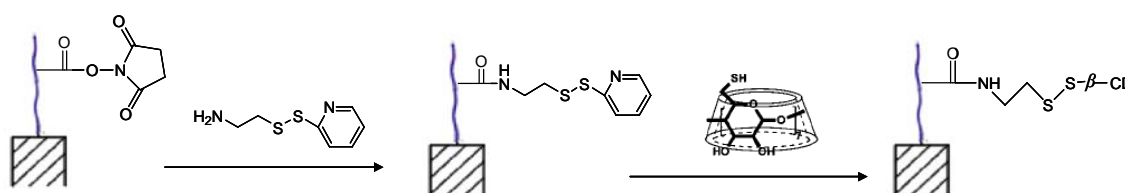
per-6-iodo-β-cyclodextrin. and 0.301g of thiourea was dissolved in 10ml of DMF (10 mL).and the mixture was heated to 70 °C under N₂ atmosphere for 19 h. The DMF was removed under reduced pressure to obtain the yellow oily product. The reaction mixture was dissolved in water (50 mL), subsequently sodium hydroxide (0.26 g) was added and the reaction mixture refluxed for 1 h under N₂ atmosphere. The resulting suspension was acidified with aqueous potassium hydrogensulfate and the precipitate was filtered off, washed thoroughly with water. The product was suspended in water (50 mL) and the minimum amount of potassium hydroxide added to give a clear solution; the product was then reprecipitated by acidifying with aqueous KHSO₄. The resulting fine powdered precipitate was carefully dried under vacuum over P₂O₅ to yield white powder. ¹H NMR (400 MHz, CD₃SOCD₃) 5.90(d, 7H), 5.78(s, 7H), 4.9(d, 7H), 3.4-3.7(m, 28H), 3.2(overlap with water peak), 2.7(m,7H), 2.1(t, 7H)

1,1'-bis{4-[(E)-phenyldiazenyl] benzyl}-4,4'-bipyridium (Br₂) was chosen as water soluble diazo-linker and prepared by the reported method¹⁰ Nitrosobenzene (0.54 g) and *p*-aminotoluene (0.54 g) were dissolved in 5 mL acetic acid. The mixture was stirred for 24 h under N₂ atmosphere. The formed precipitate (A) was filtered and recrystallized from ethanol/water. The, A (1.07 g), *N*-bromosuccinimide (0.97 g), benzoyl peroxide (49.3 mg) and CCl₄ (20 mL) were refluxed for 24 h under N₂ atmosphere. The resulting solution was filtered while it was hot, and the filtrate was concentrated under reduced pressure to give B. B (0.27 g) and 4,4'-dipyridine (70.0

mg) in 5 mL DMF was allowed to react at 100 °C for 24 h. After being cooled to room temperature, the orange precipitate was collected by filtration and washed with petroleum ether and ethyl acetate respectively. ¹H NMR (400 MHz, CD₃SOCD₃): 9.5(d, 4H), 8.8(d, 4H), 7.98(d, 4H), 7.90(m, 8H), 7.6(m, 6H), 6.0(s, 4H)

Synthesis of Poly-CD-MS (Scheme 5.2): MCM-41-type mesoporous silica(MS) nanosphere was synthesized using reported method¹⁵ with mean diameter ~140nm, which is suitable for drug delivery application^{2g}. PNAS-MS was synthesized by our reported method.⁹ 50mg PNAS-MS and 50mg *S*-(2-Aminoethylthio)-2-thiopyridine Hydrochloride in 5ml PBS buffer (100mM, pH 7.4) were stirred at 40°C for 24h to give Poly-Py-MS. Poly-CD-MS was obtained by reaction of 20mg Poly-Py-MS and 70mg per-6-thio-β-cyclodextrin in 2ml DMF for 24h.

Scheme 5.2. Schematic outline of synthesis of Poly-CD-MS



Characterization: Powder X-ray diffraction (XRD) patterns were recorded on a Bruker D8 Advance diffractometer with Cu K α radiation (40 kV, 40 mA). N₂ sorption analysis was performed on a Micromeritics ASAP2010 volumetric adsorption analyzer at 77 K. Fourier transform infrared (FT-IR) spectra were performed on Bruker Equinox 55 with KBr plates. Thermal gravimetric analysis was carried out on

a TA Instruments SDT Q600 simultaneous DSC/TGA thermal analyzer under flowing N₂ at a heating rate of 10 °C/min.

Loading, capping and release experiments: Poly-CD-MS (5.0mg) was stirred in 2.5 ml 3.2 mM calcein in PBS solution(100mM, pH 7.4) at room temperature for 24h. Then diazo linker (0.336mg, 1:2 molar ratio of diazo-linker and β -CD in Poly-CD-MS) was added to the suspension and the mixture was stirred for another 24h before the precipitate was centrifuged, washed extensively with water. To investigate the multi-responsive properties, calcein-loaded silica particle (1.0mg) was dispersed in 1ml PBS solution. Release profiles were obtained by plotting the absorbance intensity of calcein in solution at 495 nm as a function of time. The activation of nanogate was accomplished by applying the different external stimuli. For the UV irradiation, UV light (0.3W cm⁻² and 365 nm) from handheld UV lamp is directly focused on the whole releasing body solution

5.3 Results and Discussion

Poly(*N*-acryloxysuccinimide) grafted mesoporous silica (denoted as PNAS-MS) was obtained by using a previously reported method.⁹ Substitution of *N*-oxysuccinimide group along the polymer with *S*-(2-Aminoethylthio)-2-thiopyridine gave an intermediate material (denoted as Poly-Py-MS) with pyridyldithio functionality, which was confirmed by the characteristic peaks of acylamide at 1650 cm⁻¹ and of pyridine ring at 1450 cm⁻¹ in FTIR spectra. (Figure 5.1). Since pyridyldithio

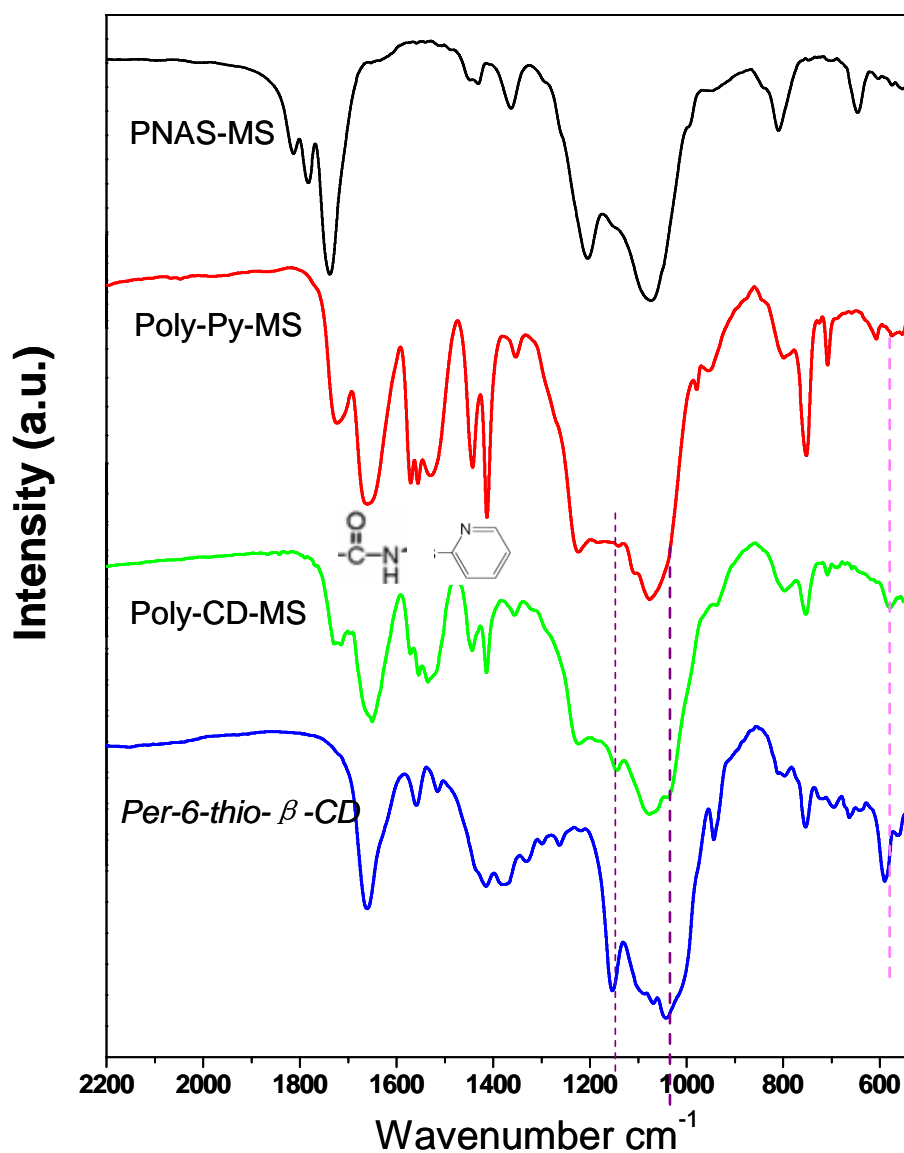


Figure 5.1. FTIR of PNAS-MS, Poly-Py-MS, Poly-CD-MS and per-6-thio-β-cyclodextrin

functionality is widely used for efficient thiol-coupling¹⁶, β-CD was easily immobilized onto the polymer via the S-S linkages by thiol-coupling reaction between pyridyldithio group and per-6-thio-β-cyclodextrin in DMF to give desired hybrid materials, Poly-CD-MS.

X-ray diffraction and N₂ sorption measurements showed the hybrid materials retain

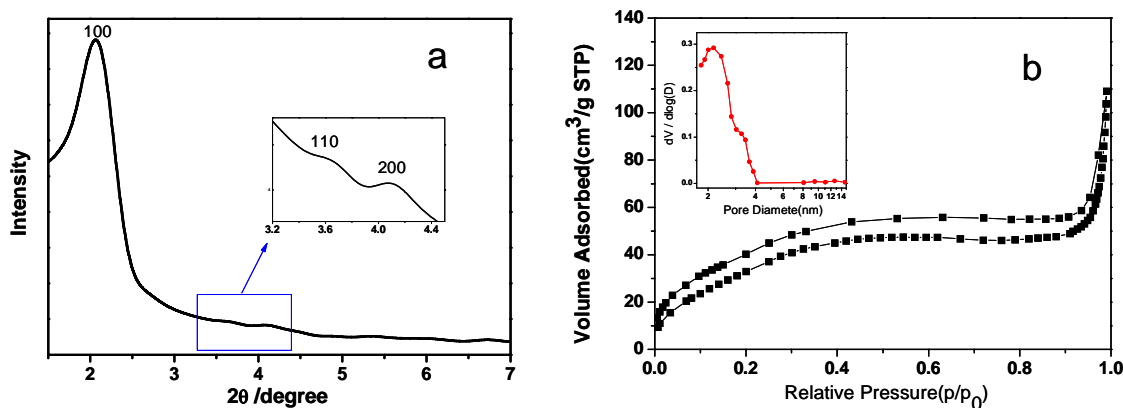


Figure 5.2. (a)XRD and (b) BET nitrogen sorption isotherms and BJH pore size distribution plots (inset) of Poly-CD-MS

the mesoporous structure upon functionalization with β -CD (Figure 5.2). The relative IR peak intensity of pyridine ring in Poly-CD-MS decreased while several new characteristic peaks from per-6-thio- β -cyclodextrin were observed after β -CD immobilization (Figure 5.1), which confirmed the successful substitution of pyridyldithio groups by β -CD through S-S bonds. Pyridinethione released from thiol coupling reaction exhibited a strong absorption at $\sim 370\text{nm}$ (Figure 5.3) and the released amount of pyridinethione was estimated to be 1.17mmol/g Poly-Py-MS by using the reported molar extinction coefficient ($5800\text{ M}^{-1}\text{ cm}^{-1}$) of pyridinethione in DMF^{16b}. Thermogravimetric analysis (TGA) showed 6% more weight loss for Poly-CD-MS (61% weight loss) than that for Poly-Py-MS(55% weight loss), resulting from the weight difference of conjugated β -CD and the released pyridinethione. From the released amount of pyridinethione and difference between TGA weight losses, the concentration of β -CD in the hybrid materials is about 0.196 mmol/g Poly-CD-MS.

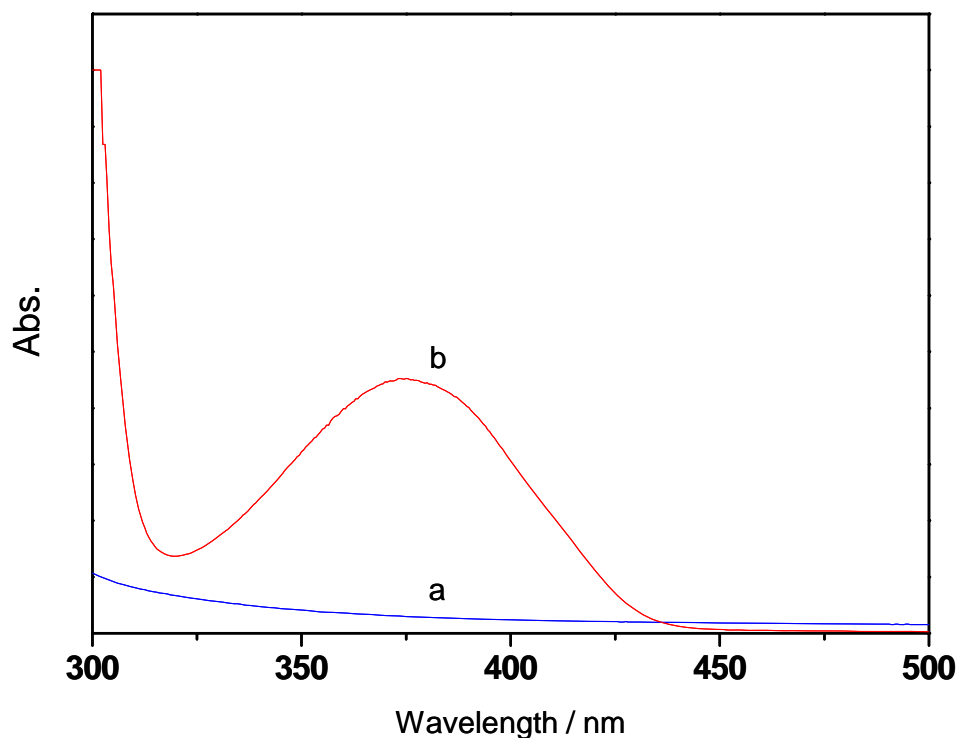


Figure 5.3. UV-vis spectra of per-6-thio- β -cyclodextrin in DMF (a) before and (b) after the coupling reaction with Poly-Py-MS

To investigate the multi-responsive gating behavior of the hybrid nanomaterials, calcein was loaded as model molecule by soaking Poly-CD-MS in a phosphate-buffered saline (PBS) solution (pH 7.4) of calcein. Then, appropriate amount of diazo-linker(1:2 molar ratio of diazo-linker and β -CD in Poly-CD-MS) was added into the mixture to cross-link the polymer chains around mesoporous silica. The excess calcein was removed by centrifugation and repeated washing with PBS buffer. The loading of calcein was determined to be 0.080 mmol/g hybrid materials. The calcein-loaded particles were then dispersed in the PBS buffer to test their controlled release property. As shown in Figure 5.4(curve a), without the application

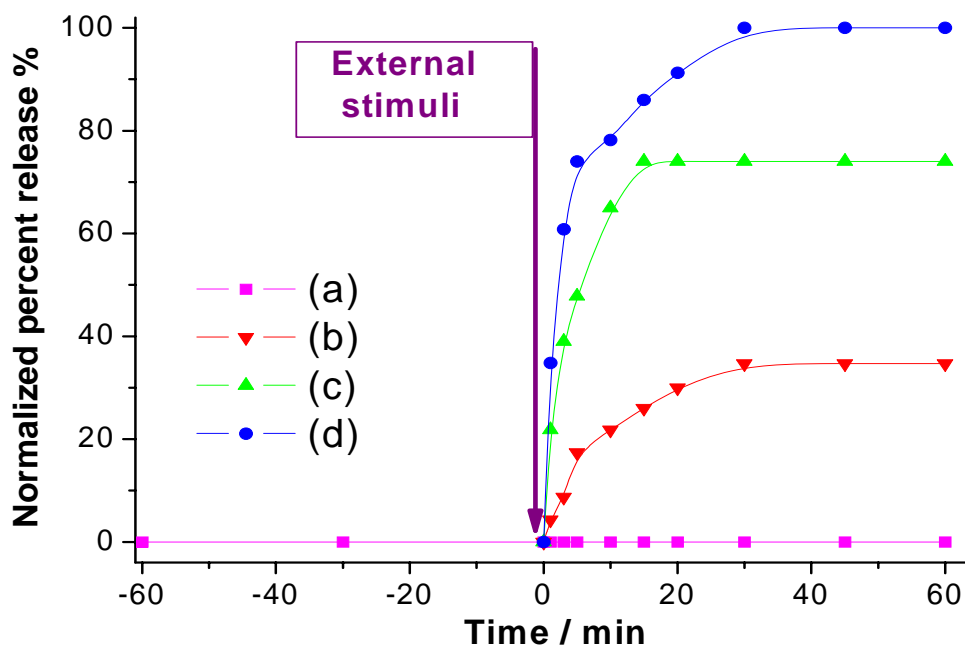


Figure 5.4 Controlled release of calcein from cross-linked Poly-CD-MS (1.0 mg) in 1 mL of PBS solution (100.0 mm, pH 7.4). (a) no noticeable release was observed in the absence of external stimuli. At time 0, triggered by (b)UV, (c) 5mg DTT (after 60min, 5mg more DTT did not induce more release), (d) 5mg α -cd (~30 equiv to β -cd of Poly-CD-MS, after 60min, 5mg more α -cd did not induce more release)

of external stimuli, no release was observed, indicating no leakage of the entrapped molecules and good efficiency of supramolecular network to retain entrapped molecules. When UV light (0.3W cm^{-2} and 365 nm) was focused on the releasing solution, the release of calcein was observed due to the dissociation of cross-linked polymer complex resulting from the *trans*-to-*cis* isomerization of azobenzene group under UV light (Figure 5.4, curve b). The release reached equilibrium about 30% at 30min, which is consistent with the reported 30min required for *trans/cis* photostationary state.¹⁷ The lower releasing saturation amount under UV irradiation may be ascribed to the existence of some *cis*-azo/ β -CD complex and hence the partial

stable cross-linker network. The addition of DTT also induced the release of entrapped molecules and the release profile (Figure 2, curve c) exhibited faster releasing dynamics than that under UV light. The presence of excess α -CD induced molecule transport at much faster rate with saturated releasing concentration at 0.0056 mM than that of DTT, which is believed to be the result of higher solubility¹⁸ and association complex constant¹² of α -CD than thiolated β -CD released through the S-S breaking. Such different releasing behavior under the different environment conditions can be used to meet the desirable nanogating requirements.

5.4 Conclusion

In conclusion, we reported here the controlled release of molecules from mesoporous silica particles by using supramolecular polymer network as multi-responsive valve. Poly-CD-MS was filled with model molecules and then blocked by adding diazo-linker to cross-link the β -CD bearing polymer chains around outer surface of mesoporous silica. The trapped molecules were released from the hybrid materials by the cleavage of polymeric network using UV irradiation, competitive binding, or with the addition of disulfide reducing agents, dithiothreitol (DTT). The multi-responsive supramolecular nanogating hybrid materials exhibit distinct releasing property under the different external stimuli, which make the system reported here promising to meet the various requirements in biosensor and *in vivo* sites-specific drug delivery applications.

5.5 References

1. (a) Harada, A. *Acc. Chem. Res.* **2001**, *34*, 456. (b) Angelos, S.; Johansson, E.; Stoddart, J. F.; Zink, J. I. *Adv. Funct. Mater.* **2007**, *17*, 2261.
2. (a) Kesanli, B.; Lin, W. *Chem. Comm.* **2004**, 2284. (b) Mihalcik, DJ; Lin, W. *Angew. Chem. Int. Ed.* **2008**, *47*, 6229. (c) Zhu, H.; Liang, C.; Yan, W.; Overbury, S. H.; Dai, S. *J. Phys. Chem. B* **2006**, *110*, 10842. (d) Lei, C.; Shin, Y.; Liu, J.; Ackerman, E. J. *J. Am. Chem. Soc.* **2002**, *124*, 11242. (e) Lei, C.; Shin, Y.; Liu, J.; Ackerman, E. J. *Nano Lett.* **2007**, *7*, 1050. (f) Trewyn, B. G.; Slowing, I. I.; Giri, S.; Chen, H.; Lin, V. S.-Y. *Acc. Chem. Res.* **2007**, *40*, 846. (g) Slowing, I. I.; Trewyn, B. G.; Giri, S.; Lin, V. S.-Y. *Adv. Funct. Mater.* **2007**, *17*, 1225. (h) Trewyn, B. G.; Giri, S.; Slowing, I. I.; Lin, V. S.-Y. *Chem. Comm.* **2007**, 3236. (i) Taylor, K. M. L.; Kim, J. S.; Rieter, W. J.; An, H.; Lin, W.; Lin, W. *J. Am. Chem. Soc.* **2008**, *130*, 2154.
3. (a) Hernandez, R.; Tseng, H.-R.; Wong, J. W.; Stoddart, J. F.; Zink, J. I. *J. Am. Chem. Soc.* **2004**, *126*, 3370. (b) Nguyen, T. D.; Tseng, H.-R.; Celestre, P. C.; Flood, A. H.; Liu, Y.; Stoddart, J. F.; Zink, J. I. *Proc. Natl. Acad. Sci. U.S.A.* **2005**, *102*, 10029.
4. (a) Leung, K. C. F.; Nguyen, T. D.; Stoddart, J. F.; Zink, J. I. *Chem. Mater.* **2006**, *18*, 5919. (b) Nguyen, T. D.; Leung, K. C. F.; Liang, M.; Pentecost, C. D.; Stoddart, J. F.; Zink, J. I. *Org. Lett.* **2006**, *8*, 3363.
5. Park, C.; Oh, K.; Lee, S.; Kim, C. *Angew. Chem. Int. Ed.* **2007**, *46*, 1455.
6. Patel, K.; Angelos, S.; Dichtel, W. R.; Coskun, A.; Yang, Y.-W.; Zink, J. I.; Stoddart, J. F. *J. Am. Chem. Soc.* **2008**, *130*, 2382.
7. Ferris, D. P.; Zhao, Y.; Khashab, N. M.; Khatib, H. A.; Stoddart, J. F.; Zink, J. I. *J. Am. Chem. Soc.* **2009**, *131*, 1686.
8. (a) Fu, Q.; Rao, G. V. R.; Ista, L. K.; Wu, Y.; Andrzejewski, B. P.; Sklar, L. A.; Ward, T. L.; Lopez, G. P. *Adv. Mater.* **2003**, *15*, 1262. (b) You, Y.; Kalebaila, K. K.; Brock, S. L.; Oupicky, D. *Chem. Mater.* **2008**, *20*, 3354.
9. Liu, R.; Zhao, X.; Wu, T.; Feng, P. *J. Am. Chem. Soc.* **2008**, *130*, 14418.
10. Liu, Z.; Jiang, M. *J. Mater. Chem.* **2007**, *17*, 4249.
11. (a) Yang, L.; Takisawa, N.; Kaikawa, T.; Shirahama, K. *Langmuir* **1996**, *12*,

1154. (b) Takashima, Y.; Nakayama, T.; Miyauchi, M.; Kawaguchi, Y.; Yamaguchi, H.; Harada, A. *Chem. Lett.* **2004**, 890. (c) Zou, J.; Tao, F.; Jiang, M. *Langmuir* **2007**, *23*, 12791.
12. (a) Wang, Y. P.; Ma, N.; Wang, Z. Q.; Zhang, X. *Angew. Chem., Int. Ed.* **2007**, *46*, 2823. (b) Lahav, M.; Ranjit, K. T.; Katz, E.; Willner, I. *Chem. Commun.* **1997**, 259. 4254. The association constants constants for 1:1 complexation of *trans*-azo with α -CD and β -CD are 2.8×10^4 and 1700 M^{-1} , respectively.
13. You, Y.-Z.; Chun-Yan Hong, C.-Y.; Cai-Yuan Pan, C.-Y. *Adv. Funct. Mater.* **2007**, *17*, 2470.
14. Rojas, M.T.; Koniger, R.; Stoddart, J.F.; Kaifer, A.E. *J. Am. Chem. Soc.* **1995**, *117*, 336.
15. Lai, C.-Y.; Trewyn, B. G.; Jeftinija, D. M.; Jeftinija, K.; Xu, S.; Jeftinija, S.; Lin, V. S.-Y. *J. Am. Chem. Soc.* **2003**, *125*, 4451.
16. (a) Bontempo, D.; Heredia, K L.; Fish, B.A.; Maynard, H. D. *J. Am. Chem. Soc.*, **2004**, *126*,15372.(b) Liu, J.; Bulmus, V. Barner-Kowollik, C.; Stenzel, M. H.; Davis, T. P. *Macromol. Rapid Commun.* **2007**,*28*,305.
17. Zhu, Y., Fujiwara, M. *Angew. Chem., Int. Ed.* **2007**, *46*, 2241.
18. (a) Kitano, H.; Taira, Y. *Langmuir*, **2002**, *18*, 5835. (b) Kaifer, A.E. In *Nanoparticles: Building Blocks for Nanotechnology*, Rotello, V. M., Ed.; Kluwer: New York, **2004**, pp89-112.

Chapter Six

A Water-Soluble Deep Cavitand Acts as a Release Trigger for a Supramolecular Nanocap*

2.1 Introduction

Mesoporous silica is widely used as a porous solid support to construct various hybrid materials in catalysis, enzyme immobilization, drug delivery and imaging.¹ Mesoporous silica nanoparticles are also an attractive target for the encapsulation and controlled release of target molecules for targeted drug delivery. The ordered arrays of nanopores in these particles are of suitable size to contain the desired small molecules.² The concept of targeted delivery requires that the nanopores be “capped” with the substrate bound inside, and a mechanical release mechanism be incorporated to allow specificity in delivery. Most examples of this concept use covalent derivatization of the nanopores to introduce a blocking agent.³ Tetracationic cyclophane-based rotaxane and pseudorotaxane caps that can undergo conformational changes triggered by redox chemistry were reported as gatekeepers for mesoporous silica MCM-41.⁴ These blocking agents are moved from the pore opening by mechanical switching or fragmentation. Supramolecular association can also be used to control switching processes; supramolecular nanovalves controlled by pH and competitive binding have been developed,⁵ and cyclodextrin-based polypseudorotaxanes control the release of molecules from a mesopore due to pH

* Reproduced with permission from *Chem. Mater.* **2010**, 22,5797. copyright 2010 American Chemical Society

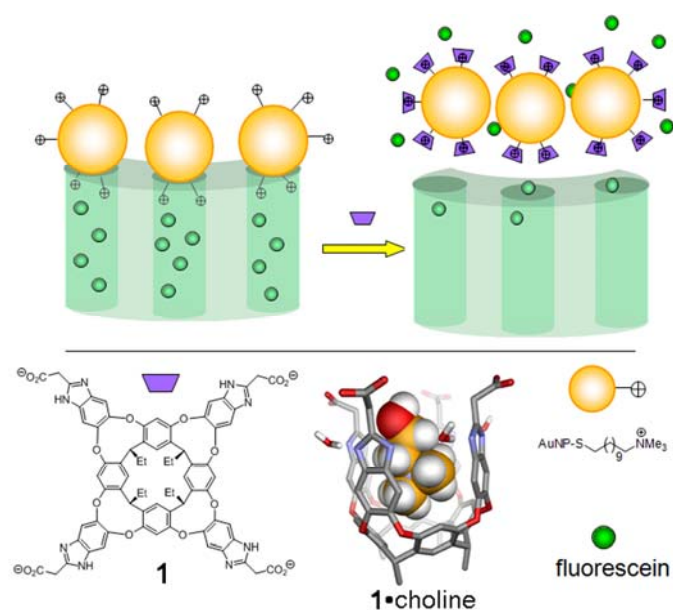
changes,⁶ enzymes and light.⁷ Nanoparticles have also been used to cap/uncap mesoporous silica channels under different stimuli.⁸ All these “cap-and-release” methods require covalent derivatization of the mesoporous silica. A far more attractive method is to use non-covalent forces to coordinate the cap itself. Derivatized gold nanoparticles can also be used for this procedure, and their coordination is dependent on charge: positive nanoparticles have a far greater affinity for the silica than neutral or negative equivalents.⁹ Changing the charge profile of the nanoparticles is a mild method of guest release.⁹ Here, we discuss a different method; the use of targeted supramolecular assemblies to disrupt the nanoparticle: silica association and release the entrapped guest species.

To favor the nanoparticle:silica assembly, alkyl-trimethylammonium ligands are attached to the gold nanoparticles. These provide positive charge to the nanoparticle, and are resistant to changes in pH. By introducing water-soluble deep cavitands as host molecules that can *selectively* bind trimethylammonium groups and interrupt the charge-based interaction between the nanoparticle and silica, guest release is possible. Cavitands are open-ended hosts that bind small molecules of complementary size, shape and chemical surface.¹⁰ Deep cavitands such as **1** self-assemble to form a cavity whose interior is surrounded by aromatic rings. The electron rich walls confer an ability to recognize suitable sized molecules with a thin layer of positive charge on the surface. Tetracarboxylate cavitand **1**¹¹ shows millimolar water solubility and forms kinetically stable complexes with substituted trimethylammonium cations in water

with binding affinities $>10^4 \text{ M}^{-1}$.¹² The strong binding is dominated by cation- π interactions between the surface of the guest and the polarized aromatic inner face of the deep cavitand.¹³ The positive charge is surrounded by a hydrophobic pocket, effectively shielding this charge from the exterior milieu.

The experiment is shown in Scheme 6.1. The nanopores in mesoporous silica can be filled with guest molecules by simple diffusion, then the pore openings can be blocked by gold nanoparticles through electrostatic interaction. Upon introduction of cavitand **1**, a strong host: guest interaction will take place, shielding the positively charged NMe_3 groups, lowering the silica: nanoparticle affinity and freeing the entrapped guests.

Scheme 6.1 a) Schematic illustration of the experiment; b) plan view of cavitand **1** and minimized structure of the **1**•choline complex (SPARTAN, AM1).



6.2 Experimental Section

^1H spectra were recorded on a Varian Inova 400 spectrometer. Proton (^1H) chemical shifts are reported in parts per million (δ) with respect to tetramethylsilane (TMS, $\delta=0$), and referenced internally with respect to the protio solvent impurity. Deuterated NMR solvents were obtained from Cambridge Isotope Laboratories, Inc., Andover, MA, and used without further purification. Powder X-ray diffraction (XRD) patterns were recorded on a Bruker D8 Advance diffractometer with Cu $K\alpha$ radiation (40 kV, 40 mA). N_2 sorption analysis was performed on a Micromeritics ASAP2010 volumetric adsorption analyzer at 77 K. Zeta potential analysis was performed on a ZetaPALS system. Fluorescence was taken using Spex Fluorolog Tau-3 fluorescence spectrophotometer. TEM images were recorded on a Philips Tecnai 12 transmission electron microscope. Cavitand **1**,^{12b} and *N,N*-trimethyl(undecylmercapto)ammonium iodide¹⁴ were synthesized according to literature procedures. All other materials were obtained from Aldrich Chemical Company, St. Louis, MO and were used as received.

Synthesis: MCM-41 was synthesized according to literature procedures:^{8b} *n*-Cetyl-trimethylammonium bromide (CTAB, 1.0 g) was dissolved in 480 mL of distilled water. NaOH (aq) (2.00 M, 3.50 mL) was added to CTAB solution, and the solution temperature was adjusted to 80 °C. Triethoxysilane (5.00 mL) was added drop-wise to the solution, and the mixture allowed to stir for 2 h at 80 °C. The resultant white precipitate was isolated by filtration. The silica particles were then calcinated at 550 °C for 5 h to remove the template.

The positively charged gold nanoparticles were synthesized according to literature procedures.¹⁴ Equimolar amounts of *N,N*-trimethyl(undecylmercapto)ammonium iodide and HAuCl₄ were combined in aqueous solution. The solution was stirred for 60 min before addition of a 10-fold molar excess of aqueous NaBH₄. After the solution was stirred for an hour, the AuNPs were purified by repeated washing and centrifugation. TEM analysis confirmed formation of nanoparticles, with a particle diameter of ~8 nm (see Figure 2).

Loading, capping and uncapping experiments: MCM-41 (25 mg) was stirred in 3 ml of 25 μM fluorescein aqueous solution at room temperature for 24 h. Positively charged AuNPs (5 mg) were added to the suspension and stirred for another 24 h. The suspension was centrifuged and washed extensively with water and isopropanol. To investigate responsive release properties, the fluorescein-loaded particle (2.0 mg) was dispersed in water (1 mL). The release of the fluorescein from the pore was monitored by measuring the fluorescence emission spectra with excitation at 490 nm.

6.3 Results and Discussion

Mesoporous silica MCM-41 was synthesized according to literature procedures.^{8b} The honeycomb-like structure of MCM-41 was confirmed by TEM analysis (Figure 6.1). The silica displayed a BET surface area of 973 m²/g and average pore diameter of 3.0 nm, as determined by N₂ sorption analysis (Figure 6.2). The positively charged gold nanoparticles (AuNP) were synthesized¹⁴ with a particle diameter of ~8 nm as

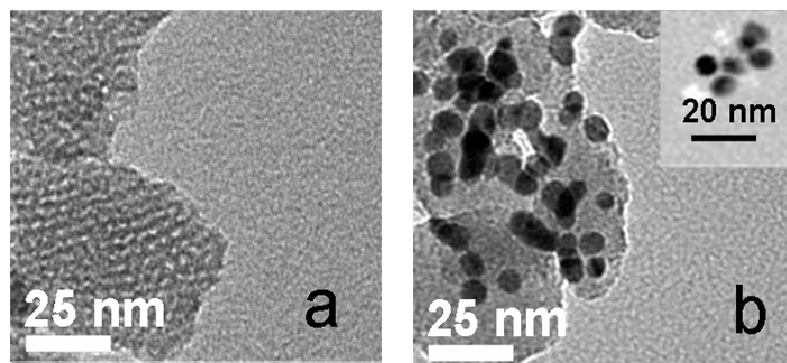


Figure 6.1. TEM of a) MCM-41, b) assembly of MCM-41 with AuNPs and inset in b) AuNPs

determined by TEM analysis (Figure 6.1 inset). The positive charge of the nanoparticle is conferred by attached mercapto-undecyl-trimethylammonium (TMA) ligands; charge measurements show a ζ potential of $+55.1 \pm 3.5$ mV. The aggregation of positively charged AuNPs around negatively charged MCM-41 (ζ potential: -48.5 ± 1.3 mV) can be confirmed by TEM microscopy. Figure 6.1 shows the TEM of

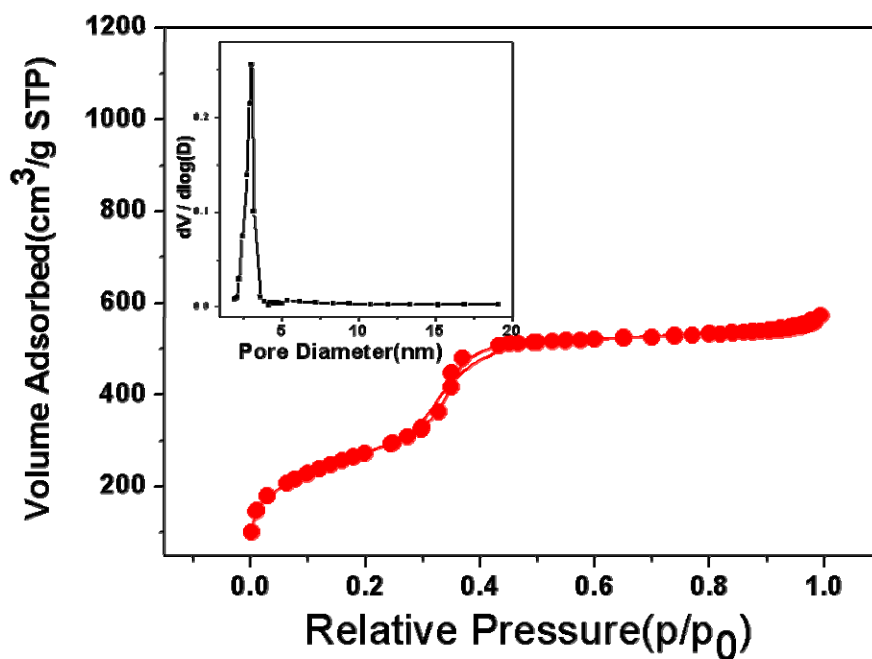


Figure 6.2 BET nitrogen sorption isotherms and BJH pore size distribution plots (inset) of MCM-41

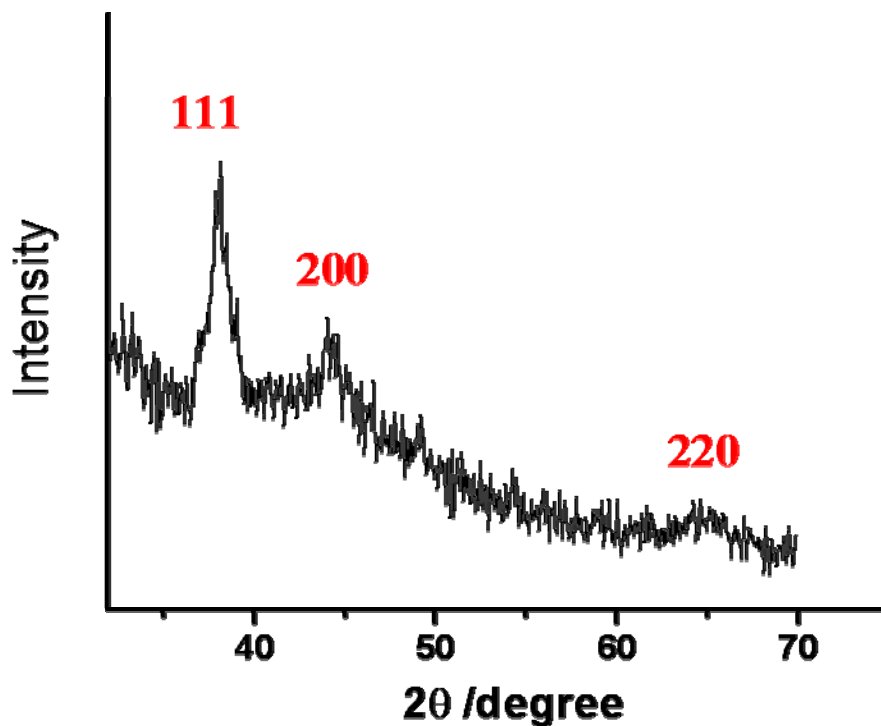


Figure 6.3. XRD of gold nanoparticles capped MCM-41

MCM-41 before and after capping with AuNPs. The hexagonally packed mesoporous channels could be clearly visualized before capping. In contrast, the TEM of AuNPs-capped MCM-41 (Figure 6.1b) shows dark spots on the exterior surface of the mesoporous silica, representing the aggregation of AuNPs around MCM-41. The presence of AuNPs was also confirmed by the appearance of (111), (200) and (220) diffraction peaks of AuNP in the powder XRD spectrum(Figure 6.3).

Cavitand **1** was prepared according to literature procedures.^{12b} The vase-like shape of the cavitand is stabilized by an array of hydrogen bonds incorporating water along its upper rim, and one molecule of THF is retained in its hydrophobic cavity during

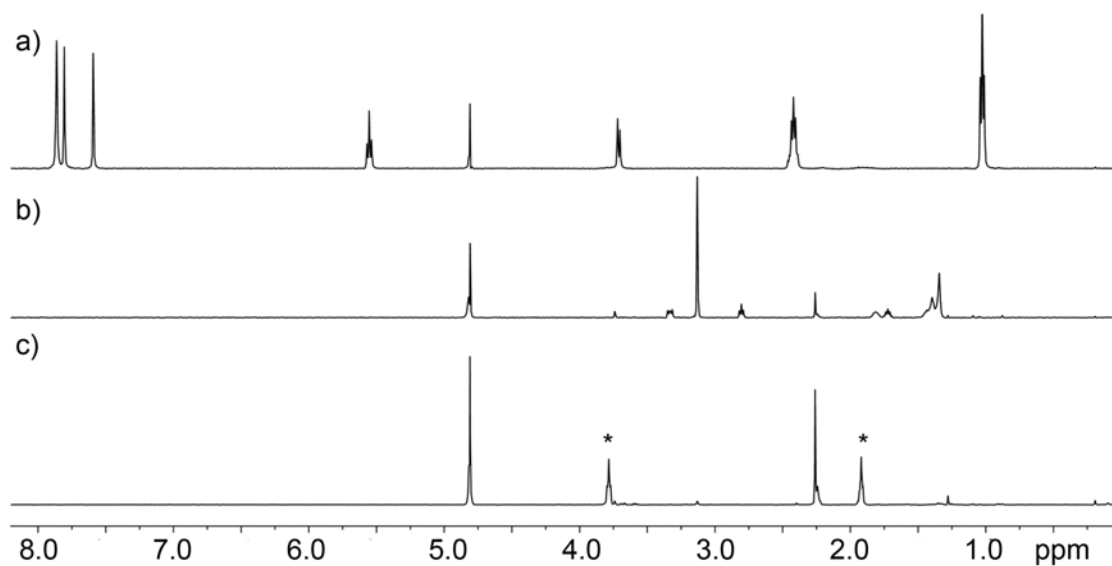


Figure 6.4. ^1H NMR of (a) Cavitand **1**, (b) AuNP and (c) AuNP after addition of Cavitand **1** in D_2O . * THF peaks in D_2O

the final synthetic step. When cavitand **1** was added to an aqueous solution of the TMA gold nanoparticles, assembly was observed. The large molecular mass of the cavitand: nanoparticle conjugate prevents ^1H NMR analysis due to slow tumbling rate, but an indirect analysis of the complex formation was possible by monitoring the displaced THF upon nanoparticle addition (Figure 6.4).^{12a} The cavitand aggregates with the nanoparticles and all cavitand signals disappear from the ^1H NMR spectrum. THF displaced from the cavity by the trimethylammonium groups is observed, and no precipitation of cavitand from solution is seen. No aggregation was observed when cavitand was exposed to nanoparticles lacking the TMA ligands.

To investigate the ability of this cavitand:AuNP association to control the capping effect of the nanoparticles, fluorescein was loaded into the MCM-41 nanoparticles. MCM-41 was soaked in an aqueous fluorescein solution for 24 h to allow complete

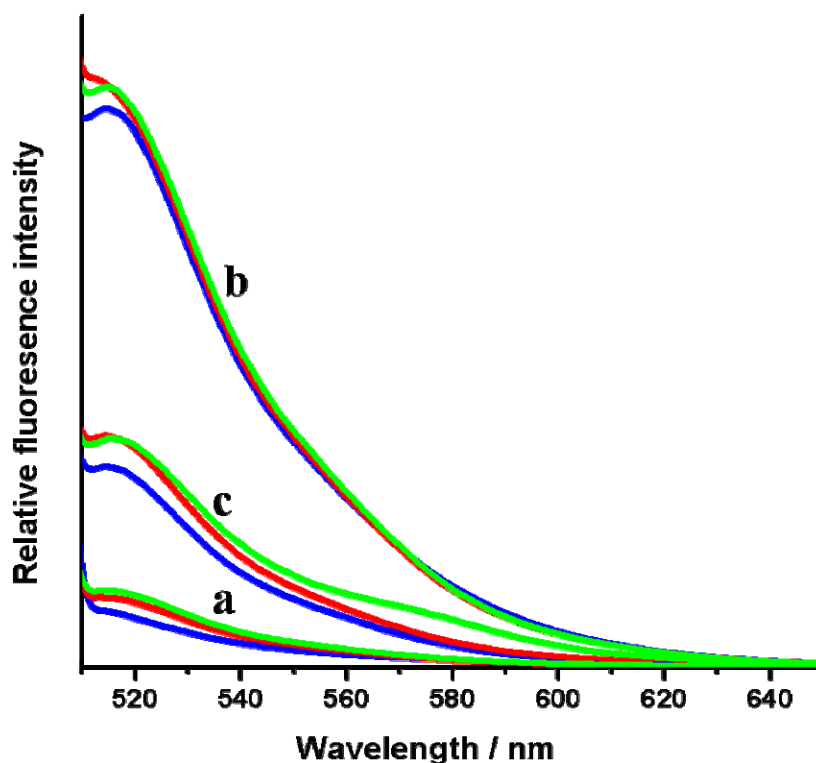


Figure 6.5 Fluorescence emission spectra of the released fluorescein under a) no additive, b) 1 mg (0.73 μmol) of cavitand 1 and c) 1 mg (6.94 μmol) of sodium benzoate. Blue line: 10 min, red line: 30 min, green line: 60 min.

saturation. The fluorescein-filled MCM-41 was capped by addition of the positively charged AuNPs. The excess fluorescein was removed by centrifugation and repeated washing with water and isopropanol. The resulting particles were then dispersed in water to test their release properties. As shown in Figure 6.5, without the application of external stimuli the intensity of fluorescein is essentially constant, indicating no leakage of the entrapped molecules and good efficiency of AuNP to retain entrapped molecules. This system was treated with 0.7 μmol of cavitand 1 in water. Upon addition of cavitand, the release of fluorescein was observed and quickly reached equilibrium within 30 min, indicating the ability of the cavitand to bind to the TMA

groups of the AuNPs, uncapping the silica and allowing guest release.

To determine whether this was a truly *supramolecular* effect, sodium benzoate was used as a control. The tetracarboxylate cavitand could conceivably interfere with the AuNP: silica interaction by non-specific interactions due to the charge of the host, rather than a specific non-covalent binding event occurring between the host and TMA groups. Sodium benzoate mimics the charge of the cavitand, but lacks any host properties. Upon addition of an excess of sodium benzoate to the system (Figure 6.5) a minimal amount of fluorescein leakage was observed, far less than that observed upon cavitand treatment.

The effect of the cavitand: AuNP association is best shown by the change in surface ζ -potential of the nanoparticles. The TMA-AuNPs have $\zeta = +55.1 \pm 3.5$ mV. Upon treatment with cavitand, positively charged NMe_3^+ groups are surrounded by the cavity (a molecular minimization of the structure of **1** binding choline is shown in Scheme 6.1b). Not only does this “hide” the charge of the headgroups, but displays the overall negative charge of the tetracarboxylate cavitand on the nanoparticle surface. The effect of this association reverses the overall charge of the nanoparticle assembly ($\zeta = -47.4 \pm 3.8$ mV), removing the AuNP: MCM-41 interaction. If sodium benzoate is used instead of **1**, the ζ potential is lowered somewhat, (ζ potential: $+22.5 \pm 0.9$ mV) but remains overall positive. The large difference can be ascribed to the strong supramolecular interaction between cavitand and nanoparticle that is not observed with sodium benzoate. The reversal of overall charge of the gold

nanoparticle aggregate allows rapid and facile guest release.

6.4 Conclusion

In this report, we describe a novel supramolecular nano-switch based on the specific host-guest interactions of a deep cavitand. The guest molecules trapped inside the nanopore and blocked by AuNPs can be released in the presence of cavitand due to the strong binding of cavitand with AuNPs and reversal of AuNP surface charge. No covalent attachments are necessary; the system switches between two host: guest interactions in aqueous solution. The results make the system reported here a promising candidate in the formulation of various responsive nanodevices. This approach could also open new applications of deep cavitands in the construction of molecular nanomachines.

6.5 References

1. (a) Angelos, S.; Johansson, E.; Stoddart, J. F.; Zink, J. I. *Adv. Funct. Mater.* **2007**, *17*, 2261; (b) Cotí, K. K.; Belowich, M. E.; Liang, M.; Ambrogio, M. W.; Lau, Y. A.; Khatib, H. A.; Zink, J. I.; Khashab N. M.; Stoddart, J. F. *Nanoscale* **2009**, *1*, 16.
2. (a) Kesanli, B.; Lin, W. *Chem. Comm.* **2004**, 2284; (b) Mihalcik, D. J.; Lin, W. *Angew. Chem. Int. Ed.* **2008**, *47*, 6229; (c) Zhu, H.; Liang, C.; Yan, W.; Overbury, S. H.; Dai, S. *J. Phys. Chem. B* **2006**, *110*, 10842; (d) Lei, C.; Shin, Y.; Liu, J.; Ackerman, E. J. *J. Am. Chem. Soc.* **2002**, *124*, 11242; (e) Taylor, K. M. L.; Kim, J. S.; Rieter, W. J.; An, H.; Lin, W.; Lin, W. *J. Am. Chem. Soc.* **2008**, *130*, 2154; (f) Liu, R.; Zhao, X.; Wu, T.; Feng, P. *J. Am. Chem. Soc.* **2008**, *130*, 14418; (g) Liu, R.; Zhang, Y.; Feng, P. *J. Am. Chem. Soc.* **2009**, *131*, 15128.
3. Klajn, R.; Stoddart, J. F.; Grzybowski, B. A. *Chem. Soc. Rev.* **2010**, *39*, 2203.

4. (a) Hernandez, R.; Tseng, H.-R.; Wong, J. W.; Stoddart, J. F.; Zink, J. I. *J. Am. Chem. Soc.* **2004**, *126*, 3370. (b) Nguyen, T. D.; Tseng, H.-R.; Celestre, P. C.; Flood, A. H.; Liu, Y.; Stoddart, J. F.; Zink, J. I. *Proc. Natl. Acad. Sci. U.S.A.* **2005**, *102*, 10029.
5. (a) Leung, K. C. F.; Nguyen, T. D.; Stoddart, J. F.; Zink, J. I. *Chem. Mater.* **2006**, *18*, 5919. (b) Nguyen, T. D.; Leung, K. C. F.; Liong, M.; Pentecost, C. D.; Stoddart, J. F.; Zink, J. I. *Org. Lett.* **2006**, *8*, 3363; (c) Angelos, S.; Yang, Y. W.; Patel, K.; Stoddart, J. F.; Zink, J. I. *Angew. Chem. Int. Ed.* **2008**, *47*, 2222. (d) Khashab, N. M.; Trabolsi, A. Lau, Y. A.; Ambrogio, M. W.; Friedman, D. C.; Khatib, H. A.; Zink, J. I.; Stoddart, J. F. *Eur. J. Org. Chem.* **2009**, 1669.
6. Park, C.; Oh, K.; Lee, S.; Kim, C. *Angew. Chem. Int. Ed.* **2007**, *46*, 1455.
7. (a) Patel, K.; Angelos, S.; Dichtel, W. R.; Coskun, A.; Yang, Y.-W.; Zink, J. I.; Stoddart, J. F. *J. Am. Chem. Soc.* **2008**, *130*, 2382, (b) Ferris, D. P.; Zhao, Y.; Khashab, N. M.; Khatib, H. A.; Stoddart, J. F.; Zink, J. I. *J. Am. Chem. Soc.* **2009**, *131*, 1686.
- 8 (a) Liu, R.; Zhang, Y.; Zhao, X.; Agarwal, A.; Mueller, L. J.; Feng, P. *J. Am. Chem. Soc.* **2010**, *132*, 1500; (b) Lai, C.-Y.; Trewyn, B. G.; Jeftinija, D. M.; Jeftinija, K.; Xu, S.; Jeftinija, S.; Lin, V. S.-Y. *J. Am. Chem. Soc.* **2003**, *125*, 4451; (c) Torney, F.; Trewyn, B. G.; Lin, V. S.-Y.; Wang, K. *Nat. Nanotechnol.* **2007**, *2*, 295; (d) Giri, S.; Trewyn, B. G.; Stellmaker, M. P.; Lin, V. S.-Y. *Angew. Chem., Int. Ed.* **2005**, *44*, 5038.
9. Vivero-Escoto, J. L.; Slowing, I. I.; Wu, C.-W.; Lin, V. S.-Y. *J. Am. Chem. Soc.* **2009**, *131*, 3462.
10. (a) Cram, D. J.; Cram, J. M. In *Container Molecules and Their Guests*; Stoddart, F., Ed.; The Royal Society of Chemistry: London, 1994. (b) Rudkevich, D. M.; Hilmersson, G.; Rebek, J. Jr. *J. Am. Chem. Soc.* **1998**, *120*, 12216; (c) Hooley, R.J.; Rebek, J., Jr. *Chem. Biol.* **2009**, *16*, 255.
11. Hof, F.; Trembleau, L.; Ullrich, E. C.; Rebek, J., Jr. *Angew. Chem. Int. Ed.* **2003**, *42*, 3150.
12. (a) Hooley, R.J., van Anda, H.J., Rebek, J., Jr. *J. Am. Chem. Soc.* **2007**, *129*, 13464; b) Biro, S. M.; Ullrich, E. C.; Hof, F.; Trembleau, L.; Rebek, J., Jr. *J. Am. Chem. Soc.* **2004**, *126*, 2870.
13. Liu, Y., Liao, P., Cheng Q., Hooley, R. J., *J. Am. Chem. Soc.* **2010**, *132*, 10383.

14. (a) Tien, J.; Terfort, A.; Whitesides, G. M. *Langmuir* **1997**, *13*, 5349. (b) Cliffler, D. E.; Zamborini, F. P.; Gross, S. M.; Murray, R. W. *Langmuir* **2000**, *16*, 9699

Chapter Seven

Sulfonated Ordered Mesoporous Carbon for Catalytic Preparation of Biodiesel*

7.1. Introduction

Due to the limited traditional fossil energy resources and increased environmental concerns, a search for alternative renewable fuels has received significant attention in recent years. Among the different possible resources, biodiesel, a nonpetroleum-based fuels, has exhibited great potential as substitutes for petroleum-based fuels. Biodiesel, produced through the process of either transesterification of triglycerides or esterification of free fatty acids(FFA), is regarded as “green fuel” because of its low emissions, biodegradability, and non-toxicity. Current biodiesel production technology using toxic, corrosive homogeneous base catalysts (e.g. NaOH, KOH or NaOCH₃) or acid catalysts (e.g.H₂SO₄) involves the costly processes of neutralization and separation. Biodiesel synthesis using solid catalysts instead of homogeneous liquid catalysts has been the main focus in recent biodiesel catalyst research¹⁻¹⁰. Solid catalysts could avoid the corrosion and environmental problems associated with liquid catalysts and could also lead to lower production costs because of easy product separation. Rothenberg et al^{11, 12} compared the catalytic activity of various solid acids such as zeolites, ion-exchange resin, and mixed metal oxide and found that the hydrophobicity of the catalyst surface and the density of the acid sites are of paramount importance in determining the catalyst’s activity and selectivity.

* Reproduced with permission from *Carbon* **2008**, 46, 1664. copyright 2008 Elsevier

Mesostructured silicas have recently emerged as a new biodiesel catalyst due to the combination of high surface area, flexible pore size and tunable surface property^{13,14}. For example, Shanks et al¹³ used organosulfonic acid-functionalized mesoporous silicas as catalysts in the esterification of fatty acid with methanol to produce methyl esters. The catalysts showed higher reactivity than commercially available solid acid esterification catalysts such as Amberlyst-15 and Nafion. However, the hydrophilic surface of silica makes effective absorption of long chain molecules difficult and the byproduct water is easily absorbed to the surface leading to deactivation of the catalysts¹⁴.

Mesoporous carbon, which can be replicated from mesoporous silica and whose surface is hydrophobic, can be an ideal candidate for the development of biodiesel catalyst. Ordered mesoporous carbons (OMCs) can be synthesized through the nanocasting technique using ordered mesoporous silicas (e.g., MCM-48 and SBA-15) as templates¹⁵. OMCs not only keep the unique porous properties of mesoporous materials, but also show chemical inertness and good mechanical and thermal stabilities. One of the most important features of carbon materials is that their surface is hydrophobic so that it can effectively absorb long chain organic molecule such as free fatty acids and avoid the absorption of water byproduct that can lead to deactivation. At the same time, efficient modification methods on carbon surface, such as grafting through electrochemical^{16,17} or chemical reduction^{18,19} of aryl diazoniums, reductive alkylation and arylation²⁰, have been developed and can be

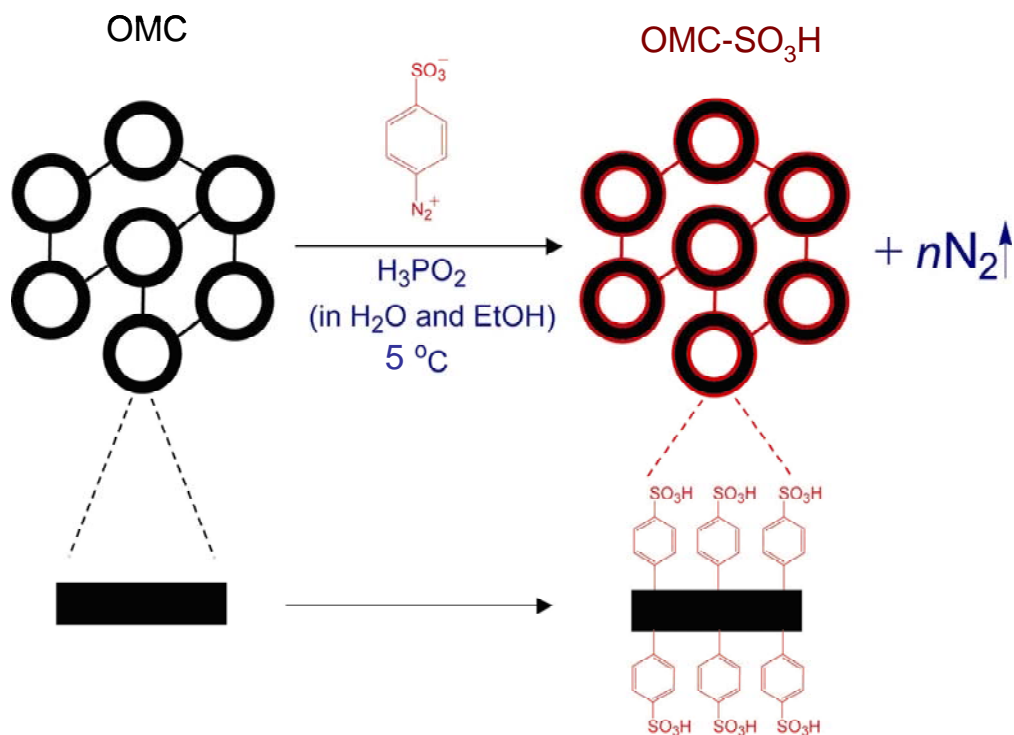
applied for functionalization of OMCs. We have recently reported a new method to prepare sulfonic acid functionalized OMC by covalent attachment of sulfonic acid-containing aryl radical and demonstrated their catalytic properties in the synthesis of ethyl acetate and bisphenol-A ²¹. In this paper, a series of sulfonated OMCs are synthesized and examined as solid acid catalysts in biodiesel synthesis. Through the combination of the advantages of carbon-based catalysts (e.g., excellent stability) and the unique features of OMCs (e.g., large surface area, uniform porosity), the resulting materials show higher activity for acid-catalyzed biodiesel reactions compared with other solid acid catalysts. The catalytic ability is further tested by tuning the pore size of sulfonated OMC.

7.2 Experimental Section

7.2.1 OMC and sulfonated OMC

Three types of SBA-15 materials were synthesized at 100°C, 130°C and 150°C, respectively, according to the reported method ²². Ordered mesoporous carbons with different pore diameters were prepared by using SBA-15 materials as templates and furfuryl alcohol (FA) as the carbon precursor ^{23, 24}. The obtained carbon materials were denoted as OMC-100, OMC-130 and OMC-150, respectively, where the number indicates the aging temperature of SBA-15 template. Preparation of sulfonated OMC(OMC- SO₃H) was carried out from a mixture with a starting composition of 1/20(w/w) OMC/4-benzene-diazoniumsulfonate in ethanol/water solution in the

Scheme 7.1. Functionalization of OMC with sulfonic acid groups



presence H_3PO_2 (Scheme 7.1). In a typical procedure, 0.15 g of OMC was added in a three-necked ground flask containing 3.0 g of 4-benzene-diazoniumsulfonate in 50 ml of distilled water and 50 ml of ethanol. Subsequently, the mixture was cooled down to $5\text{ }^\circ\text{C}$ and 50 ml of 50 wt % H_3PO_2 aqueous solution was added. After stirring for 30 min, another 50 ml of H_3PO_2 aqueous solution was added and the mixture was stirred at $5\text{ }^\circ\text{C}$ for another 30 min. The sulfonic acid functionalized carbon material (OMC- SO_3H) was recovered by filtration, washed thoroughly with distilled water and finally acetone, and dried in an oven at 100°C . The obtained sulfonated OMCs were denoted as OMC- SO_3H -100, OMC- SO_3H -130, OMC- SO_3H -150 from OMC-100, OMC-130, OMC-150, respectively.

7.2.2 Other acid catalysts

Nafion(NR50, Aldrich) was obtained commercially without any further purification. Mesoporous silica functionalized with benzenesulfonic acid groups, SBA-15-Ph-SO₃H, was synthesized by reported method ¹³. Typically, 4g of Pluronic P123 was dissolved in 125 ml of 1.9 M HCl at room temperature. 8.76g of TEOS was added after the solution was heated to 35 °C. Following TEOS prehydrolysis, 2.66 mL of 2-(4-chlorosulfonylphenyl)ethyltrimethoxysilane (CSPTMS, Gelest) solution in methylene chloride was added and the resulting mixture was stirred for 20 h at 35°C , and aged at 95°C for another 24 h. The solid was recovered and the surfactant template was removed by suspending the solid material in ethanol and refluxing for 48 h. The sulfonyl chloride groups underwent hydrolysis in the acidic media of the reaction.

7.2.3 Catalyst characterization

Powder X-ray diffraction (XRD) patterns were recorded on a Bruker D8 Advance diffractometer with Cu K α radiation (40 kV, 40 mA). SEM images were recorded on a Philips XL30 scanning electron microscope. N₂ sorption analysis was performed on a Micromeritics ASAP2010 volumetric adsorption analyzer at 77 K. Prior to the measurement, the samples were degassed at 120 °C for 4 h. The specific surface area was calculated using the BET method from the nitrogen adsorption data in the relative pressure range (P/P₀) of 0.05 ~ 0.30. The total pore volume was determined from the amount of N₂ uptake at P/P₀ of 0.99. Acid capacity was determined by titration with

0.01M NaOH aqueous solution.

7.2.4 Catalytic reactions

Catalytic esterification of oleic acid with ethanol was performed under N₂ atmosphere in a closed flask at 80 °C. 50 mg of catalyst was degassed at 100 °C for 1 h prior to the addition of ethanol (0.05 mol) and oleic acid (0.005 mol). The reaction aliquots (about 0.1 ml) were taken out at regular intervals. After centrifugation at 12000 rpm, the clear supernatant solution was analyzed on an Shimadzu GC-2010 gas chromatographic (GC) system equipped with a FID detector and an Alltech AT-5 capillary column (15 m * 0.32 mm * 1 μm), where hexadecane was used as the internal standard. The products were identified by HP 5989A GC/MS.

7.3 Results and Discussion

By using SBA-15 materials as templates, OMCs were synthesized following a reported procedure^{23, 24}. Three OMC materials were obtained and designated as OMC-100, OMC-130, and OMC-150. The functionalization of OMC was carried out by covalent attachment of sulfonic acid-containing aryl radicals through reaction OMC with 4-benzene-diazoniumsulfonate in the presence of hypophosphorous acid. Three sulfonated OMCs, OMC-SO₃H-100, OMC-SO₃H-130, and OMC-SO₃H-150 are obtained from OMC-100, OMC-130 and OMC-150, respectively. The XRD patterns of OMCs and sulfonated OMCs in Figure 7.1 show 4 peaks, which can be

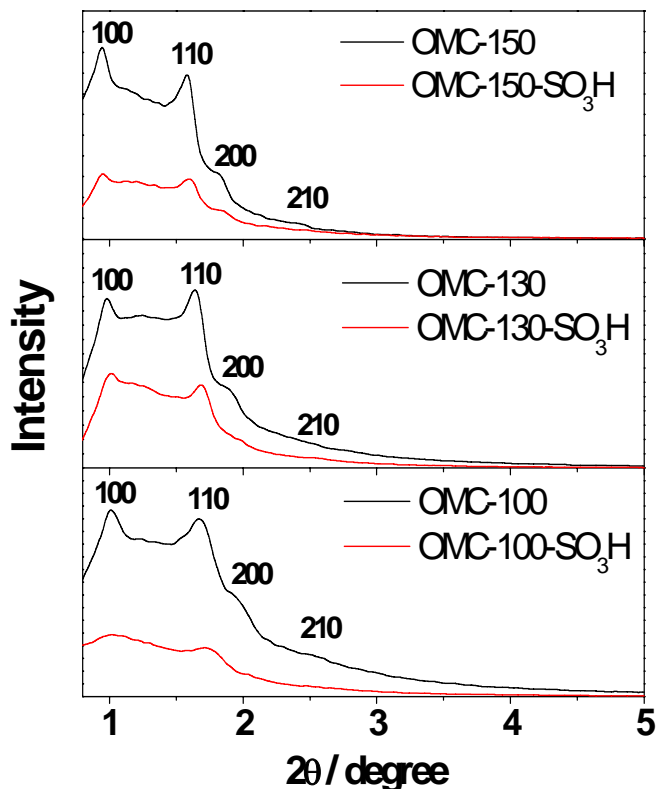


Figure 7.1 XRD patterns of OMCs and sulfonated OMCs

indexed as 100, 110, 200 and 210 reflections based on CMK-5 type 2D hexagonal $p6m$ symmetry. After modification, the sulfonated OMC retains the pore structure, but the intensity of XRD peaks is lower and some peaks can be difficult to detect due to the decreased scattering contrast between walls and channels after modification. As shown in Figure 7.2, the synthesized OMC-SO₃H possesses the tube-type morphology because of the rod-shaped SBA-15 template^{21, 22}. The N₂-adsorption data of three sulfonated OMCs in Figure 4 show that both the BET surface area and pore volume decrease after sulfonation. It can be seen (inset of Figure 7.3) that pore

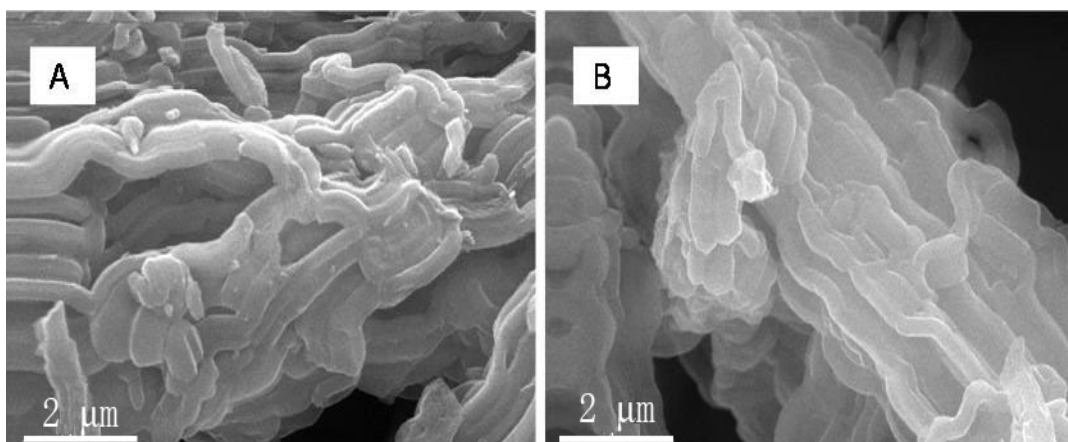


Figure 7.2 SEM of OMC-150(A) and OMC-150-SO₃H(B)

size of all sulfonated OMCs exhibits a decrease of 1.3nm compared with parent OMCs, which indicates the successful grafting of functional group. The acid exchange capacity of OMC-SO₃H determined by potentiometric titration was above 1.70 mmol H⁺/g (or 2.20×10^{-3} mmol H⁺/m²) for all three sulfonated OMC and even reach 1.95 mmol H⁺/g (or 2.83×10^{-3} mmol H⁺/m²) for OMC-SO₃H-100, which is higher than most of the other sulfonic acid functionalized mesoporous materials reported so far²⁵⁻²⁹. Specific textural parameters of OMCs and sulfonated OMCs are listed in Table 7.1.

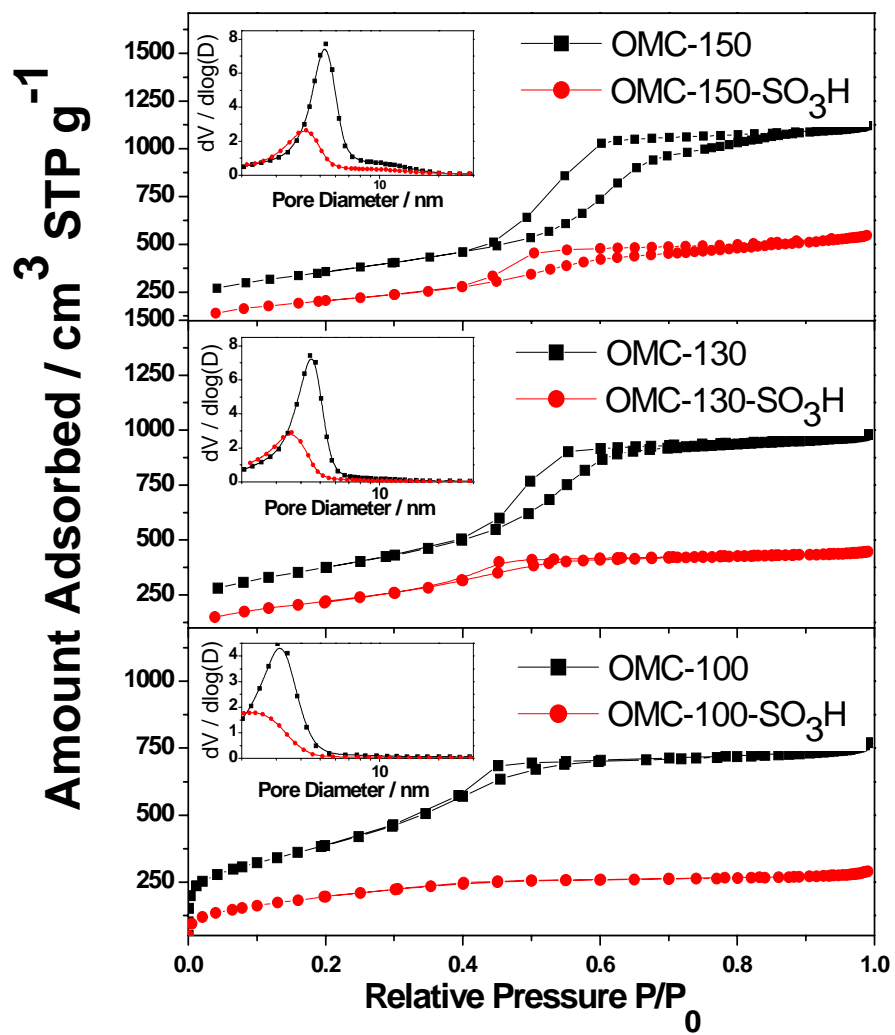


Figure 7.3 N₂ sorption isotherms and BJH pore size distribution plots (inset) of OMCs and OMC-SO₃Hs

Table 7.1 Textural properties of OMCs and sulfonated ordered mesoporous carbons and catalytic properties of OMC-SO₃Hs

| | Textural properties | | | | Catalytic properties ^d | | |
|-----------------------------|---------------------|---|----------------------------------|---------------------|--|--|----------------|
| | Pore diameter (nm) | S _{BET} ^a (m ² /g) | Pore volume (cm ³ /g) | a ^b (nm) | Acid density ^c mmol H ⁺ /g, 10 ⁻³ mmol H ⁺ /m ² | Initial formation rate (μmol min ⁻¹) | Conversion (%) |
| OMC-150 | 5.5 | 1254 | 1.75 | 11.18 | | | |
| OMC-130 | 4.5 | 1338 | 1.52 | 10.21 | | | |
| OMC-100 | 3.4 | 1384 | 1.20 | 9.93 | | | |
| OMC-150-SO ₃ H | 4.2 | 741 | 0.85 | 10.75 | 1.70 ± 0.07 | 2.29 ± 0.10 | 73.59 |
| OMC-130-SO ₃ H | 3.2 | 813 | 0.69 | 10.07 | 1.82 ± 0.06 | 2.24 ± 0.08 | 69.12 |
| OMC-100-SO ₃ H | 2.1 | 689 | 0.45 | 9.85 | 1.95 ± 0.01 | 2.83 ± 0.01 | 69.21 |
| SBA-15-Ph-SO ₃ H | 10.0 | 610 | 0.79 | 13.21 | 1.17 ± 0.09 | 1.92 ± 0.14 | 50.95 |

^a S_{BET}: BET surface area; ^b a: unit cell parameter, $a = d_{100} \sqrt{3}$; ^c determined by potentiometric titration; ^d reaction condition: acid catalyzed (50 mg catalyst) esterification of oleic acid (0.005 mol) with ethanol (0.05 mol) at 80 °C for 10h

The catalytic performance of OMC-SO₃Hs in biodiesel synthesis was investigated by esterification of oleic acid with ethanol at 80°C. Figure 7.4 shows time courses of acid conversion on OMC-SO₃Hs, SBA-15-Ph-SO₃H (see experimental detail and Table 7.1) and protonated Nafion(NR50, Aldrich, acid capacity 0.8 mmol g⁻¹). In the absence of acid catalyst, the conversion of oleic acid was only 5.78% after 10h of reaction. In comparison, all three OMC-SO₃Hs gave above 69.00 % yield of ethyl oleate (based on oleic acid). Under identical condition, the conversion of oleic acid was only 26.69% for Nafion and 50.95% for organosulfonic acid-functionalized mesoporous silica, SBA-15-Ph-SO₃H. Compared with sulfonated mesoporous silica, the larger amount of active sites of sulfonated OMC may not be the only reason for its high catalytic activity since the initial biodiesel formation rate of OMC-SO₃H-150 (e.g. 30.03μmol min⁻¹) is almost 3 times that of mesoporous silica (e.g. 10.23μmol min⁻¹)

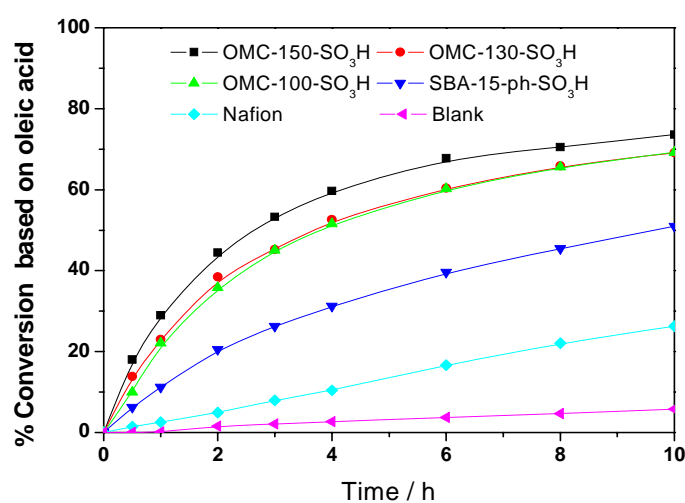


Figure 7.4 Comparison of catalytic activity for conversion of oleic acid over different catalysts. Reaction condition: acid catalyzed (50 mg catalyst) esterification of oleic acid (0.005 mol) with ethanol (0.05 mol)

while the acid capacity is only 1.5 times(based on weight) and 1.2 times(based on surface area) that of sulfonated mesoporous silica. Hydrophobic substrate of carbon-based catalyst is believed to contribute to the superior performance on catalyzed formation of ethyl oleate, because it can lead to effective absorption of the long chain fatty acid molecules and leaching of byproduct water, especially at the beginning stage.

Pore size is another concern for mesoporous materials in catalytic application, such as biodiesel synthesis involving large organic molecules. Three sulfonated OMCs with different pore diameters are synthesized by templating with different SBA-15 materials as discussed above. The results of catalytic ability in oleic acid esterification from the three materials are shown in Table 7.1. Although both the surface area and amount of acid site of OMC-SO₃H-150 used in the catalytic reaction are lower than OMC-SO₃H-130, the initial formation rate for ethyl oleate and final conversion of OMC-SO₃H-150 with larger pore size are higher than that of OMC-SO₃H-130. Furthermore, OMC-SO₃H-100 with the smallest pore size and surface area shows the lowest initial formation rate compared with larger pore sized OMC-SO₃Hs even though OMC-SO₃H-100 has the highest acid density(both per unit weight and per unit area) and the final conversion is almost identical as OMC-SO₃H-130. The effect of pore size on the catalytic performance demonstrates that the factors favoring the diffusion of large organic molecules contribute to the enhancement of catalytic property.

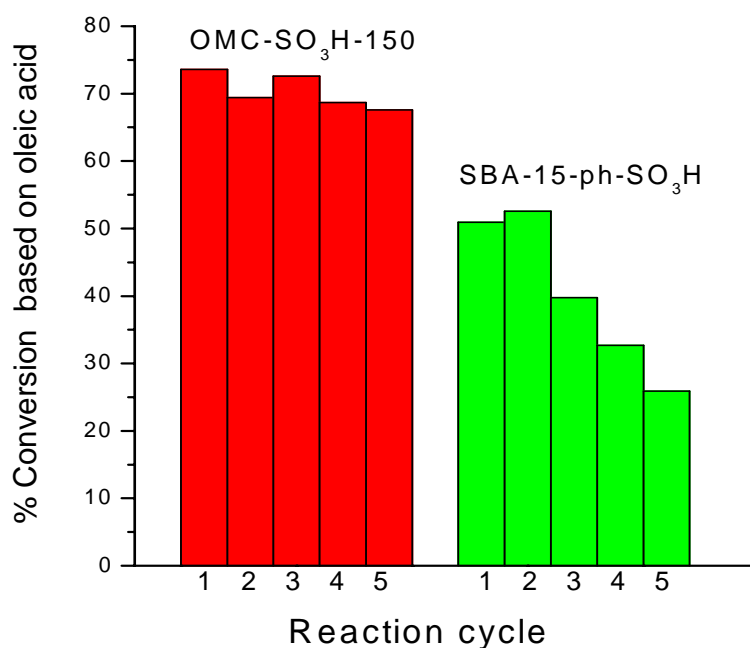


Figure 7.5 Repeating use of OMC-SO₃H-150 and SBA-15-ph-SO₃H for esterification of oleic acid (0.005 mol) with ethanol (0.05 mol) at 80 °C. The yields of ethyl oleate produced after reaction for 10 h are shown.

The stability of OMC-SO₃Hs was investigated by performing the esterification reaction with the same catalyst five times. After each use, the catalyst was recycled by simple centrifugation, followed by washing with distilled water and drying in an oven at 100 °C overnight. Figure 7.5 shows the recyclable ability for different mesoporous catalysts. The yield of ethyl oleate for carbon-based catalysts almost remained unchanged even after four cycles while the catalytic activity of SBA-15-ph-SO₃H gradually decreases after two runs. The low stability of the latter may be due to the weak attachment of functional groups on the silica surface through unstable Si-O-Si-R siloxane bonds, which are susceptible to hydrolysis especially at low pH values³⁰. The

good recycleability of sulfonated OMC can be attributed to high stability of ordered mesoporous carbon and strong attachment of aryl sulfonic acid group on the substrate through the robust C-C bond. Therefore the materials presented here have great potential to be a stable and highly active solid acid catalyst.

7.4. Conclusions

The preparation of mesoporous solid acid catalysts for biodiesel synthesis based on sulfonic acid functionalized OMC is reported. The obtained materials exhibit high surface area and uniform pore size. The high acid density and hydrophobic surface property of OMC-SO₃H make it a highly efficient biodiesel catalyst. Large pore size that favors the diffusion of large organic molecules contributes to the enhancement of catalytic ability. Another unique feature of OMC-SO₃H is its reusable ability without noticeable loss of activity due to the stability of carbon-based materials and the strong attachment of sulfonic acid group. The application of sulfonated OMC can also be extended to other acid-catalyzed reactions.

7.5 References

1. Furuta, S.; Matsushashi, H.; Arata, K. *Catal Commun* **2004**; 5(12): 721.
2. Kim, H.; Kang, B.; Kim, M.; Park, Y. M.; Kim, D.; Lee, J.; Lee, K. *Catal Today* **2004**; 93-95: 315.
3. Toda, M.; Takagaki, A.; Okamura, M.; Kondo, J. N.; Hayashi, S.; Domen, K.; Hara, M. *Nature* **2005**; 438: 178.

4. Lotero, E.; Liu, Y.; Lopez, D. E.; Suwannakarn, K.; Bruce, D. A.; Goodwin, J. G. Jr. *Ind Eng Chem Res* **2005**; 44(14): 5353.
5. Lopez, D. E.; Goodwin, J. G. Jr.; Bruce, D. A.; Lotero, E. *Appl Catal A Gen* **2005**; 295(2): 97.
6. Xie, W.; Peng, H.; Chen, L. *J Mol Catal A Chem* **2006**; 246(1-2): 24.
7. Xie, W.; Peng, H.; Chen, L. *Appl Catal A Gen* **2006**; 300(1): 67.
8. Kulkarni, M. G.; Gopinath, R.; Meher, L. C.; Dalai, A. K. *Green Chemistry* **2006**; 8(12): 1056.
9. Rao, K. N.; Sridhar, A.; Lee, A. F.; Tavener, S. J.; Young, N. A.; Wilson, K. *Green Chemistry* **2006**; 8(9): 790.
10. Jitputti, J.; Kitiyanan, B.; Rangsunvigit, P.; Bunyakiat, K.; Attanatho, L.; Jenvanitpanjakul, P. *Chem Eng J* **2006**; 116(1): 61.
11. Kiss, A. A.; Omota, F.; Dimian, A. C.; Rothenberg, G. *Top Catal* **2006**; 40(1-4): 141.
12. Kiss, A. A.; Dimian, A.C.; Rothenberg, G. *Adv Synth Catal* **2006**; 348(1-2): 75.
13. Mbaraka, I. K.; Radu, D. R.; Lin, V. S. Y.; Shanks, B. H. *J Catal* **2003**; 219(2): 329.
14. Mbaraka, I. K.; Shanks, B. H. *J Catal* **2005**; 229(2): 365.
15. Ryoo, R.; Joo, S. H.; Jun, S.; Tsubakiyama, T.; Terasaki, O. *Stud Surf Sci Catal* **2001**; 135: 150.
16. Delamar, M.; Hitmi, R.; Pinson, J.; Savéant, J. M. *J Am Chem Soc* **1992**; 114(14): 5883.
17. Bahr, J. L.; Yang, J.; Kosynkin, D. V.; Bronikowshi, M. J.; Smalley, R. E.; Tour, J. M. *J Am Chem Soc* **2001**; 123(27): 6536.
18. Pandurangappa, M.; Lawrence, N. S.; Compton, R. G. *Analyst* **2002**; 127(12): 1568.

19. Wildgoose, G. G.; Leventis, H. C.; Davies, I. J.; Crossley, A.; Lawrence, N. S.; Jiang, L.; Jones, T. G. J.; Compton, R. G. *J Mater Chem* **2005**; 15(24): 2375.
20. Stephenson, J.J.; Sadana, A. K.; Higginbotham, A. L.; Tour, J. M. *Chem Mater* **2006**; 18(19): 4658.
21. Wang, X.; Liu, R.; Waje, M. M.; Chen, Z.; Yan, Y.; Bozhilov, K. N.; Feng, P. *Chem Mater* **2007**; 19(10): 2395.
22. Yu, C.; Fan, J.; Tian, B.; Zhao, D.; Stucky, G. D. *Adv Mater* **2002**; 14(23): 1742.
23. Joo, S. H.; Choi, J.; Oh, I.; Kwak, J.; Liu, Z.; Terasaki, O.; Ryoo, R. *Nature* **2001**; 412: 169.
24. Kurk, M.; Jaroniec, M.; Kim, T. W.; Ryoo, R. *Chem Mater* **2003**; 15(14): 2815.
25. Dufaud, V.; Davis, M. E. *J Am Chem Soc* **2003**; 125(31): 9403.
26. Yang, Q.; Liu, J.; Yang, J.; Kapoor, M. P.; Inagaki, S.; Li, C. *J Catal* **2004**; 228(2): 265.
27. Yang, Q.; Kapoor, M. P.; Inagaki, S.; Shirokura, N.; Kondo, J. N.; Domen, K. *J Mol Catal A Chem* **2005**; 230(1-2): 85.
28. Macquarrie, D. J.; Tavener, S. J.; Harmer, M. A. *Chem Commun* **2005**; 2363.
29. Rác, B.; Molnár Forgo, A. P.; Mohai, M.; Bertóti, J. *J Mol Catal A Chem* **2006**; 244(1-2): 46.
30. Brown, L.; Ciccone, B.; Pesek, J. J.; Matyska, M. T. *American Lab* **2003**; 35(24):23.